VOLUME XXIX JANUARY, 1950 NO. 1

THE BELL SYSTEM TECHNICAL JOURNAL

DEVOTED TO THE SCIENTIFIC AND ENGINEERING ASPECTS OF ELECTRICAL COMMUNICATION

50¢ per copy

$1.50 per Year

THE BELL SYSTEM TECHNICAL JOURNAL

Published quarterly by the
American Telephone and Telegraph Company
195 Broadway, New York, N. Y.

SUBSCRIPTIONS

Subscriptions are accepted at $1.50 per year. Single copies are 50 cents each. The foreign postage is 35 cents per year or 9 cents per copy.

PRINTED IN U. S. A.

The Bell System Technical Journal

Vol. XXIX *January, 1950* *No. 1*

Traveling-Wave Tubes

By J. R. PIERCE

The following material on traveling-wave tubes is taken from a book which will be published by Van Nostrand in September, 1950. Substantially the entire contents of the book will be published in this and the three succeeding issues of the Bell System Technical Journal.

This material will cover in detail the theory of traveling-wave amplifiers. In addition, brief discussions of magnetron amplifiers and double-stream amplifiers are included. Experimental material is drawn on in a general way only, as indicating the range of validity of the theoretical treatments.

The material deals only with the high-frequency electronic and circuit behavior of tubes. Such matters as matching into circuits are not considered; neither are problems of beam formation and electron focusing, which have been dealt with elsewhere.[1]

The material opens with the presentation of a simplified theory of the traveling-wave tube. A discussion of circuits follows, including helix calculations, a treatment of filter-type circuits, some general circuit considerations which show that gain will be highest for low group velocities and low stored energies, and a justification of a simple transmission line treatment of circuits by means of an expansion in terms of the normal modes of propagation of a circuit. Then a detailed analysis of overall electronic and circuit behavior is made, including a discussion of various electronic and circuit waves, the fitting of boundary conditions to obtain overall gain, noise figure calculations, transverse motions of electrons and field solutions appropriate to broad electron streams. Short treatments of the magnetron amplifier and the double-stream amplifier follow.

[1] For instance, "Theory and Design of Electron Beams," J. R. Pierce, Van Nostrand, 1949.

CHAPTER I

INTRODUCTION

ASTRONOMERS are interested in stars and galaxies, physicists in atoms and crystals, and biologists in cells and tissues because these are natural objects which are always with us and which we must understand. The traveling-wave tube is a constructed complication, and it can be of interest only when and as long as it successfully competes with older and newer microwave devices. In this relative sense, it is successful and hence important.

This does not mean that the traveling-wave tube is better than other microwave tubes in all respects. As yet it is somewhat inefficient compared with most magnetrons and even with some klystrons, although efficiencies of over 10 per cent have been attained. It seems reasonable that the efficiency of traveling-wave tubes will improve with time, and a related device, the magnetron amplifier, promises high efficiencies. Still, efficiency is not the chief merit of the traveling-wave tube.

Nor is gain, although the traveling-wave tubes have been built with gains of over 30 db, gains which are rivaled only by the newer double-stream amplifier and perhaps by multi-resonator klystrons.

In noise figure the traveling-wave tube appears to be superior to other microwave devices, and noise figures of around 12 db have been reported. This is certainly a very important point in its favor.

Structurally, the traveling-wave tube is simple, and this too is important. Simplicity of structure has made it possible to build successful amplifiers for frequencies as high as 48,000 megacycles (6.25 mm). When we consider that successful traveling-wave tubes have been built for 200 mc, we realize that the traveling-wave amplifier covers an enormous range of frequencies.

The really vital feature of the traveling-wave tube, however, the new feature which makes it different from and superior to earlier devices, is its tremendous bandwidth.

It is comparatively easy to build tubes with a 20 per cent bandwidth at 4,000 mc, that is, with a bandwidth of 800 mc, and L. M. Field has reported a bandwidth of 3 to 1 extending from 350 mc to 1,050 mc. There seems no reason why even broader bandwidths should not be attained.

As it happens, there is a current need for more bandwidth in the general field of communication. For one thing, the rate of transmission of intelli-

gence by telegraph, by telephone or by facsimile is directly proportional to bandwidth; and, with an increase in communication in all of these fields, more bandwidth is needed.

Further, new services require much more bandwidth than old services. A bandwidth of 4,000 cycles suffices for a telephone conversation. A bandwidth of 15,000 cycles is required for a very-high-fidelity program circuit. A single black-and-white television channel occupies a bandwidth of about 4 mc, or approximately a thousand times the bandwidth required for telephony.

Beyond these requirements for greater bandwidth to transmit greater amounts of intelligence and to provide new types of service, there is currently a third need for more bandwidth. In FM broadcasting, a radio frequency bandwidth of 150 kc is used in transmitting a 15 kc audio channel. This ten-fold increase in bandwidth does not represent a waste of frequency space, because by using the extra bandwidth a considerable immunity to noise and interference is achieved. Other attractive types of modulation, such as PCM (pulse code modulation) also make use of wide bandwidths in overcoming distortion, noise and interference.

At present, the media of communication which have been used in the past are becoming increasingly crowded. With a bandwidth of about 3 mc, approximately 600 telephone channels can be transmitted on a single coaxial cable. It is very hard to make amplifiers which have the high quality necessary for single sideband transmission with bandwidths more than a few times broader than this. In television there are a number of channels suitable for local broadcasting in the range around 100 mc, and amplifiers sufficiently broad and of sufficiently good quality to amplify a single television channel for a small number of times are available. It is clear, however, that at these lower frequencies it would be very difficult to provide a number of long-haul television channels and to increase telephone and other services substantially.

Fortunately, the microwave spectrum, which has been exploited increasingly since the war, provides a great deal of new frequency space. For instance, the entire broadcast band, which is about 1 mc wide, is not sufficient for one television signal. The small part of the microwave spectrum in the wavelength range from 6 to $7\frac{1}{2}$ cm has a frequency range of 1,000 mc, which is sufficient to transmit many simultaneous television channels, even when broad-band methods such as FM or PCM are used.

In order fully to exploit the microwave spectrum, it is desirable to have amplifiers with bandwidths commensurate with the frequency space available. This is partly because one wishes to send a great deal of information in the microwave range: a great many telephone channels and a substantial number of television channels. There is another reason why very broad

bands are needed in the microwave range. In providing an integrated nationwide communication service, it is necessary for the signals to be amplified by many repeaters. Amplification of the single-sideband type of signal used in coaxial systems, or even amplification of amplitude modulated signals, requires a freedom from distortion in amplifiers which it seems almost impossible to attain at microwave frequencies, and a freedom from interfering signals which it will be very difficult to attain. For these reasons, it seems almost essential to rely on methods of modulation which use a large bandwidth in order to overcome both amplifier distortion and also interference.

Many microwave amplifiers are inferior in bandwidth to amplifiers available at lower frequencies. Klystrons give perhaps a little less bandwidth than good low-frequency pentodes. The type 416A triode, recently developed at Bell Telephone Laboratories, gives bandwidths in the 4,000 mc range somewhat larger than those attainable at lower frequencies. Both the klystron and the triode have, however, the same fundamental limitation as do other conventional tubes. As the band is broadened at any frequency, the gain is necessarily decreased, and for a given tube there is a bandwidth beyond which no gain is available. This is so because the signal must be applied by means of some sort of resonant circuit across a capacitance at the input of the tube.

In the traveling-wave tube, this limitation is overcome completely. There is no input capacitance nor any resonant circuit. The tube is a smooth transmission line with a negative attenuation in the forward direction and a positive attenuation in the backward direction. The bandwidth can be limited by transducers connecting the circuit of the tube to the source and the load, but the bandwidth of such transducers can be made very great. The tube itself has a gradual change of gain with frequency, and we have seen that this allows a bandwidth of three times and perhaps more. This means that bandwidths of more than 1,000 mc are available in the microwave range. Such bandwidths are indeed so great that at present we have no means for fully exploiting them.

In all, the traveling-wave tube compares favorably with other microwave devices in gain, in noise figure, in simplicity of construction and in frequency range. While it is not as good as the magnetron in efficiency, reasonable efficiencies can be attained and greater efficiencies are to be expected. Finally, it does provide amplification over a bandwidth commensurate with the frequency space available at microwaves.

The purpose of this book is to collect and present theoretical material which will be useful to those who want to know about, to design or to do research on traveling-wave tubes. Some of this material has appeared in print. Other parts of the material are new. The old material and the new material have been given a common notation.

The material covers the radio-frequency aspects of the electronic behavior of the tube and its internal circuit behavior. Matters such as matching into and out of the slow-wave structures which are described are not considered. Neither are problems of producing and focusing electron beams, which have been discussed elsewhere,[1] nor are those of mechanical structure nor of heat dissipation.

In the field covered, an effort has been made to select material of practical value, and to present it as understandably as possible. References to various publications cover some of the finer points. The book refers to experimental data only incidentally in making general evaluations of theoretical results.

To try to present the theory of the traveling-wave tube is difficult without some reference to the overall picture which the theory is supposed to give. One feels in the position of lifting himself by his bootstraps. For this reason the following chapter gives a brief general description of the traveling-wave tube and a brief and specialized analysis of its operation. This chapter is intended to give the reader some insight into the nature of the problems which are to be met. In Chapters III through VI, slow-wave circuits are discussed to give a qualitative and quantitative idea of their nature and limitations. Then, simplified equations for the overall behavior of the tube are introduced and solved, and matters such as overall gain, insertion of loss, a-c space-charge effects, noise figure, field analysis of operation and transverse field operation are considered. A brief discussion of power output is given.

Two final chapters discuss briefly two closely related types of tube; the traveling-wave magnetron amplifier and the double-stream amplifier.

[1] loc. cit.

CHAPTER II

SIMPLE THEORY OF TRAVELING-WAVE TUBE GAIN

Synopsis of Chapter

IT IS difficult to describe general circuit or electronic features of traveling-wave tubes without some picture of a traveling-wave tube and traveling-wave gain. In this chapter a typical tube is described, and a simple theoretical treatment is carried far enough to describe traveling-wave gain in terms of an increasing electromagnetic and space-charge wave and to express the rate of increase in terms of electronic and circuit parameters.

In particular, Fig. 2.1 shows a typical traveling-wave tube. The parts of this (or of any other traveling-wave tube) which are discussed are the electron beam and the slow-wave circuit, represented in Fig. 2.2 by an electron beam and a helix.

In order to derive equations covering this portion of the tube, the properties of the helix are simulated by the simple delay line or network of Fig. 2.3, and ordinary network equations are applied. The electrons are assumed to flow very close to the line, so that all displacement current due to the presence of electrons flows directly into the line as an impressed current

For small signals a wave-type solution of the equations is known to exist, in which all a-c electronic and circuit quantities vary with time and distance as $\exp(j\omega t - \Gamma z)$. Thus, it is possible to assume this from the start.

On this basis the excitation of the circuit by a beam current of this form is evaluated (equation (2.10)). Conversely, the beam current due to a circuit voltage of this form is calculated (equation (2.22)). If these are to be consistent, the propagation constant Γ must satisfy a combined equation (2.23).

The equation for the propagation constant is of the fourth degree in Γ, so that any disturbance of the circuit and electron stream may be expressed as a sum of four waves.

Because some quantities are in practical cases small compared with others, it is possible to obtain good values of the roots by making an approximation. This reduces the equation to the third degree. The solutions are expressed in the form

$$-\Gamma = -j\beta_e + \beta_e C\delta$$

Here β_e is a phase constant corresponding to the electron velocity (2.16) and C is a gain parameter depending on circuit and beam impedance (2.43). A solution of the equation for the case of an electron speed equal to the speed of the undisturbed wave yields 3 values of δ which are shown in Fig. 2.4. These represent an increasing, a decreasing and an unattenuated wave. The increasing wave is of course responsible for the gain of the tube. A different approximation yields the missing backward unattenuated wave (2.32).

The characteristic impedance of the forward waves is expressed in terms of β_e, C, and δ (2.36) and is found to differ little from the impedance in the absence of electrons.

The gain of the increasing wave is expressed in terms of C and the length of the tube in wavelengths, N

$$G = 47.3\,CN \text{ db} \tag{2.37}$$

It will be shown later that the gain of the tube can be expressed approximately as the sum of the gain of the increasing wave plus a constant to take into account the setting up of the increasing wave, or the boundary conditions (2.39).

Finally, the important gain parameter C is discussed. The circuit part of this parameter is measured by the cube root of an impedance, $(E^2/\beta^2 P)^{1/3}$, which relates the peak field E acting on the electrons, the phase constant $\beta = \omega/v$, and the power flow. $(E^2/\beta^2 P)^{1/3}$ is a measure of circuit goodness as far as gain is concerned.

We should note also that a desirable circuit property is constancy of phase velocity with frequency, for the electron velocity must be near to the circuit phase velocity to produce gain.

Evaluation of the effects of attenuation, of varying the electron velocity and many other matters are treated in later chapters.

2.1 Description of a Traveling-Wave Tube

Figure 2.1 shows a typical traveling-wave tube such as may be used at frequencies around 4,000 megacycles. Such a tube may operate with a cathode current of around 10 ma and a beam voltage of around 1500 volts. There are two essential parts of a traveling-wave amplifier; one is the helix, which merely serves as a means for producing a slow electromagnetic wave with a longitudinal electric field; and the other is the electron flow. At the input the wave is transferred from a wave guide to the helix by means of a short antenna and similarly at the output the wave is transferred from the helix to a short antenna from which it is radiated into the output wave guide. The wave travels along the wire of the helix with approximately the speed of light. For operation at 1500 volts, corresponding to about $\frac{1}{13}$ the

speed of light, the wire in the helix will be about thirteen times as long as the axial length of the helix, giving a wave velocity of about $\frac{1}{13}$ the speed of light along the axis of the helix. A longitudinal magnetic focusing field of a few hundred gauss may be used to confine the electron beam and enable it to pass completely through the helix, which for 4000 megacycle operation may be around a foot long.

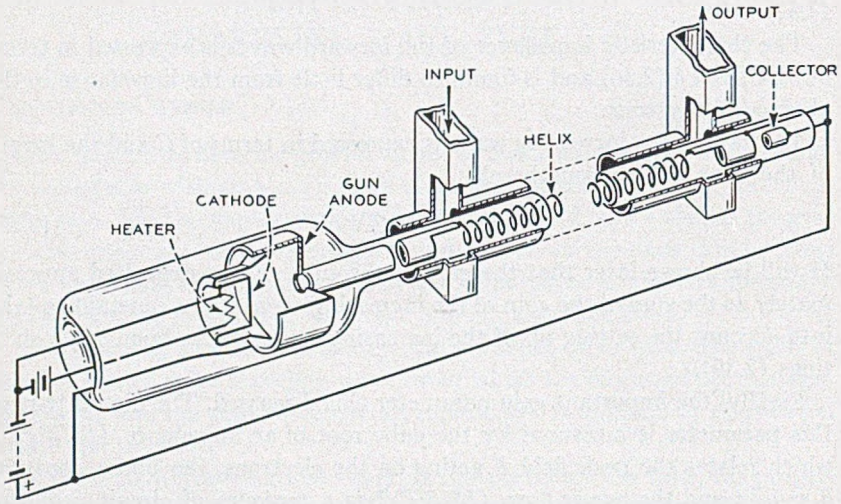

Fig. 2.1—Schematic of the traveling-wave amplifier.

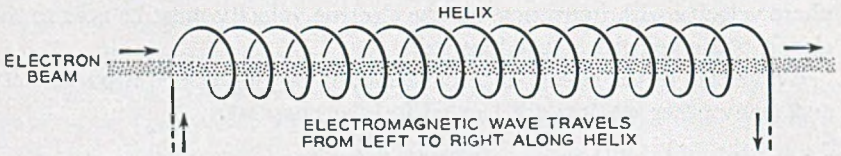

Fig. 2.2—Portion of the traveling-wave amplifier pertaining to electronic interaction with radio-frequency fields and radio-frequency gain.

In analyzing the operation of the traveling-wave tube, it is necessary to focus our attention merely on the two essential parts shown in Fig. 2.2, the circuit (helix) and the electron stream.

2.2 The Type of Analysis Used

A mathematical treatment of the traveling-wave tube is very important, not so much to give an exact numerical prediction of operation as to give a picture of the operation and to enable one to predict at least qualitatively the effect of various physical variations or features. It is unlikely that all of

the phenomena in a traveling-wave tube can be satisfactorily described in a theory which is simple enough to yield useful results. Most analyses, for instance, deal only with the small-signal or linear theory of the traveling-wave tube. The distribution of current in the electron beam can have an important influence on operation, and yet in an experimental tube it is often difficult to tell just what this distribution is. Even the more elaborate analyses of linear behavior assume a constant current density across the beam. Similarly, in most practical traveling-wave tubes, a certain fraction of the current is lost on the helix and yet this is not taken into account in the usual theories.

It has been suggested that an absolutely complete theory of the traveling-wave tube is almost out of the question. The attack which seems likely to yield the best numerical results is that of writing the appropriate partial differential equations for the disturbance in the electron stream inside the helix and outside of the helix. This attack has been used by Chu and Jackson[2] and by Rydbeck.[3] While it enables one to evaluate certain quantities which can only be estimated in a simpler theory, the general results do not differ qualitatively and are in fair quantitative agreement with those which are derived here by a simpler theory.

In the analysis chosen here, a number of approximations are made at the very beginning. This not only simplifies the mathematics but it cuts down the number of parameters involved and gives to these parameters a simple physical meaning. In terms of the parameters of this simple theory, a great many interesting problems concerning noise, attenuation and various boundary conditions can be worked out. With a more complicated theory, the working out of each of these problems would constitute essentially a new problem rather than a mere application of various formulae.

There are certain consequences of a more general treatment of a traveling-wave tube which are not apparent in the simple theory presented here. Some of these matters will be discussed in Chapters XII, XIII and XIV.

The theory presented here is a small signal theory. This means that the equations governing electron flow have been linearized by neglecting certain quantities which become negligible when the signals are small. This results in a wave-type solution. Besides the small signal limitation of the analyses presented here, the chief simplifying assumption which has been made is that all the electrons in the electron flow are acted on by the same a-c field, or at least by known fields. The electrons will be acted on by essentially the same field when the diameter of the electron beam is small enough or when

[2] L. J. Chu and J. D. Jackson, "Field Theory of Traveling-Wave Tubes," *Proc. I. R. E.*, Vol. 36, pp. 853–863, July 1948.

[3] Olof E. H. Rydbeck, "The Theory of the Traveling-Wave Tube," *Ericsson Technics*, No. 46, 1948.

the electrons form a hollow cylindrical beam in an axially symmetrical circuit, a case of some practical importance.

Besides these assumptions, it is assumed in this section that the electrons are displaced by the a-c field in the axial direction only. This may be approximately true in many cases and is essentially so when a strong magnetic focusing field is used. The effects of transverse motion will be discussed in Chapter XIII.

In this chapter an approximate relation suitable for electron speeds small compared to the velocity of light is used in computing interaction between electrons and the circuit.

A more general relation between impressed current and circuit field, valid for faster waves, will be given in Chapter VI. Non-relativistic equations of motion will, however, be used throughout the book. With whatever speed the waves travel, it will be assumed that the electron speed is always small compared with the speed of light.

We consider here the interaction between an electric circuit capable of propagating a slow electromagnetic wave and a stream of electrons. We can consider that the signal current in the circuit is the result of the disturbed electron stream acting on the circuit and we can consider that the disturbance on the electron stream is the result of the fields of the circuit acting on the electrons. Thus the problem naturally divides itself into two parts.

2.3 The Field Caused by an Impressed Current

We will first consider the problem of the disturbance produced in the circuit by a bunched electron stream. In considering this problem in this section in a manner valid for slow waves and small electron velocities, we will use the picture in Fig. 2.3. Here we have a circuit or network with uniformly

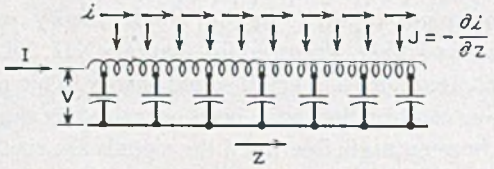

Fig. 2.3—Equivalent circuit of a traveling-wave tube. The distributed inductance and capacitance are chosen to match the phase velocity and field strength of the field acting on the electrons. The impressed current due to the electrons is $-\partial i/\partial z$, where i is the electron convection current.

distributed series inductance and shunt capacitance and with current I and voltage V. The circuit extends infinitely in the z direction. An electron convection current i flows along very close to the circuit. The sum of the displacement and convection current into any little volume of the electron beam must be zero. Because the convection current varies with distance in

the direction of flow, there will be a displacement current J amperes per meter impressed on the transmission circuit. We will assume that the electron beam is very narrow and very close to the circuit, so that the displacement current along the stream is negligible compared with that from the stream to the circuit. In this case the displacement current to the circuit will be given by the rate of change of the convection current with distance.

If the convection current i and the impressed current J are sinusoidal with time, the equations for the network shown in Fig. 2.3 are

$$\frac{\partial I}{\partial z} = -jBV + J \tag{2.1}$$

$$\frac{\partial V}{\partial z} = -jXI \tag{2.2}$$

Here I and V are the current and the voltage in the line, B and X are the shunt susceptance and series reactance per unit length and J is the impressed current per unit length.

It may be objected that these "network" equations are not valid for a transmission circuit operating at high frequencies. Certainly, the electric field in such a circuit cannot be described by a scalar electric potential. We can, however, choose BX so that the phase velocity of the circuit of Fig. 2.3 is the same as that for a particular traveling-wave tube. We can further choose X/B so that, for unit power flow, the longitudinal field acting on the electrons according to Fig. 2.3, that is, $-\partial V/\partial z$, is equal to the true field for a particular circuit. This lends a plausibility to the use of (2.1) and (2.2). The fact that results based on these equations are actually a good approximation for phase velocities small compared with the velocity of light is established in Chapter VI.

We will be interested in cases in which all quantities vary with distance as $\exp(-\Gamma z)$. Under these circumstances, we can replace differentiation with respect to z by multiplication by $-\Gamma$. The impressed current per unit length is given by

$$J = -\frac{\partial i}{\partial z} = \Gamma i \tag{2.3}$$

Equations (2.1) and (2.2) become

$$-\Gamma I = -jBV + \Gamma i \tag{2.4}$$

$$-\Gamma V = -jXI \tag{2.5}$$

If we eliminate I, we obtain

$$V(\Gamma^2 + BX) = -j\Gamma Xi \tag{2.6}$$

Now, if there were no impressed current, the righthand side of (2.6) would be zero and (2.6) would be the usual transmission-line equation. In this case, Γ assumes a value Γ_1, the natural propagation constant of the line, which is given by

$$\Gamma_1 = j\sqrt{BX} \tag{2.7}$$

The forward wave on the line varies with distance as $\exp(-\Gamma_1 z)$ and the backward wave as $\exp(+\Gamma_1 z)$.

Another important property of the line itself is the characteristic impedance K, which is given by

$$K = \sqrt{X/B} \tag{2.8}$$

We can express the series reactance X in terms of Γ_1 and K

$$X = -jK\Gamma_1 \tag{2.9}$$

Here the sign has been chosen to assure that X is positive with the sign given in (2.7). In terms of Γ_1 and K, (2.6) may be written

$$V = \frac{-\Gamma\Gamma_1 Ki}{(\Gamma^2 - \Gamma_1^2)} \tag{2.10}$$

In (2.10), the convection current i is assumed to vary sinusoidally with time and as $\exp(-\Gamma z)$ with distance. This current will produce the voltage V in the line. The voltage of the line given by (2.10) also varies sinusoidally with time and as $\exp(-\Gamma z)$ with distance.

2.4 Convection Current Produced by the Field

The other part of the problem is to find the disturbance produced on the electron stream by the fields of the line. In this analysis we will use the quantities listed below, all expressed in M.K.S. units.[4]

η—charge-to-mass ratio of electrons
$\eta = 1.759 \times 10^{11}$ coulomb/kg
u_0—average velocity of electrons
V_0—voltage by which electrons are accelerated to give them the velocity u_0. $u_0 = \sqrt{2\eta V_0}$
I_0—average electron convection current
ρ_0—average charge per unit length
$\rho_0 = -I_0/u_0$
v—a-c component of velocity
ρ—a-c component of linear charge density
i—a-c component of electron convection current

[4] Various physical constants are listed in Appendix I.

The quantities v, ρ, and i are assumed to vary with time and distance as $\exp(j\omega t - \Gamma z)$.

One equation we have concerning the motion of the electrons is that the time rate of change of velocity is equal to the charge-to-mass ratio times the electric gradient.

$$\frac{d(u_0 + v)}{dt} = \eta \frac{\partial V}{\partial z} \tag{2.11}$$

In (2.11) the derivative represents the change of velocity observed in following an individual electron. There is, of course, no change in the average velocity u_0. The change in the a-c component of velocity may be expressed in terms of partial derivatives, $\frac{\partial v}{\partial t}$, which is the rate of change with time of the velocity of electrons passing a given point, and $\frac{\partial v}{\partial z}$, which is variation of electron velocity with distance at a fixed time.

$$\frac{dv}{dt} = \frac{\partial v}{\partial t} + \frac{\partial v}{\partial z}\frac{dz}{dt} = \eta \frac{\partial V}{\partial z} \tag{2.12}$$

Equation (2.12) may be rewritten

$$\frac{\partial v}{\partial t} + \frac{\partial v}{\partial z}(u_0 + v) = \eta \frac{\partial V}{\partial z} \tag{2.13}$$

Now it will be assumed that the a-c velocity v is very small compared with the average velocity u_0, and v will be neglected in the parentheses. The reason for doing this is to obtain differential equations which are linear, that is, in which products of a-c terms do not appear. Such linear equations necessarily give a wave type of variation with time and distance, such as we have assumed. The justification for neglecting products of a-c terms is that we are interested in the behavior of traveling-wave tubes at small signal levels, and that it is very difficult to handle the non-linear equations. When we have linearized (2.13) we may replace the differentiation with a respect to time by multiplication by $j\omega$ and differentiation with respect to distance by multiplication by $-\Gamma$ and obtain

$$(j\omega - u_0\Gamma)v = -\eta\Gamma V \tag{2.14}$$

We can solve (2.14) for the a-c velocity and obtain

$$v = \frac{-\eta\Gamma V}{u_0(j\beta_e - \Gamma)} \tag{2.15}$$

Where

$$\beta_e = \omega/u_0 \tag{2.16}$$

We may think of β_e as the phase constant of a disturbance traveling with the electron velocity.

We have another equation to work with, a relation which is sometimes called the equation of continuity and sometimes the equation of conservation of charge. If the convection current changes with distance, charge must accumulate or decrease in any small elementary distance, and we see that in one dimension the relation obeyed must be

$$\frac{\partial i}{\partial z} = -\frac{\partial \rho}{\partial t} \tag{2.17}$$

Again we may proceed as before and solve for the a-c charge density ρ

$$-\Gamma i = -j\omega\rho$$

$$\rho = \frac{-j\Gamma i}{\omega} \tag{2.18}$$

The total convection current is the total velocity times the total charge density

$$-I_0 + i = (u_0 + v)(\rho_0 + \rho) \tag{2.19}$$

Again we will linearize this equation by neglecting products of a-c quantities in comparison with products of a-c quantities and a d-c quantity. This gives us

$$i = \rho_0 v + u_0 \rho \tag{2.20}$$

We can now substitute the value ρ obtained from (2.18) into (2.20) and solve for the convection current in terms of the velocity, obtaining

$$i = \frac{j\beta_e \rho_0 v}{(j\beta_e - \Gamma)} \tag{2.21}$$

Using (2.15) which gives the velocity in terms of the voltage, we obtain the convection current in terms of the voltage

$$i = \frac{jI_0\beta_e \Gamma V}{2V_0(j\beta_e - \Gamma)^2} \tag{2.22}$$

2.5 Overall Circuit and Electronic Equation

In (2.22) we have the convection current in terms of the voltage. In (2.10) we have the voltage in terms of the convection current. Any value of Γ for which both of these equations are satisfied represents a natural mode of

propagation along the circuit and the electron stream. When we combine (2.22) and (2.10) we obtain as the equation which Γ must satisfy:

$$1 = \frac{jKI_0\beta_e\Gamma^2\Gamma_1}{2V_0(\Gamma_1^2 - \Gamma^2)(j\beta_e - \Gamma)^2} \tag{2.23}$$

Equation (2.23) applies for any electron velocity, specified by β_e, and any wave velocity and attenuation, specified by the imaginary and real parts of the circuit propagation constant Γ_1. Equation (2.23) is of the fourth degree. This means that it will yield four values of Γ which represent four natural modes of propagation along the electron stream and the circuit. The circuit alone would have two modes of propagation, and this is consistent with the fact that the voltages at the two ends can be specified independently, and hence two boundary conditions must be satisfied. Four boundary conditions must be satisfied with the combination of circuit and electron stream. These may be taken as the voltages at the two ends of the helix and the a-c velocity and a-c convection current of the electron stream at the point where the electrons are injected. The four modes of propagation or the waves given by (2.23) enable us to satisfy these boundary conditions.

We are particularly interested in a wave in the direction of electron flow which has about the electron speed and which will account for the observed gain of the traveling-wave tube. Let us assume that the electron speed is made equal to the speed of the wave in the absence of electrons, so that

$$-\Gamma_1 = -j\beta_e \tag{2.24}$$

As we are looking for a wave with about the electron speed, we will assume that the propagation constant differs from β_e by a small amount ξ, so that

$$\begin{aligned} -\Gamma &= -j\beta_e + \xi \\ &= -\Gamma_1 + \xi \end{aligned} \tag{2.25}$$

Using (2.24) and (2.25) we will rewrite (2.23) as

$$1 = \frac{-KI_0\beta_e^2(-\beta_e^2 - 2j\beta_e\xi + \xi^2)}{2V_0(2j\beta_e\xi - \xi^2)(\xi^2)} \tag{2.26}$$

Now we will find that, for typical traveling-wave tubes, ξ is much smaller than β_e; hence we will neglect the terms involving $\beta_e\xi$ and ξ^2 in the numerator in comparison with β_e^2 and we will neglect the term ξ^2 in the denominator in comparison with the term involving $\beta_e\xi$. This gives us

$$\xi^3 = -j\beta_e^3\frac{KI_0}{4V_0} \tag{2.27}$$

While (2.27) may seem simple enough, it will later be found very convenient

to rewrite it in terms of other parameters, and we will introduce them now. Let

$$KI_0/4V_0 = C^3 \tag{2.28}$$

C is usually quite small and is typically often around .02. Instead of ξ we will use a quantity or a parameter δ

$$\xi = \beta_e C\delta \tag{2.29}$$

In terms of δ and C, (2.27) becomes

$$\delta = (-j)^{1/3} = (e^{j(2n-1/2)\pi})^{1/3} \tag{2.30}$$

This has three roots which will be called δ_1, δ_2 and δ_3, and these represent three forward waves. They are

$$\begin{aligned} \delta_1 &= e^{-j\pi/6} = \sqrt{3}/2 - j/2 \\ \delta_2 &= e^{-j5\pi/6} = -\sqrt{3}/2 - j/2 \\ \delta_3 &= e^{j\pi/2} = j \end{aligned} \tag{2.31}$$

Figure 2.4 shows the three values of δ. Equation (2.23) was of the fourth degree, and we see that a wave is missing. The missing root was eliminated

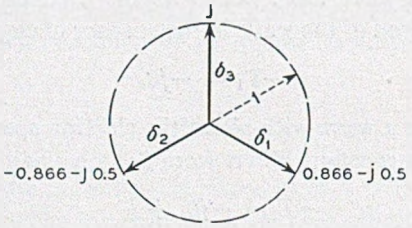

Fig. 2.4—There are three forward waves, with fields which vary with distance as $\exp(-j\beta_e + \beta_e C\delta)z$. The three values of δ for the case discussed, in which the circuit is lossless and the electrons move with the phase velocity of the unperturbed circuit wave, are shown in the figure.

by the approximations made above, which are valid for forward waves only. The other wave is a backward wave and its propagation constant is found to be

$$-\Gamma = j\beta_e \left(1 - \frac{C^3}{4}\right) \tag{2.32}$$

As C is a small quantity, C^3 is even smaller, and indeed the backward wave given by (2.32) is practically the same as the backward wave in the absence of electrons. This is to be expected. In the forward direction, there is a cumulative interaction between wave and the electrons because both are moving

at about the same speed. In the backward direction there is no cumulative action, because the wave and the electrons are moving in the opposite directions.

The variation in the z direction for three forward waves is as

$$\exp -\Gamma z = \exp -j\beta_e z \exp \delta C\beta_e z \tag{2.33}$$

We see that the first wave is an increasing wave which travels a little more slowly than the electrons. The second wave is a decreasing wave which travels a little more slowly than the electrons. The third wave is an unattenuated wave which travels faster than the electrons. It can be shown generally that when a stream of electrons interacts with a wave, the electrons must go faster than the wave in order to give energy to it.

It is interesting to know the ratio of line voltage to line current, or the characteristic impedance, for the three forward waves. This may be obtained from (2.5). We see that the characteristic impedance K_n for the nth wave is given in terms for the propagation constant for the nth wave, Γ_n, by

$$K_n = V/I = jX/\Gamma_n \tag{2.34}$$

In terms of δ_n this becomes

$$K_n = K(1 - \beta_e C\delta_n/\Gamma_1) \tag{2.35}$$

$$K_n = K(1 - jC\delta_n) \tag{2.36}$$

We see that the characteristic impedance for the forward waves differs from the characteristic impedance in the absence of electrons by a small amount proportional to C, and that the characteristic impedance has a small reactive component.

We are particularly interested in the rate at which the increasing wave increases. In a number of wave lengths N, the total increase in db is given by

$$\begin{aligned} &20 \log_{10} \exp [(\sqrt{3}/2)(C)(2\pi N)] \text{ db} \\ &= 47.3\, CN \text{ db} \end{aligned} \tag{2.37}$$

We will see later that the overall gain of the traveling-wave tube with a uniform helix can be expressed in the form

$$G = A + BCN \text{ db} \tag{2.38}$$

Here A is a loss relating voltage associated with the increasing wave to the total applied voltage. This loss may be evaluated and will be evaluated later by a proper examination of the boundary conditions at the input of the tube. It turns out that for the case we have considered

$$G = -9.54 + 47.3\, CN \text{ db} \tag{2.39}$$

In considering circuits for traveling-wave tubes, and in reformulating the theory in more general terms later on, it is valuable to express C in terms of parameters other than the characteristic impedance. Two physically significant parameters are the power flow in the circuit and the electric field associated with it which acts on the electron stream. The ratio of the square of the electric field to the power can be evaluated by physical measurement even when it cannot be calculated. For instance, Cutler[5] did this by allowing the power from a wave guide to flow into a terminated helix, so that the power in the helix was the same as the power in the wave guide. He then compared the field in the helix with the field in the wave guide by probe measurements. The field strength in the wave guide could be calculated in terms of the power flow, and hence Cutler's measurements enabled him to evaluate the field in the helix for a given power flow.

The magnitude of the field is given in terms of the magnitude of the voltage by

$$E = |\Gamma V| \tag{2.40}$$

Here E is taken as the magnitude of the field. The power flow in the circuit is given in terms of the circuit voltage by

$$P = |V|^2/2K \tag{2.41}$$

A quantity which we will use as a circuit parameter is

$$E^2/\beta^2 P = 2K \tag{2.42}$$

Here it has been assumed that we are concerned with low-loss circuits, so that Γ_1^2 can be replaced by the phase constant β^2. Usually, β can be taken as equal to β_e, the electron phase constant, with small error, and in the preceding work this has been assumed to be exactly true in (2.23).

In terms of this new quantity, C is given by

$$C^3 = (2K)(I_0/8V_0) = (E^2/\beta^2 P)(I_0/8V_0) \tag{2.43}$$

If we call V_0/I_0 the beam impedance, C^3 is $\frac{1}{4}$ the circuit impedance divided by the beam impedance. It would have been more sensible to use $E^2/2\beta^2 P$ instead of $E^2/\beta^2 P$. Unfortunately the writer feels stuck with his benighted first choice because of the number of curves and published equations which make use of it.

Besides the circuit impedance, another important circuit parameter is the phase velocity. As the electron velocity is made to deviate from the phase velocity of the circuit, the gain falls off. An analysis to be given later

[5] C. C. Cutler, "Experimental Determination of Helical-Wave Properties," *Proc. IRE*, Vol. 36, pp. 230–233, February 1948.

discloses that the allowable range of velocity Δv is of the order of

$$\Delta v \approx \pm C u_0 \tag{2.44}$$

Thus, the allowable difference between the phase velocity of the circuit and the velocity of the electrons increases as circuit impedance and beam current are increased and decreases as voltage is increased.

We have illustrated the general method of attack to be used and have introduced some of the important parameters concerned with the circuit and with the overall behavior of the tube. In later chapters, the properties of various circuits suitable for traveling-wave tubes will be discussed in terms of impedance and phase velocity and various cases of interest will be worked out by the methods presented.

CHAPTER III

THE HELIX

Synopsis of Chapter

ANY circuit capable of propagating a slow electromagnetic wave can be used in a traveling-wave tube. The circuit most often used is the helix. The helix is easy to construct. In addition, it is a very good circuit. It has a high impedance and a phase velocity that is almost constant over a wide frequency range.

In this chapter various properties of helices are discussed. An approximate expression for helix properties can be obtained by calculating the properties, not of a helix, but of a helically conducting cylindrical sheet of the same radius and pitch as the helix. An analysis of such a sheet is carried out in Appendix II and the results are discussed in the text.

Parameters which enter into the expressions are the free-space phase constant $\beta_0 = \omega/c$, the axial phase constant $\beta = \omega/v$, where v is the phase velocity of the wave, and the radial phase constant γ. The arguments of various Bessel functions are, for instance, γr and γa, where r is the radial coordinate and a is radius of the helix. The parameters β_0, β and γ are related by

$$\beta^2 = \beta_0^2 + \gamma^2$$

For tightly wound helices in which the phase velocity v is small compared with the velocity of light, γ is very nearly equal to β. For instance, at a velocity corresponding to that of 1,000 volt electrons, γ and β differ by only 0.4%.

Figure 3.1 illustrates two parameters of the helically conducting sheet, the radius a and pitch angle ψ. For an actual helix, a will be taken to mean the mean radius, the radius to the center of the wire.

Figure 3.2 shows a single curve which enables one to obtain γ, and hence β, for any value of the parameter

$$\beta_0 a \cot \psi = \frac{\omega a \cot \psi}{c}.$$

This parameter is proportional to frequency. The curve is an approximate representation of velocity vs. frequency. At high frequencies γ approaches

$\beta_0 \cot \psi$ and β thus approaches $\beta_0/\sin \psi$; this means that the wave travels with the velocity of light around the sheet in the direction of conduction. In the case of an actual helix, the wave travels along the wire with the velocity of light.

The gain parameter C is given by

$$C = (I_0/8V_0)^{1/3}(E^2/\beta^2 P)^{1/3}$$

Values of $(E^2/\beta^2 P)^{1/3}$ on the axis may be obtained through the use of Fig. 3.4, where an impedance parameter $F(\gamma a)$ is plotted vs. γa, and by use of (3.9). For a given helix, $(E^2/\beta^2 P)^{1/3}$ is approximately proportional to $F(\gamma a)$. $F(\gamma a)$ falls as frequency increases. This is partly because at high frequencies and short wavelengths, for which the sign of the field alternates rapidly with distance, the field is strong near the helix but falls off rapidly away from the helix and so the field is weak near the axis. At very high frequencies the field falls off away from the helix approximately as $\exp(-\gamma \Delta r)$, where Δr is distance from the helix, and we remember that γ is very nearly proportional to frequency. $(E^2/\beta^2 P)^{1/3}$ measured at the helix also falls with increasing frequency.

In many cases, a hollow beam of radius r (the dashed lines of Fig. 3.5 refer to such a beam) or a solid beam of radius r (the solid lines of Fig. 3.5 refer to such a beam) is used. For a hollow beam we should evaluate E^2 in $(E^2/\beta^2 P)^{1/3}$ at the beam radius, and for a solid beam we should use the mean square value of E averaged over the beam.

The ordinate in Fig. 3.5 is a factor by which $(E^2/\beta^2 P)^{1/3}$ as obtained from Fig. 3.4 and (3.9) should be multiplied to give $(E^2/\beta^2 P)^{1/3}$ for a hollow or solid beam.

The gain of the increasing wave is proportional to $F(\gamma a)$ times a factor from Fig. 3.5, and times the length of the tube in wavelengths, N. N is very nearly proportional to frequency. Also γ, and hence γa, are nearly proportional to frequency. Thus, $F(\gamma a)$ from Fig. 3.4 times the appropriate factor from Fig. 3.5 times γa gives approximately the gain vs. frequency, (if we assume that the electron speed matches the phase velocity over the frequency range). This product is plotted in Fig. 3.6. We see that for a given helix size the maximum gain occurs at a higher frequency and the bandwidth is broader as r/a, the ratio of the beam radius to the helix radius, is made larger.

It is usually desirable, especially at very short wavelengths, to make the helix as large as possible. If we wish to design the tube so that gain is a maximum at the operating frequency, we will choose a so that the appropriate curve of Fig. 3.6 has its maximum at the value of γa corresponding to the operating frequency. We see that this value of a will be larger the larger is r/a. In an actual helix, the maximum possible value of r/a is less than unity,

since the inside diameter of the helix is less than a by the radius of the wire. Further, focusing difficulties preclude attaining a beam radius equal even to the inside radius of the helix.

Experience indicates that at very short wavelengths (around 6 millimeters, say) it is extremely important to have a well-focused electron beam with as large a value of r/a as is attainable.

A characteristic impedance K_t may be defined in terms of a "transverse" voltage V_t, obtained by integrating the peak radial field from a to ∞, and from the power flow. In Fig. 3.7, $(v/c)\ K_t$ is plotted vs. γa. A "longitudinal" characteristic impedance $K\ell$ is related to K_t (3.13). For slow waves $K\ell$ is nearly equal to K_t. The impedance parameter $E^2/\beta^2 P$ evaluated at the surface of the cylinder is twice $K\ell$. We see that $K\ell$ falls with increasing frequency.

A simplified approach in analysis of the helically conducting sheet is that of "developing" the sheet; that is, slitting it normal to the direction of conduction and flattening it out as in Fig. 3.8. The field equations for such a flattened sheet are then solved. For large values of γa the field is concentrated near the helically conducting sheet, and the fields near the developed sheet are similar to the fields near the cylindrical sheet. Thus the dashed line in Fig. 3.7 is for the developed sheet and the solid line is for a cylindrical sheet.

For the developed sheet, the wave always propagates with the speed of light in the direction of conduction. In a plane normal to the direction of conduction, the field may be specified by a potential satisfying Laplace's equation, as in the case, for instance, of a two-wire or coaxial line. Thus, the fields can be obtained by the solution of an electrostatic problem.

One can develop not only a helically conducting sheet, but an actual helix, giving a series of straight wires, shown in cross-section in Fig. 3.9. In Case I, corresponding to approximately two turns per wavelength, successive wires are $-$, $+$, $-$, $+$ etc.; in case II, corresponding to approximately four turns per wavelength, successive wires are $+$, 0, $-$, 0, $+$, 0 etc.

Figures 3.10 and 3.11 illustrate voltages along a developed sheet and a developed helix.

Figure 3.13 shows the ratio, $R^{1/3}$, of $(E^2/\beta^2 P)^{1/3}$ on the axis to that for a developed helically conducting sheet, plotted vs. d/p. We see that, for a large wire diameter d, $(E^2/\beta^2 P)^{1/3}$ may be larger on the axis than for a helically conducting sheet with the same mean radius and hence the same pitch angle and phase velocity. This is merely because the thick wires extend nearer to the axis than does the sheet. The actual helix is really inferior to the sheet.

We see this by noting that the highest value of $(E^2/\beta^2 P)^{1/3}$ for a helically conducting sheet is that at the sheet $(r = a)$. With a finite wire size, the

largest value r can have is the mean helix radius a minus the wire radius. In Fig. 3.14, the ratio of $(E^2/\beta^2P)^{1/3}$ for this largest allowable radius to $(E^2/\beta^2P)^{1/3}$ at the surface of the developed sheet is plotted vs. d/p. We see that, in terms of maximum available field, $(E^2/\beta^2P)^{1/3}$ is no more than 0.83 as high as for the sheet for four turns per wavelength and 0.67 as high as for the sheet for two turns per wavelength. We further see that there is an optimum ratio of wire diameter to pitch; about 0.175 for four turns per wavelength and about 0.125 for two turns per wavelength. Because the maxima are so broad, it is probably better in practice to use larger wire, and in most tubes which have been built, d/p has been around 0.5.

In designing tubes it is perhaps best to do so in terms of field on the axis (Fig. 3.13), the allowable value of r/a and the curves of Fig. 3.6.

Figure 3.15 compares the impedance of the developed helix with that of the developed sheet as given by the straight line of Fig. 3.7.

There are factors other than wire size which can cause the value of E^2/β^2P for an actual helix to be less than the value for the helically conducting sheet. An important cause of impedance reduction is the influence of dielectric supporting members. Even small ceramic or glass supporting rods can cause some reduction in helix impedance. In some tubes the helix is supported inside a glass tube, and this can cause a considerable reduction in helix impedance.

When a field analysis seems too involved, it may be possible to obtain some information by considering the behavior of transmission lines having parameters adjusted to make the phase constant and the characteristic impedance equal to those of the helix. For instance, suppose that the presence of dielectric material results in an actual phase constant β_d as opposed to a computed phase constant β. Equation (3.64) gives an estimate of the consequent reduction of $(E^2/\beta^2P)^{1/3}$ on the axis.

This method is of use in studying the behavior of coupled helices. For instance, concentric helices may be useful in producing radial fields in tubes in which transverse fields predominate in the region of electron flow (see Chapter XIII). A concentric helix structure might be investigated by means of a field analysis, but some interesting properties can be deduced more simply by considering two transmission lines with uniformly distributed self and mutual capacitances and inductances, or susceptance and reactances. The modes of propagation on such lines are affected by coupling in a manner similar to that in which the modes of two resonant circuits are affected by coupling.

If two lines are coupled, their two independent modes of propagation are mixed up to form two modes of propagation in which both lines participate. If the original phase velocities differ greatly, or if the coupling between the lines is weak, the fields and velocity of one of these modes will be almost

like the original fields and velocity of one line, and the fields and velocity of the other mode will be almost like the original fields and velocity of the other line. However, if the coupling is strong enough compared with the original separation of phase velocities, both lines will participate almost equally in each mode. One mode will be a "longitudinal mode" for which the excitations on the two lines are substantially equal, and the other mode will be a "transverse" mode for which the excitations are substantially equal and opposite.

The ratios of the voltages on the lines for the two modes are given by (3.75). Here it is assumed that the series reactances X and shunt susceptances B of the lines are almost equal, differing only enough to make a difference $\Delta\Gamma_0$ in the propagation constants. B_{12} and X_{12} are the mutual susceptance and reactance. We see that to make the voltages on the two lines nearly equal or equal and opposite, B_{12} and X_{12} should have the same sign, so that capacitive and inductive couplings add.

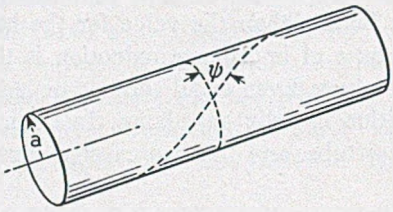

Fig. 3.1—A helically conducting sheet of radius a. The sheet is conducting along helical paths making an angle ψ with a plane normal to the axis.

Increasing the coupling increases the velocity separation between the two modes, and this is desirable. When there is a substantial difference in velocity, operation in the desired mode can be secured by making the electron velocity equal to the phase velocity of the desired mode.

To make the capacitive and inductive couplings add in the case of concentric helices (Fig. 3.17), the helices should be wound in opposite directions.

3.1 The Helically Conducting Sheet

In computing the properties of a helix, the actual helix is usually replaced by a helically conducting cylindrical sheet of the same mean radius. Such a sheet is illustrated in Fig. 3.1. This sheet is perfectly conducting in a helical direction making an angle ψ, the pitch angle, with a plane normal to the axis (the direction of propagation), and is non-conducting in a helical direction normal to this ψ direction, the direction of conduction. Appropriate solutions of Maxwell's equations are chosen inside and outside of the cylindrical sheet. At the sheet, the components of the electric field in the ψ direction are made zero, and those normal to the ψ direction are made equal inside and outside. Since there can be no current in the sheet normal to the ψ direction, the

components of magnetic field in the ψ direction must be the same inside and outside of the sheet. When these boundary conditions are imposed, one can solve for the propagation constant and $E^2/\beta^2 P$ can then be obtained by integrating the Poynting vector.

The helically conducting sheet is treated mathematically in Appendix II. The results of this analysis will be presented here.

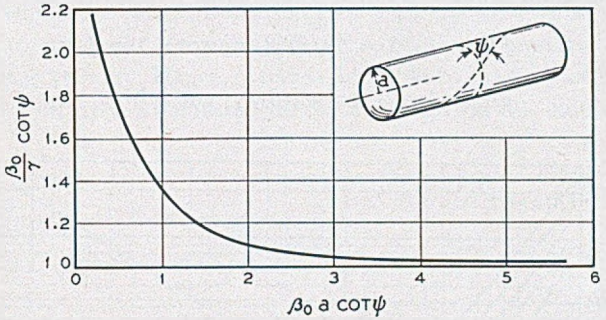

Fig. 3.2—The radial propagation constant is $\gamma^2 = (\beta^2 - \beta_0^2)^{1/2}$. Here (β_0/γ) cot ψ is plotted vs $\beta_0 a$ cot ψ, a quantity proportional to frequency. For slow waves the ordinate is roughly the ratio of the wave velocity to the velocity the wave would have if it traveled along the helically conducting sheet with the speed of light in the direction of conduction.

3.1a *The Phase Velocity*

The results for the helically conducting sheet are expressed in terms of three phase or propagation constants. These are

$$\beta_0 = \omega/c, \qquad \beta = \omega/v \tag{3.1}$$

$$\gamma = \sqrt{\beta^2 - \beta_0^2} \tag{3.2}$$

$$\gamma = \beta\sqrt{1 - (v/c)^2} \tag{3.3}$$

Here c is the velocity of light and v is the phase velocity of the wave. β_0 is the phase constant of a wave traveling with the speed of light, which would vary with distance in the z direction as $\exp(-j\beta_0 z)$. The actual axial phase constant is β, and the fields vary with distance as $\exp(-j\beta z)$.

γ is the radial propagation constant. Various field components vary as modified Bessel functions of argument γr, where r is the radius. Particularly, the longitudinal electric field, which interacts with the electrons, varies as $I_0(\gamma r)$.

For the phase velocities usually used, γ is very nearly equal to β, as may be seen from the following table of accelerating voltages V_0 (to give an electron the velocity v), v/c and γ/β.

V	v/c	γ/β
100	.0198	1.000
1,000	.0625	.998
10,000	.1980	.980

Figure 3.2 gives information concerning the phase velocity of the wave in the form of a plot of $(\beta_0/\gamma)\cot\psi$ as a function of $\beta_0 a \cot\psi$.

The ratio of the phase velocity v to the velocity of light c may be expressed

$$v/c = \beta_0/\beta = (\gamma/\beta)(\beta_0/\gamma)\cot\psi\tan\psi \tag{3.4}$$

$$v/c = (\gamma/\beta)\tan\psi\,[(\beta_0/\gamma)\cot\psi\,]$$

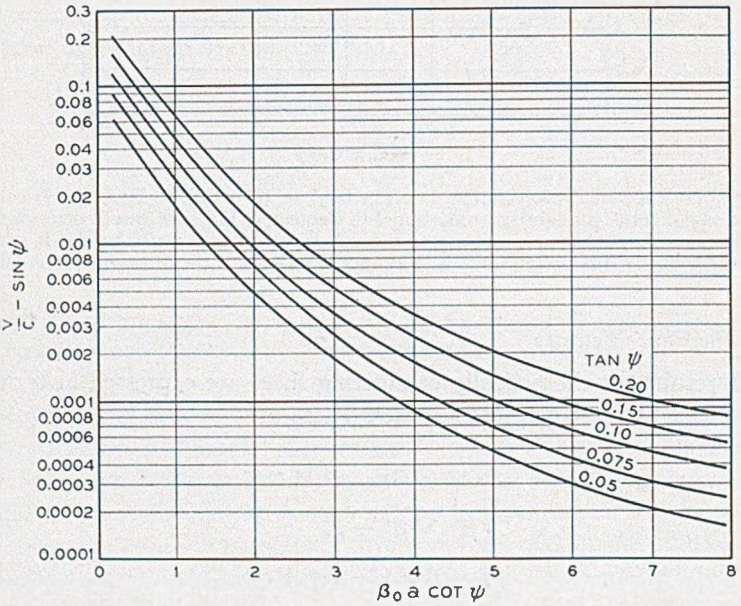

Fig. 3.3—From these curves one can obtain v/c, the ratio of the phase velocity of the wave to the velocity of light, for various values of tan ψ and $\beta_0 a$ cot ψ.

From Fig. 3.2 we see that, for large values of $\beta_0 a \cot\psi$, $(\beta_0/\gamma)\cot\psi$ approaches unity. For slow waves γ/β approaches unity. Under these circumstances, very nearly

$$v/c = \tan\psi \tag{3.5}$$

If the wave traveled in the direction of conduction with the speed of light we would have

$$v/c = \sin\psi$$

This is essentially the same as (3.5) for small pitch angles ψ. Thus, for large values of the abscissa in Fig. 3.2, the phase velocity is just about that corresponding to propagation along the sheet in the direction of conduction with the speed of light and hence in the axial direction at a much reduced speed. For helices of smaller radius compared with the wavelength, the speed is greater.

The bandwidth of a traveling-wave tube is in part determined by the range over which the electrons keep in step with the wave. The abscissa of Fig. 3.2 is proportional to frequency, but the ordinate is not strictly proportional to phase velocity. Hence, it seems desirable to have a plot which does show velocity directly. To obtain this we can assign various values to cot ψ.

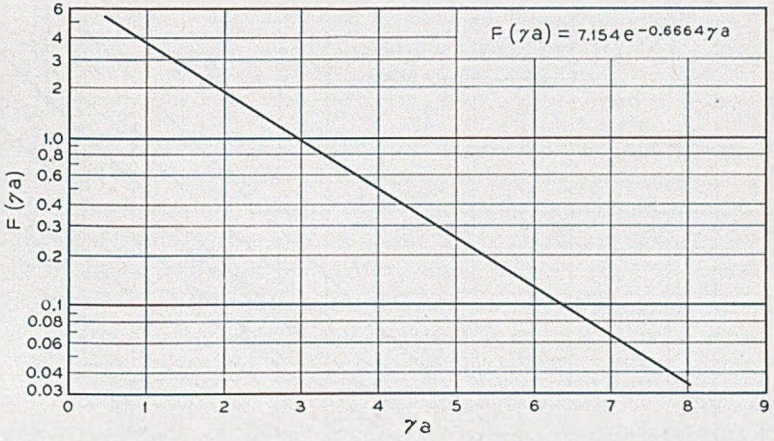

Fig. 3.4—A curve giving the impedance function $F(\gamma a)$ vs. γa. On the axis, $(E^2/\beta^2 P)^{1/3} = (\beta/\beta_0)^{1/3}(\gamma/\beta)^{4/3}F(\gamma a)$.

The ordinate (β_0/γ) cot ψ then gives us γ/β_0 and from (3.2) we see that

$$v/c = \beta_0/\beta = (1 + (\gamma/\beta_0)^2)^{-1/2} \tag{3.6}$$

We have seen that, for large values of $\beta_0 a$ cot ψ, (β_0/γ) cot ψ approaches unity, and v/c approaches a value

$$v/c = (1 + \cot^2 \psi)^{-1/2} = \sin \psi \tag{3.7}$$

To emphasize the change in velocity with frequency it seems best to plot the difference between the actual velocity ratio and this asymptotic velocity ratio on a semi-log scale. Accordingly, Fig. 3.3 shows $(v/c) - \sin \psi$ vs. $\beta_0 a$ cot γ for tan ψ = .05, .075, .1, .15, .2.

For large values of the abscissa the velocities are those corresponding to

about 640 volts ($\tan\psi = .05$), 1,400 volts (.075), 2,500 volts (.1), 5,600 volts (.15), 9,800 volts (.2).

3.1b *The Impedance Parameter* (E^2/β^2P)

Figure 3.4 shows a plot of a quantity $F(\gamma a)$ vs. γa. This quantity is computed from a very complicated expression (Appendix II), but it is accurately given over the range shown by the empirical relation

$$F(\gamma a) = 7.154\, e^{-.6664\gamma a} \tag{3.8}$$

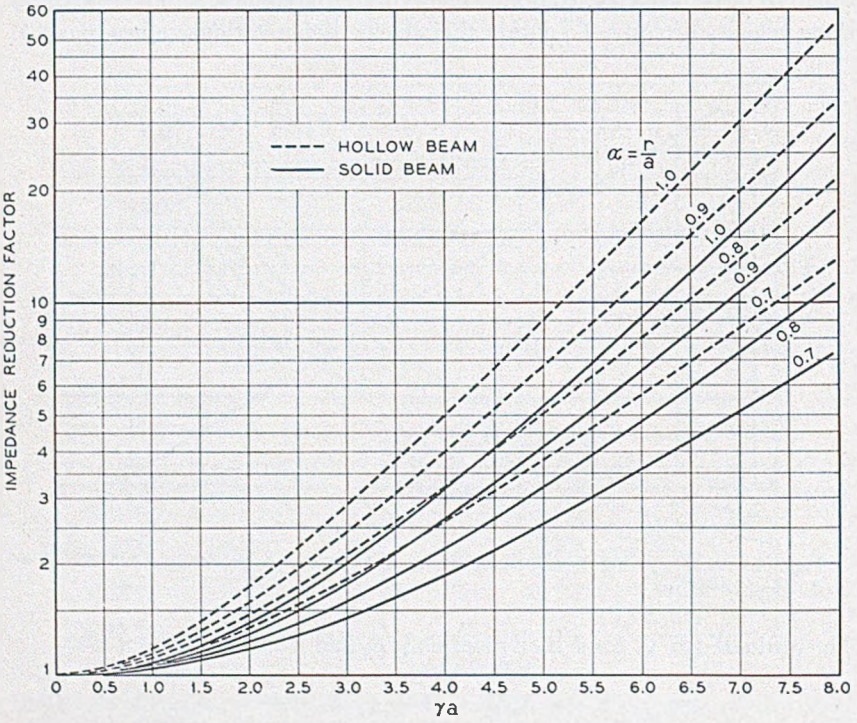

Fig. 3.5—Factors by which $(E^2\beta/^2P)^{1/3}$ on the axis should be multiplied to give the correct value for hollow and solid beams of radius r.

For the field on the axis of the helix,

$$(E^2/\beta^2P)^{1/3} = (\beta/\beta_0)^{1/3}(\gamma/\beta)^{4/3}F(\gamma a) \tag{3.9}$$

We should remember that $\beta/\beta_0 = c/v$ and that γ/β is nearly unity for velocities small compared with the velocity of light.

In the expression for the gain parameter C, the square of the field E is multiplied by the current I_0 (2.28). If we were to assume that two electron

streams of different currents, I_1 and I_2, were coupled to the circuit through transformers, so as to be acted on by fields E_1 and E_2, but that the streams did not interact directly with one another, we would find the effective value of C^3 to be given by

$$C^3 = (E_1^2/\beta^2 P)(I_1/8V_0) + (E_2^2/\beta^2 P)(I_2/8V_0)$$

Thus, if we neglect the direct interaction of electron streams through fields due to local space charge, we can obtain an effective value of C^3 by integrating $E^2 dI_0$ over the beam. If we assume a constant current density, we can merely use the mean square value of E over the area occupied by electron flow.

The axial component of electric field at a distance r from the axis is $I_0(\gamma r)$ times the field on the axis. Hence, if we used a tubular beam of radius r, we should multiply $(E^2/\beta^2 P)^{1/3}$ as obtained from Fig. 3.4 by $[I_0(\gamma r)]^{2/3}$. The quantity $[I_0(\gamma r)]^{2/3}$ is plotted vs. γa for several values of r/a as the dashed lines in Fig. 3.5.

Suppose the current density is uniform out to a radius r and zero beyond this radius. The average value of E^2 is greater than the value on the axis by a factor $[I_0^2(\gamma r) - I_1^2(\gamma r)]$ and $(E^2/\beta^2 P)^{1/3}$ from Fig. 3.4 should in this case be multiplied by this factor to the $\frac{1}{3}$ power. The appropriate factor is plotted vs. γa as the solid lines of Fig. 3.5.

We note from (2.39) that the gain contains a term proportional to CN, where N is the number of wavelengths. For slow waves and usual values of γa, very nearly, N will be proportional to the frequency and hence to γ, while C is proportional to $(E^2/\beta^2 P)^{1/3}$. We can obtain $(E^2/\beta^2 P)^{1/3}$ from Figs. 3.4 and 3.5. The gain of the increasing wave as a function of frequency will thus be very nearly proportional to this value of $(E^2/\beta^2 P)^{1/3}$ times γ, or, times γa if we prefer.

In Fig. 3.6, $\gamma a F(\gamma a)$ is plotted vs. γa for hollow beams of radius r for various values of r/a (dashed lines) and for uniform density beams of radius r for various values of r/a (solid lines). If we assume that the electron speed is adjusted to equal the phase velocity of the wave, we can take the ordinate as proportional to gain and the abscissa as proportional to frequency.

We see that the larger is r/a, the larger is the value of γa for maximum gain. For one typical 7.5 cm wavelength traveling-wave tube, γa was about 2.8. For this tube, the ratio of the inside radius of the helix to the mean radius of the helix was 0.87. We see from Fig. 3.6 that, if a solid beam just filled this helix, the maximum gain should occur at about the operating wavelength. As a matter of fact, the beam was somewhat smaller than the inside diameter of the helix, and there was an observed increase of gain with an increase in wavelength (a higher gain at a lower frequency). In a particular

tube for 0.625 cm wavelength, it was felt desirable to use a relatively large helix diameter. Accordingly, a value of γa of 6.7 was chosen. We see that, unless r/a is 0.9 or larger, this must result in an appreciable increase in gain at some frequency lower than operating frequency. It was only by use of great care in focusing the beam that gain was attained at 0.625 cm wavelength, and there was a tendency toward oscillation, presumably at longer wavelengths. This discussion of course neglects the effect of transmission

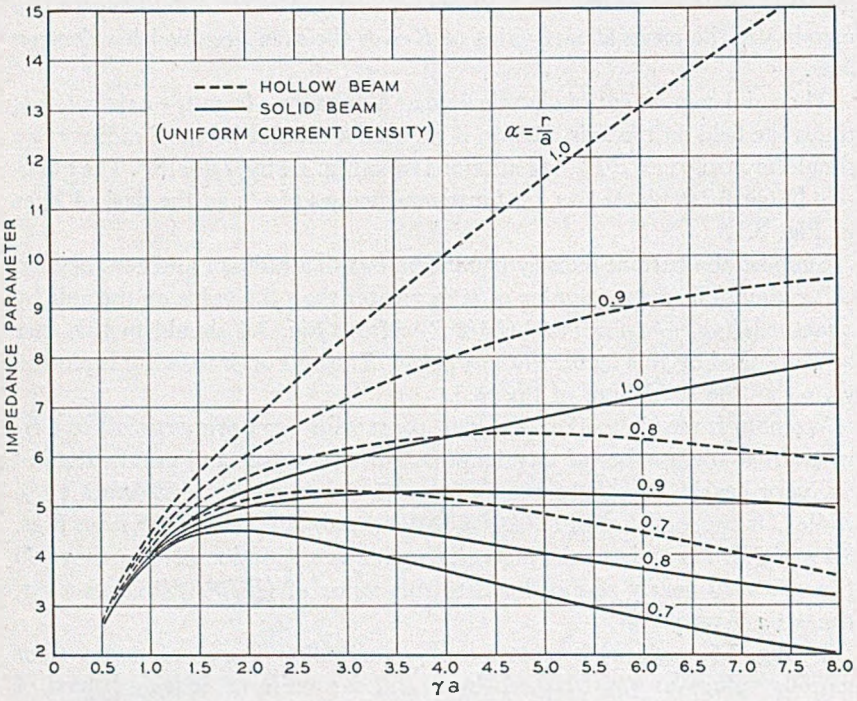

Fig. 3.6—The ordinate is $\gamma aF(\gamma a)$ times the parameters from Fig. 3.5. For a fixed current and voltage it is nearly proportional to gain per unit length, and hence the curves give roughly the variation of gain with frequency.

loss or gain. Usually the loss decreases when the frequency is decreased, and this favors oscillation at low frequencies.

3.1c *Impedance of the Helix*

No impedance which can be assigned to the helically conducting sheet can give full information for matching a helix to a waveguide or transmission line. As in the case of transducers between a coaxial line and a waveguide or between waveguides of different cross-section, the impedance is important,

but discontinuity effects are also important. However, a suitably defined helix impedance is of some interest.

Figure 3.7 presents the impedance as defined on a voltage-power basis. The peak "transverse" voltage V_t is obtained by integrating the radial electric field from the radius a of the helically conducting sheet to ∞. The "transverse" characteristic impedance K_t is defined by the relation

$$P = (\tfrac{1}{2})(V_t^2/K_t)$$

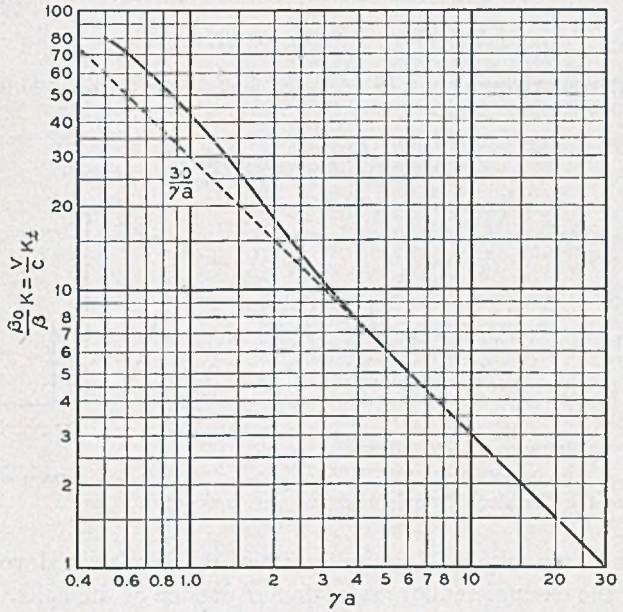

Fig. 3.7—Curves giving the variation of transverse impedance, K_t, with γa.

The impedance is found to be given by

$$\left(\frac{\beta}{\gamma}\right)^2\left(\frac{\beta_0}{\beta}\right)K_t = \frac{120I_0^2}{(\gamma a)^2}\left[\left(1+\frac{I_0K_1}{I_1K_0}\right)(I_1^2 - I_0I_2) + \left(\frac{I_0}{K_0}\right)^2\left(1+\frac{I_1K_0}{I_0K_1}\right)(K_0K_2 - K_1^2)\right]^{-1} \tag{3.10}$$

The I's and K's are modified Bessel functions of argument γa.

The dashed line on Fig. 3.7 is a plot of $30/\gamma a$ vs. γa. It may be seen that, for large values of γa, very nearly

$$K_t = (\beta/\beta_0)(\gamma/\beta)^2(30/\gamma a) \tag{3.11}$$

and in the whole range shown the impedance differs from this value by a factor less than 1.5.

We might have defined a "longitudinal" voltage V_ℓ as half of the integral of the longitudinal component of electric field at the surface of the helically conducting sheet for a half wavelength (between successive points of zero field). We find that

$$V_\ell = \sqrt{1 - (v/c)^2}\, V_t = (\gamma/\beta) V_t \tag{3.12}$$

and, accordingly, the "longitudinal impedance" K_ℓ will be

$$K_\ell = [1 - (v/c)^2] K_t = (\gamma/\beta)^2 K_t \tag{3.13}$$

Our impedance parameter, $E^2/\beta^2 P$, is just twice this "longitudinal impedance."

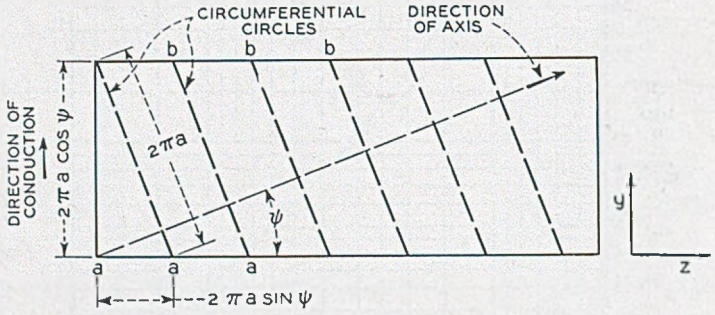

Fig. 3.8—A "developed" helically conducting sheet. The sheet has been slit along a line normal to the direction of conduction and flattened out.

The transverse voltage V_t is greater than the longitudinal voltage V_ℓ because of the circumferential magnetic flux outside of the helix. For slow waves V_ℓ is nearly equal to V_t and the fields are nearly curl-free solutions of Laplace's equation. In this case the circumferential magnetic flux is small compared with the longitudinal flux inside of the helix.

For the circuit of Fig. 2.3 the transverse and longitudinal voltages are equal, and it is interesting to note that this is approximately true for slow waves on a helix. For very fast waves, the longitudinal voltage becomes small compared with the transverse voltage.

For a typical 4,000-megacycle tube, for which $\gamma a = 2.8$, Fig. 5 indicates a value of K_t of about 150 ohms.

3.2 The Developed Helix

For large helices, i.e., for large values of γa, the fields fall off very rapidly away from the wire. Under these circumstances we can obtain quite accurate results by slitting the helically conducting sheet along a spiral line normal

to the direction of conduction and flattening it out. This gives us the plane conducting sheet shown in Fig. 3.8. The indicated coordinates are z to the right and y upward: x is positive into the paper. The fields about the developed sheet approximate those about the helically conducting sheet for distances always small compared with the original radius of curvature.

The straight dashed line shown on the helix impedance curve of Fig. 3.7 can be obtained as a solution for the "developed helix." We see that it is within 10% of the true curve for values of γa greater than 2.8. We might note that a 10% error in impedance means only a $3\frac{1}{3}$% error in the gain parameter C.

In solving for the fields around the sheet, the developed surface can be extended indefinitely in the plus and minus y directions. In order that the fields may match when the sheet is rolled up, they must be the same at $y = 0, z = 2\pi a \sin \psi$ and $y = 2\pi a \cos \psi, z = 0$. The appropriate solutions are plane electromagnetic waves traveling in the y direction with the speed of light.

For positive values of x, the appropriate electric and magnetic fields are

$$\begin{aligned} E_x &= E_0 e^{-\gamma x} e^{-j\gamma z} e^{-j\beta_0 y} \\ E_z &= jE_0 e^{-\gamma x} e^{-j\gamma z} e^{-j\beta_0 y} \\ E_y &= 0 \end{aligned} \tag{3.14}$$

We should note that the x and z components of the field can be obtained as gradients of a function

$$\Phi = -(E_0/\gamma) e^{-\gamma x} e^{-j\gamma z} e^{-j\beta_0 y} \tag{3.15}$$

where

$$\begin{aligned} E_x &= -\partial\Phi/\partial z \\ E_z &= -\partial\Phi/\partial y \end{aligned} \tag{3.16}$$

$$\partial^2\Phi/\partial x^2 + \partial^2\Phi/\partial z^2 = 0 \tag{3.17}$$

Thus, in the xz plane, Φ satisfies Laplace's equation.

The magnetic field is given by the curl[6] of the electric field times $j/\omega\mu$. Its components are:

$$\begin{aligned} H_x &= \frac{-j}{\mu c} E_0 e^{-\gamma x} e^{-j\gamma z} e^{-j\beta_0 y} \\ H_z &= \frac{-1}{\mu c} E_0 e^{-\gamma x} e^{-j\gamma z} e^{-j\beta_0 y} \\ H_y &= 0 \end{aligned} \tag{3.18}$$

[6] Maxwell's equations are given in Appendix I.

The fields in the $-x$ direction may be obtained by substituting $\exp(\gamma x)$ for $\exp(-\gamma x)$.

If the sheet is to roll up properly, the points a on the bottom coinciding with the points b on the top, we have

$$2\pi\gamma a \sin\psi - 2\pi\beta_0 a \cos\psi = 2n\pi \tag{3.19}$$

where n is an integer.

The solution corresponding most nearly to the wave on a singly-wound helix is that for $n = 0$. The others lead to a variation of field by n cycles along a circumferential line. These can be combined with the $n = 0$ solution to give a solution for a developed helix of thin tape, for instance. Or, appropriate combinations of them can represent modes of helices wound of several parallel wires. For instance, we can imagine winding a balanced transmission line up helically. One of the modes of propagation will be that in which the current in one wire is 180° out of phase with the current in the other. This can be approximated by a combination of the $n = +1$ and $n = -1$ solutions. This mode should not be confused with a fast wave, a perturbation of a transverse electromagnetic wave, which can exist around an unshielded helix.

Usually, we are interested in the slow wave on a singly-wound helix, and in this case we take $n = 0$ in (3.19), giving

$$\begin{aligned} \gamma \sin\psi - \beta_0 \cos\psi &= 0 \\ \tan\psi &= \beta_0/\gamma \end{aligned} \tag{3.20}$$

$$\sin\psi = \frac{\beta_0}{(\gamma^2 + \beta_0^2)^{1/2}} \tag{3.21}$$

$$\cos\psi = \frac{\gamma}{(\gamma^2 + \beta_0^2)^{1/2}} \tag{3.22}$$

Let us evaluate the propagation constant in the axial direction. From Fig. 3.8 we see that, in advancing unit distance in the axial direction, we proceed a distance $\cos\psi$ in the z direction and $\sin\psi$ in the y direction. Hence, the phase constant β in the axial direction must be

$$\beta = \beta_0 \sin\psi + \gamma \cos\psi \tag{3.23}$$

Using (3.18) and (3.19), we obtain

$$\beta = (\beta_0^2 + \gamma^2)^{1/2} \tag{3.24}$$

$$\gamma = (\beta^2 - \beta_0^2)^{1/2} \tag{3.25}$$

These are just relations (3.2, 3.3).

The power flow along the axis is that crossing a circumferential circle, represented by lines a-b in Fig. 3.8. As the power flows in the y direction, this is the power associated with a distance $2\pi a \sin \psi$ in z direction. Also, the power flow in the $+x$ region will be equal to the power flow in the $-x$ region. Hence, the power flow in the helix will be twice that in the region $x = 0$ to $x = +\infty$, $z = 0$ to $z = 2\pi a \sin \psi$.

$$P = 2 \int_{z=0}^{2\pi a \sin \psi} \int_{x=0}^{\infty} (\tfrac{1}{2})(E_z H_x^* - E_x H_z^*)\, dx\, dz \tag{3.26}$$

This is easily integrated to give

$$P = \frac{2\pi a \sin \psi E_0^2}{\gamma \mu c} \tag{3.27}$$

The magnitude E of the axial component of field is

$$E = E_0 \cos \psi \tag{3.28}$$

Using (3.21), (3.22), (3.24) and (3.28) in connection with (3.27) we obtain

$$(E^2/\beta^2 P) = (\gamma/\beta)^4(\beta/\beta_0)(\mu c/2\pi\gamma a) \tag{3.29}$$

We have

$$\mu c = \mu/\sqrt{\mu\epsilon} = \sqrt{\mu/\epsilon} = 377 \text{ ohms}$$

Thus

$$E^2/\beta^2 P = (\gamma/\beta)^4(\beta/\beta_0)(60/\gamma a) \tag{3.30}$$

The longitudinal impedance is half this, and the transverse impedance is $(\beta/\gamma)^2$ times the longitudinal impedance.

3.3 Effect of Wire Size

An actual helix of round wire, as used in traveling-wave tubes, will of course differ somewhat in properties from the helically conducting sheet for which the foregoing material applies.

One might expect a small difference if there were many turns per wavelength, but actual tubes often have only a few turns per wavelength. For instance, a typical 4,000 mc tube has about 4.8 turns per wavelength, while a tube designed for 6 mm operation has 2.4 turns per wavelength.

If the wire is made very small there will be much electric and magnetic energy very close to the wire, which is not associated with the desired field component (that which varies as $\exp(-j\beta z)$ in the z direction). If the wire is very large the internal diameter of the helix becomes considerably less than the mean diameter, and the space available for electron flow is reduced. As the field for the helically conducting sheet is greatest at the sheet, this

means that the maximum available field is reduced. Too, the impedance will depend on wire size.

It thus seems desirable to compare in some manner an actual helix and the helically conducting sheet. It would be very difficult to solve the problem of an actual helix. However, we can make an approximate comparison by a method suggested by R. S. Julian.

In doing this we will develop the helix of wires just as the helically con-

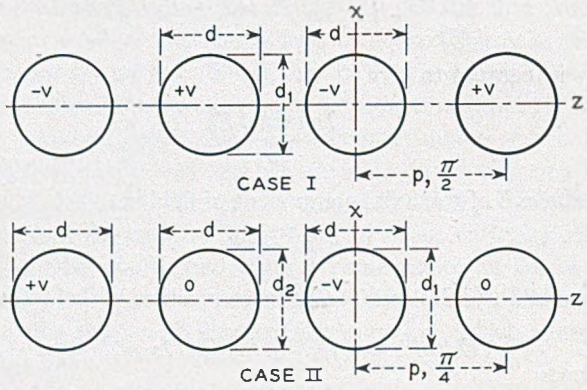

Fig. 3.9—The wires of a developed helix with about two turns per wavelength (case I) and about four turns per wavelength (case II). In the analysis used, the wires are not quite round.

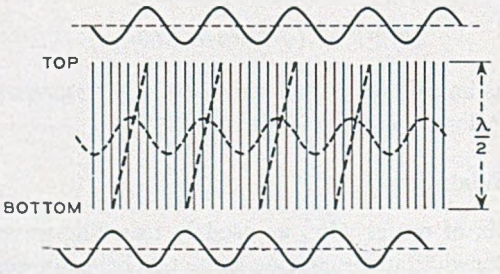

Fig. 3.10—Voltages on a developed helically conducting sheet for two turns per wavelength.

ducting sheet was developed, by slitting it along a helical line normal to the wires. We will then consider two special cases, one in which the wires of the developed helix are one half wavelength long and the other in which the wires are one quarter wavelength long.

The waves propagated on the developed helix are transverse electromagnetic waves propagated in the direction of the wires, and the electric fields normal to the direction of propagation can be obtained from a solution of Laplace's equation in two dimensions (as in (3.15)-(3.17)).

It is easy to make up two-dimensional solutions of Laplace's equation with equipotentials or conductors of approximately circular form, as shown in Fig. 3.9. In case I, the conductors are alternately at potentials $-V$, $+V$, $-V$, etc.; and in case II, the potentials are $-V$, 0, $+V$, 0, $-V$, 0, $+V$, etc. Far away in the x direction from such a series of conductors, the field will vary sinusoidally in the z direction and will vary in the same manner with x as in the developed helically conducting sheet. Hence, we can make the distant fields of the conductors of cases I and II of Fig. 3.9 equal to the distant fields of developed helically conducting sheets, and compare the $E^2/\beta^2 P$ and the impedance for the different systems. Case I would correspond to a helix of approximately two turns per wavelength and case II to four turns per wavelength.

3.3a *Two Turns per Wavelength*

Figure 3.10 is intended to illustrate the developed helically conducting sheet. The vertical lines indicate the direction of conduction. The dashed slanting lines are intersections of the original surface with planes normal to the axis. That is, on the original cylindrical surface they were circles about the surface, and they connect positions along the top and bottom which should be brought together in rolling up the flattened surface to reconstitute the helically conducting sheet.

Waves propagate on the developed sheet of Fig. 3.10 vertically with the speed of light. The vertical dimension of the sheet is in this case taken as $\lambda/2$, where λ is the free-space wavelength.[7] The sine waves above and below Fig. 3.10 indicate voltages at the top and the bottom and are, of course, 180° out of phase. As is necessary, the voltages at the ends of the dashed slanting lines, (really, the voltages at the same point before the sheet was slit) are equal.

A wave sinusoidal at the bottom of the sheet, zero half way up and 180° out of phase with the bottom at the top would constitute along any horizontal line a standing wave,not a traveling wave. Actually, this is only one component of the field. The other is a wave 90° out of phase in both the horizontal and vertical directions. Its maximum voltage is half-way up, and it is indicated by the dotted sine wave in Fig. 3.10. The voltage of this component is zero at top and bottom. It may be seen that these two components propagating upward together constitute a wave traveling to the right. The two components are orthogonal spatially, and the total power is twice the power of either component taken separately.

Figure 3.11 indicates an array of wires obtained by developing an actual

[7] Section 3.3a is referred to as "two turns per wavelength." This is not quite accurate; it is in error by the difference between the lengths of the vertical and the slanting lines in Fig. 3.10.

helix which has been slit along a helical line normal to the wire of which the helix is wound. The dashed slanting lines again connect points which were the same point before the helix was slit and developed. Again we assume a height of a half wavelength. Thus, if the polarities are maximum $+, -, +, -$ etc. as shown at the bottom, they will be maximum $-, +, -, +, -, +$ etc. as shown at the top, and zero half-way up. In this case the field is a standing wave along any horizontal line, and no other component can be introduced to make it a traveling wave. Half of the field strength can be regarded as constituting a component traveling to the right and half as a component traveling to the left.

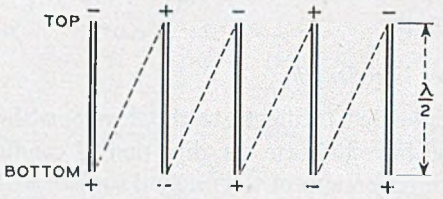

Fig. 3.11—Voltages on a developed helix for two turns per wavelength.

The equipotentials used to represent the field about the wires of Fig. 3.9, Case I and Fig. 3.10 belong to the field

$$V + j\psi = \ln \tan (z + jx) \tag{3.31}$$

Here V is potential and ψ is a stream function. There are negative equipotentials about $z = x = 0$ and positive equipotentials about $x = 0$, $z = \pm\pi/2$. For an equipotential coinciding with the surface of a wire of z-diameter, $2\,z_{\text{wire}}$, d/p is thus

$$d/p = \frac{z_{\text{wire}}}{\pi/4} \tag{3.32}$$

at $x = 0, z < \pi/4$

$$V = \ln \tan z \tag{3.33}$$

at $z = 0$

$$V = \ln \tanh x \tag{3.34}$$

Hence, for an equipotential on the wire with an z-diameter $2z$, the x-diameter $2x$ can be obtained from (3.33) and (3.34) as

$$2x = 2 \tanh^{-1} \tan z \tag{3.35}$$

Of course, the ratio of the x-diameter d_1 to the pitch is given by

$$d_1/p = \frac{x}{\pi/4} \tag{3.36}$$

where x is obtained from (3.35).

In Fig. 3.12, d_1/d is plotted vs. d/p by means of (3.35) and (3.36). This shows that for wire diameters up to $d/p = .5$ (open space equal to wire diameter) the equipotentials representing the wire are very nearly round.

The total electric flux from each wire is $2\pi\epsilon$ and the potential of a wire of z-diameter $2z$ is $V = -\ln \tan z$. Hence, the stored energy W_1 per unit length per wire, half the product of the charge and the voltage, is

$$W_1 = -\pi\epsilon \ln \tan z \tag{3.37}$$

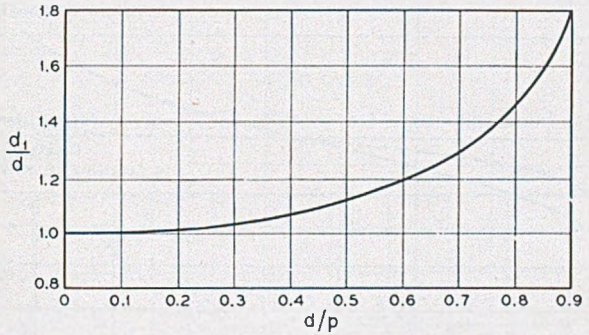

Fig. 3.12—Ratio of the two diameters of the wire of a helix for two turns per wavelength (see Fig. 3.9) vs. the ratio of one of the diameters to the pitch.

The total distant field and the useful field component are given by expanding (3.31) in Fourier series and taking the fundamental component, giving

$$V = -2 \cos 2ze^{\mp 2x} \tag{3.38}$$

The $-$ sign applies for $x > 0$ and the $+$ sign for $x < 0$. Half of this can be regarded as belonging to a field moving to the right and half to a field moving to the left.

For a field equal to half that specified by (3.38), which might be part of the field of a developed helically conducting sheet, the stored energy W_2 per unit depth can be obtained by integrating $(E_z^2 + E_x^2)\ \epsilon/2$ from $x = -\infty$ to $x = +\infty$ and from $z = -\pi/4$ to $+\pi/4$, and it turns out to be

$$W_2 = \tfrac{1}{2}\ \pi\epsilon \tag{3.39}$$

If we add another field component similar to half of (3.38), but in quadrature with respect to z and t, we will have the traveling wave of a helically conducting sheet with the same distant traveling field component as given by (3.31). Hence, the ratio R of the stored energy for the developed sheet to the stored energy for the developed helix is

$$R = 2W_2/W_1 = -\frac{1}{\ln \tan z} \tag{3.40}$$

R is the ratio of the stored energies, and hence of the power flows (since the waves both propagate with the speed of light) of a developed helically conducting sheet and a developed helix with the same distant traveling fundamental field components. Hence, at a given distance $(E^2/\beta^2 P)^{1/3}$ for the helix is $R^{1/3}$ times as great as for the helically conducting sheet. In Fig. 3.13, $R^{1/3}$ is plotted vs. d/p.

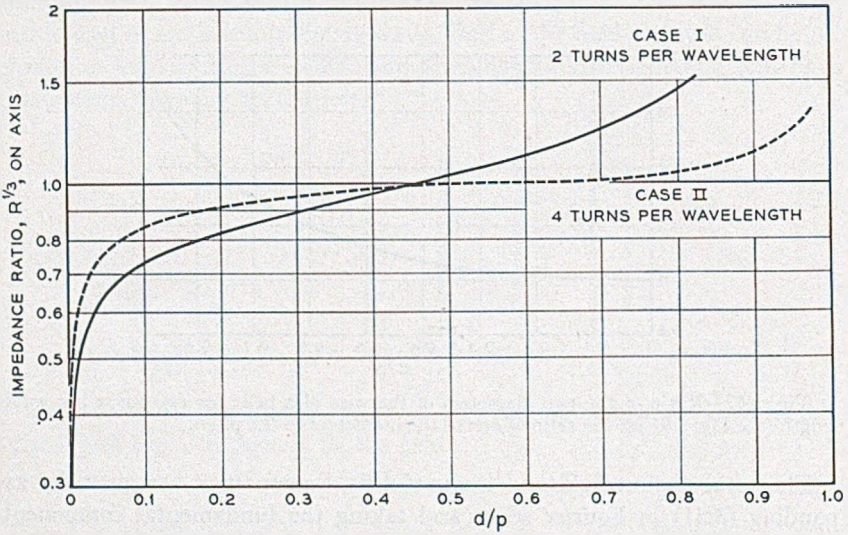

Fig. 3.13—Ratio $R^{1/3}$ of $(E^2/\beta^2 P)^{1/3}$ for a helix to the value for a helically conducting sheet for the distant field.

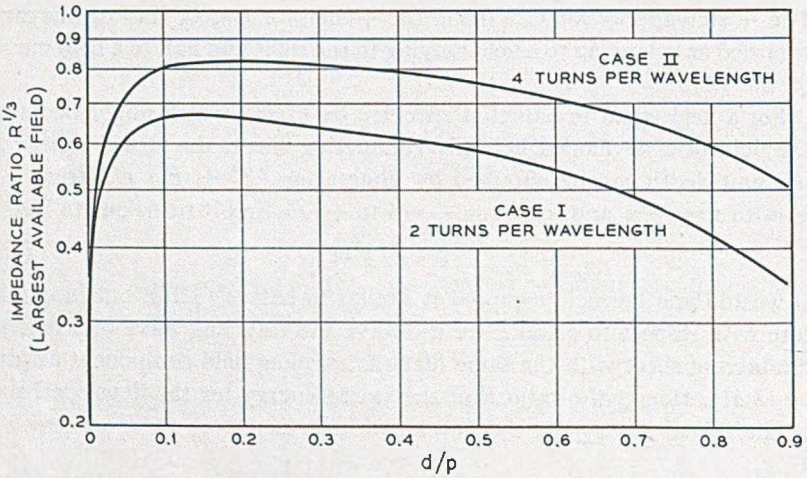

Fig. 3.14—Ratio $R^{1/3}$ of $(E^2/\beta^2 P)^{1/3}$ for a helix to the value for a helically conducting sheet, field at the inside diameter of the helix or sheet.

The maximum available field for the developed helically conducting sheet (equation (3.38)) is that for $x = 0$. The maximum available field for the developed helix (equation (3.31)) is that for an electron grazing the helix inner or outer diameter, that is, an electron at a value of x given by (3.35). The fundamental sinusoidal component of the field varies as $\exp(-2x)$ for both the sheet and the helix, and hence there is a loss in E^2 by a factor $\exp(-4x)$ because of this. We wish to make a comparison on the basis of E^2 and power or energy. Hence, on basis of maximum available field squared we would obtain from (3.40)

$$R = -\frac{1}{\ln \tan z} e^{-4x} \tag{3.41}$$

where x is obtained from (3.35). Figure 3.14 was obtained from (3.32), (3.35) and (3.41).

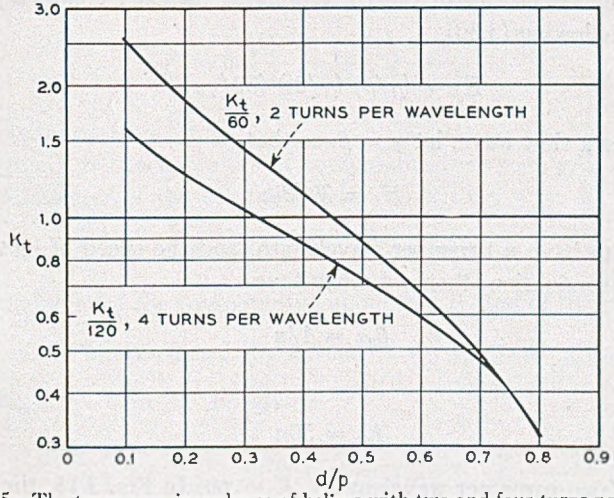

Fig. 3.15—The transverse impedance of helices with two and four turns per wavelength vs. the ratio of wire diameter to pitch.

In a transmission line the characteristic impedance is given by

$$K = \sqrt{\frac{L}{C}} \tag{3.42}$$

Here L and C are the inductance and capacitance per unit length. This impedance should be identified with the transverse impedance of the helix. We also have for the velocity of propagation, which will be the velocity of light, c,

$$c = \frac{1}{\sqrt{LC}} = \frac{1}{\sqrt{\mu\epsilon}} \tag{3.43}$$

From (3.42) and (3.43) we obtain

$$\begin{aligned} K_t &= \sqrt{\mu\epsilon}/C = \sqrt{\mu/\epsilon}(\epsilon/C) \\ &= 377\ \epsilon/C \end{aligned} \tag{3.44}$$

Now C is the charge Q divided by the voltage V. Hence

$$K_t = 377\ \epsilon V/Q \tag{3.45}$$

In this case we have

$$\begin{aligned} K_t &= \frac{337\epsilon \ln \tan z}{2\pi\epsilon} \\ K_t &= -60 \ln \tan_z \end{aligned} \tag{3.46}$$

To obtain the impedance of the corresponding helically conducting sheet we assume, following (3.30)

$$K_t = (\gamma/\beta)\ (\gamma/\beta_0)\ (30/\gamma a) \tag{3.47}$$

and assuming a slow wave, let $\gamma = \beta$, so that

$$K_t = 30/\beta_0 a \tag{3.48}$$

If we are to have n turns per wavelength, and the speed of light in the direction of conduction, then we must have

$$\beta_0 a = 1/n \tag{3.49}$$

whence

$$K_t = 30n \tag{3.50}$$

For $n = 2$ (two turns per wavelength), $K = 60$. In Fig. 3.15, the characteristic impedance K_t as obtained from (3.46) divided by 60 (from (3.50)) is plotted vs. d/p.

3.3b *Four Turns per Wavelength*

In this case there are enough wires so that we can add a quadrature component as in Fig. 3.10 and thus produce a traveling wave rather than a standing wave. Thus, we can make a more direct comparison between the developed sheet and the developed helix.

For the developed helix we have

$$V + j\psi = \ln \tan (z + jx) + \frac{A}{\cos 2\ (z + jx)} \tag{3.15}$$

If we transform this to new coordinates z_1, x_1 about an origin at $z = 0$, $x = \pi/4$ we obtain

$$V + j\psi = \ln\left(\frac{1 + \tan(z_1 + jx_1)}{1 - \tan(z_1 + jx_1)}\right) - \left(\frac{A}{\sin 2(z_1 + jx_1)}\right) \tag{3.52}$$

We can now adjust A to give a zero equipotential of diameter $2z_1$ about $x = x_1 = 0$, $z_1 = 0$ ($z = \pi/4$) by letting

$$A = (\sin 2z_1) \ln\left(\frac{1 + \tan z_1}{1 - \tan z_1}\right) \tag{3.53}$$

If A is so chosen, there will be roughly circular equipotentials of z-diameter $2z_1$ about $z = \pm \pi/4$, etc. There will also be roughly circular equipotentials of the same z-diameter about $z = 0, \pm\pi/2$, etc., of potential $\pm V$. That about $z = 0$ has a potential

$$V = \ln\left(\frac{1 + \tan z_1}{1 - \tan z_1}\right) \frac{A}{\cos 2z_1} \tag{3.54}$$

where A is taken from (3.53).

The distance between centers of equipotentials is $p = \pi/4$, so that the ratio of z-diameter of the equipotentials to pitch is

$$d/p = 2z_1/(\pi/4) = z_1/(\pi/8) \tag{3.55}$$

The x-diameter of the equipotential about $z = 0$ (and of those about $z = \pm\frac{\pi}{2}$ etc.) can be obtained as $2x$ by letting V have the value given by (3.54) and setting $z = 0$ in (3.51), giving

$$V = \ln \tanh x + \frac{A}{\cosh 2x} \tag{3.56}$$

The ratio of this x-diameter to the pitch, d_1/p, is

$$d_1/p = y/(\pi/8), \tag{3.57}$$

x is obtained from (3.56).

To obtain the x-diameter of the 0 potential electrodes we take the derivative (3.52) with respect to z_1, giving the gradient in the z direction

$$\frac{\partial V}{\partial z_1} + j\frac{\partial \psi}{\partial z_1} = \frac{\sec^2(z_1 + jx_1)}{1 + \tan(z_1 + jx_1)} + \frac{\sec^2(z_1 + jx_1)}{1 - \tan(z_1 + jx_1)} - \frac{2A\cos 2(z_1 + jx_1)}{\sin 2(z_1 + jx_1)} \tag{3.58}$$

We then let $z_1 = 0$ and find the value of x_1 for which $\partial V/\partial z_1 = 0$. When $z_1 = 0$, (3.58) becomes

$$A = \sinh 2x_1 \tanh 2x_1 \frac{(1 - \tanh^2 x_1)}{(1 + \tanh^2 x_1)} \tag{3.59}$$

As A is given by (3.53), we can obtain x, from (3.57), and the ratio of the x-diameter d_2 to the pitch is

$$d_2/p = x_1/(\pi/8) \tag{3.60}$$

Figure 3.16 shows d_1/d and d_2/d vs. d/p.

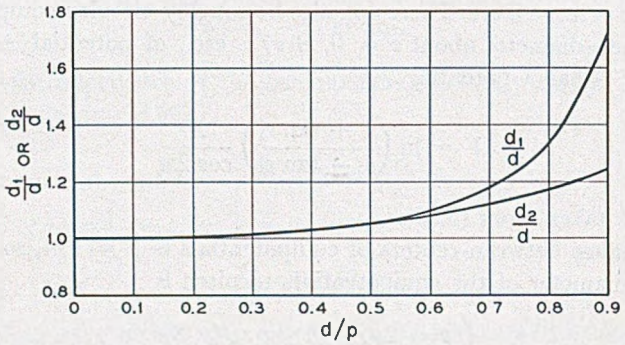

Fig. 3.16—Ratios of the wire diameters for the four turns per wavelength analysis.

The ratios R and the impedance are obtained merely by comparing the power flow for the developed sheet with a single sinusoidally distributed component with the power flow for case II for the same distant field. In a comparison with the helically conducting sheet, $n = 2$ is used in (3.50). The results are shown in Figs. 3.13, 3.14, 3.15. We see that on the basis of the largest available field, the best wire size is $d/p = .19$.

3.4 Transmission Line Equations and Helices

It is of course possible at any frequency to construct a transmission line with a distributed shunt susceptance B per unit length and a distributed shunt reactance X per unit length and, by adjusting B and X to make the phase velocity and $E^2/\beta^2 P$ the same for the artificial line as for the helix. In simulating the helix with the line, B and X must be changed as frequency is changed. Indeed, it may be necessary to change B and X somewhat in simulating a helix with a forced wave on it, as, the wave forced by an electron stream. Nevertheless, a qualitative insight into some problems can be obtained by use of this type of circuit analogue.

3.4a *Effect of Dielectric on Helix Impedance Parameter*

One possible application of the transmission line equivalent is in estimating the lowering of the helix impedance parameter $(E^2/\beta^2 P)^{1/3}$.

In the case of a transmission line of susceptance B and reactance X per unit length, we have for the phase constant β and the characteristic impedance K

$$\beta = \sqrt{BX} \tag{3.61}$$

$$K = \sqrt{X/B} \tag{3.62}$$

Now, suppose that B is increased by capacitive loading so that β has a larger value β_d. Then we see that K will have a value K_d

$$K_d = (\beta/\beta_d)K \tag{3.63}$$

Where should K be measured? It is reasonable to take the field at the surface of the helix or the helically conducting sheet as the point at which the field should be evaluated. The field at the axis will, then, be changed by a different amount, for the field at the surface of the helix is $I_0(\gamma a)$ times the field at the axis.

Suppose, then, we design a helix to have a phase constant β (a phase velocity ω/β) and, in building it, find that the dielectric supports increase the phase constant to a value β_d giving a smaller phase velocity ω/β_d. Suppose β/β_0 is large, so that γ is nearly equal to β. How will we estimate the actual axial value of $(E^2/\beta^2 P)^{1/3}$? We make the following estimate:

$$(E^2/\beta^2 P)_d^{1/3} = \left(\frac{\beta}{\beta_d}\right)^{1/3} \left(\frac{I_0(\beta a)}{I_0(\beta_d a)}\right)^{2/3} (E^2/\beta^2 P)^{1/3} \tag{3.64}$$

Here the factor $(\beta/\beta_d)^{1/3}$ is concerned with the reduction of impedance measured at the helix surface, and the other factor is concerned with the greater falling-off of the field toward the center of the helix because of the larger value of γ (taken equal to β and β_d in the two cases).

The writer does not know how good this estimate may be.

3.4b *Coupled Helices*

Another case in which the equivalent transmission line approach is particularly useful is in considering the problem of concentric helices. Such configurations have been particularly suggested for producing slow transverse fields. They can be analyzed in terms of helically conducting cylinders or in terms of developed cylinders. A certain insight can be gained very quickly, however, by the approach indicated above.

We will simulate the helices by two transmission lines of series impedances jX_1 and jX_2, of shunt admittances jB_1 and jB_2 coupled by series mutual

impedance and shunt mutual admittance jX_{12} and jB_{12}. If we consider a wave which varies as $\exp(-j\Gamma z)$ in the z direction we have

$$\Gamma I_1 - jB_1V_1 - jB_{12}V_2 = 0 \tag{3.65}$$

$$\Gamma V_1 - jX_1I_1 - jX_{12}I_2 = 0 \tag{3.66}$$

$$\Gamma I_2 - jB_2V_2 - jB_{12}V_1 = 0 \tag{3.67}$$

$$\Gamma V_2 - jX_2I_2 - jX_{12}I_1 = 0 \tag{3.68}$$

If we solve (3.65) and (3.67) for I_1 and I_2 and eliminate these, we obtain

$$\frac{V_2}{V_1} = \frac{-(\Gamma^2 + X_1B_1 + X_{12}B_{12})}{X_1B_{12} + B_2X_{12}} \tag{3.69}$$

$$\frac{V_1}{V_2} = \frac{-(\Gamma^2 + X_2B_2 + X_{12}B_{12})}{X_2B_{12} + B_1X_{12}} \tag{3.70}$$

Multiplying these together we obtain

$$\begin{aligned}\Gamma^4 &+ (X_1B_1 + X_2B_2 + 2X_{12}B_{12})\Gamma^2 \\ &+ (X_1X_2 - X_{12}^2)(B_1B_2 - B_{12}^2) = 0\end{aligned} \tag{3.71}$$

We can solve this for the two values of Γ^2

$$\begin{aligned}\Gamma^2 = &-\tfrac{1}{2}(X_1B_1 + X_2B_2 + 2X_{12}B_{12}) \\ &\pm \tfrac{1}{2}[(X_1B_1 - X_2B_2)^2 + 4(X_1B_1 + X_2B_2)(X_{12}B_{12}) \\ &+ 4(X_1X_2B_{12}^2 + B_1B_2X_{12}^2)]^{1/2}\end{aligned} \tag{3.72}$$

Each value of Γ^2 represents a normal mode of propagation involving both transmission lines. The two square roots of each Γ^2 of course indicate waves going in the positive and negative directions.

Suppose we substitute (3.72) into (3.69). We obtain

$$\frac{V_2}{V_1} = \frac{\begin{aligned}&-(X_1B_1 - X_2B_2) \pm [(X_1B_1 - X_2B_2)^2 \\ &+ 4(X_1B_1 + X_2B_2)(X_{12}B_{12}) + 4(X_1X_2B_{12}^2 + B_1B_2X_{12}^2)]^{1/2}\end{aligned}}{2(X_1B_{12} + B_2X_{12})} \tag{3.73}$$

We will be interested in cases in which X_1B_1 is very nearly equal to X_2B_2. Let

$$\Delta\Gamma_0^2 = X_1B_1 - X_2B_2 \tag{3.74}$$

and in the parts of (3.73) where the difference of (3.74) does not occur use

$$\begin{aligned}X_1 &= X_2 = X \\ B_1 &= B_2 = B\end{aligned} \tag{3.75}$$

Then, approximately

$$\frac{V_2}{V_1} = \frac{-\Delta\Gamma_0^2 \pm [(\Delta\Gamma_0^2)^2 + 4(XB_{12} + BX_{12})^2]^{1/2}}{2(XB_{12} + BX_{12})} \tag{3.76}$$

Let us assume that $\Delta\Gamma^2$ is very small and retains terms up to the first power of $\Delta\Gamma^2$

$$\frac{V_2}{V_1} = \pm 1 + \frac{\Delta\Gamma_0^2}{2(XB_{12} + BX_{12})} \tag{3.77}$$

Let

$$\Gamma_0^2 = -XB \tag{3.78}$$

$$\frac{V_2}{V_1} = \pm 1 - \frac{\Delta\Gamma_0^2/\Gamma_0^2}{2(B_{12}/B + X_{12}/X)} \tag{3.79}$$

Let us now interpret (3.79). This says that if $\Delta\Gamma_0^2$ is zero, that is, if $X_1B_1 = X_2B_2$ exactly, there will be two modes of transmission, a *longitudinal* mode in which $V_2/V_1 = +1$ and a *transverse* mode in which $V_2/V_1 = -1$. If we excite the transverse mode it will persist. However, if $\Delta\Gamma_0^2 \neq 0$, there will be two modes, one for which $V_2 > V_1$ and the other for which $V_2 < V_1$; in other words, as $\Delta\Gamma_0^2$ is increased, we approach a condition in which one mode is nearly propagated on one helix only and the other mode nearly propagated on the other helix only. Then if we drive the pair with a transverse field we will excite both modes, and they will travel with different speeds down the system.

We see that to get a good transverse field we must make

$$\frac{\Delta\Gamma_0^2}{\Gamma_0^2} \ll 2(B_{12}/B + X_{12}/X) \tag{3.80}$$

In other words, the stronger the coupling (B_{12}, X_{12}) the more the helices can afford to differ (perhaps accidentally) in propagation constant and the pair still give a distinct transverse wave.

Thus, it seems desirable to couple the helices together as tightly as possible and especially to see that B_{12} and X_{12} have the same signs.

Let us consider two concentric helices wound in opposite directions, as in Fig. 3.17. A positive voltage V_1 will put a positive charge on helix 1 while a positive voltage V_2 will put a negative charge on helix 1. Thus, B_{12}/B is negative. It is also clear that the positive current I_2 will produce flux linking helix 1 in the opposite direction from the positive current I_1, thus making X_{12}/X negative. This makes it clear that to get a good transverse field between concentric helices, the helices should be wound in opposite direc-

tions. If the helices were wound in the same direction, the "transverse" and "longitudinal" modes would cease to be clearly transverse and longitudinal should the phase velocities of the two helices by accident differ a little. Further, even if the phase velocities were the same, the transverse and longitudinal modes would have almost the same phase velocity, which in itself may be undesirable.

Field analyses of coupled helices confirm these general conclusions.

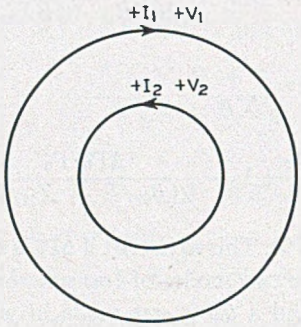

Fig. 3.17—Currents and voltages of concentric helices.

3.5 About Loss in Helices

The loss of helices is not calculated in this book. Some matters concerning deliberately added loss will be considered, however.

Loss is added to helices so that the backward loss of the tube (loss for a wave traveling from output to input) will be greater than the forward gain. If the forward gain is greater than the backward loss, the tube may oscillate if it is not terminated at each end in a good broad-band match.

In some early tubes, loss was added by making the helix out of lossy wire, such as nichrome or even iron, which is much lossier at microwave frequencies because of its ferromagnetism. Most substances are in many cases not lossy enough. Iron is very lossy, but its presence upsets magnetic focusing.

When the helix is supported by a surrounding glass tube or by parallel ceramic or glass rods, loss may be added by spraying aquadag on the inside or outside of the glass tube or on the supporting rods. This is advantageous in that the distribution of loss with distance can be controlled.

It is obvious that for lossy material a finite distance from the helix there is a resistivity which gives maximum attenuation. A perfect conductor would introduce no dissipation and neither would a perfect insulator

If lossy material is placed a little away from the helix, loss can be made greater at lower frequencies (at which the field of the helix extends out into the lossy material) than at higher frequencies (at which the fields of

the helix are crowded near the helix and do not give rise to much current in the lossy material. This construction may be useful in preventing high-frequency tubes from oscillating at low frequencies.

Loss may be added by means of tubes or collars of lossy ceramic which fit around the helix.

APPENDIX I

MISCELLANEOUS INFORMATION

This appendix presents an assortment of material which may be useful to the reader.

Constants

Electronic charge-to-mass ratio:

$\eta = e/m = 1.759 \times 10^{11}$ Coulomb/kilogram

Electronic charge: $e = 1.602 \times 10^{-19}$ Coulomb

Dielectric constant of vacuum: $\epsilon = 8.854 \times 10^{-12}$ Coulomb/meter

Permitivity of vacuum: $\mu = 1.257 \times 10^{-6}$ Henry/meter

Boltzman's constant: $k = 1.380 \times 10^{-23}$ Joule/degree

Cross Products

$$(A' \times A'')_x = A_y' A_z'' - A_z' A_y''$$
$$(A' \times A'')_y = A_z' A_x'' - A_x' A_z''$$
$$(A' \times A'')_z = A_x' A_y'' - A_y' A_x''$$

Maxwell's Equations: Rectangular Coordinates

$$\frac{\partial E_z}{\partial y} - \frac{\partial E_y}{\partial z} = -j\omega\mu H_x \qquad \frac{\partial H_z}{\partial y} - \frac{\partial H_y}{\partial z} = j\omega\epsilon E_x + J_x$$

$$\frac{\partial E_x}{\partial z} - \frac{\partial E_z}{\partial x} = -j\omega\mu H_y \qquad \frac{\partial H_x}{\partial z} - \frac{\partial H_z}{\partial x} = j\omega\epsilon E_y + J_y$$

$$\frac{\partial E_y}{\partial x} - \frac{\partial E_x}{\partial y} = -j\omega\mu H_z \qquad \frac{\partial H_y}{\partial x} - \frac{\partial H_x}{\partial y} = j\omega\epsilon E_z + J_z$$

Maxwell's Equations: Axially Symmetrical

$$\frac{\partial E_\varphi}{\partial z} = -j\omega\mu H_\rho \qquad \frac{\partial H_\varphi}{\partial z} = -(j\omega\epsilon E_\rho + J_\rho)$$

$$\frac{\partial E\rho}{\partial z} - \frac{\partial E_z}{\partial \rho} = -j\omega\mu H_\varphi \qquad \frac{\partial H_\rho}{\partial z} - \frac{\partial H_z}{\partial \rho} = j\omega\epsilon E_\varphi + J_\varphi$$

$$\frac{\partial}{\partial \rho}(\rho E_\varphi) = -j\omega\mu\rho H_z \qquad \frac{\partial}{\partial \rho}(\rho H_\varphi) = \rho(j\omega\epsilon E_z + J_z)$$

MISCELLANEOUS FORMULAE INVOLVING $I_n(x)$ AND $K_n(x)$

1. $I_{\nu-1}(Z) - I_{\nu+1}(Z) = \frac{2\nu}{Z} I_\nu(Z), \qquad K_{\nu-1}(Z) - K_{\nu+1}(Z) = -\frac{2\nu}{Z} K_\nu(Z)$

2. $I_{\nu-1}(Z) + I_{\nu+1}(Z) = 2I'_\nu(Z), \qquad K_{\nu-1}(Z) + K_{\nu+1}(Z) = -2K'_\nu(Z)$

3. $ZI'_\nu(Z) + \nu I_\nu(Z) = ZI_{\nu-1}(Z), \qquad ZK'_\nu(Z) + \nu K_\nu(Z) = -ZK_{\nu-1}(Z)$

4. $ZI'_\nu(Z) - \nu I_\nu(Z) = ZI_{\nu+1}(Z), \qquad ZK'_\nu(Z) - \nu K_\nu(Z) = -ZK_{\nu+1}(Z)$

5. $\left(\frac{d}{ZDZ}\right)^m \{Z^\nu I_\nu(Z)\} = Z^{\nu-m} I_{\nu-m}(Z), \left(\frac{d}{ZdZ}\right)^m \{Z^\nu K_\nu(Z)\}$

$$= (-)^m Z^{\nu-m} K_{\nu-m}(Z)$$

6. $\left(\frac{d}{ZdZ}\right)^m \left\{\frac{I_\nu(Z)}{Z^\nu}\right\} = \frac{I_{\nu+m}(Z)}{Z^{\nu+m}}, \qquad \left(\frac{d}{ZdZ}\right)^m \left\{\frac{K_\nu(Z)}{Z^\nu}\right\} = (-)^m \frac{K_{\nu+m}(Z)}{Z^{\nu+m}}$

7. $I'_0(Z) = I_1(Z), \qquad K'_0(Z) = -K_1(Z)$

8. $I_{-\nu}(Z) = I_\nu(Z), \qquad K_{-\nu}(Z) = K_\nu(Z)$

9. $K_{1/2}(Z) = \left(\frac{\pi}{2Z}\right)^{1/2} e^{-z}$

10. $I_\nu(Ze^{m\pi i}) = e^{m\nu\pi i} I_\nu(Z)$

11. $K_\nu(Ze^{m\pi i}) = e^{-m\nu\pi i} K_\nu(Z) - i \frac{\sin m\nu\pi}{\sin \nu\pi} I_\nu(Z)$

12. $I_\nu(Z)\, K_{\nu+1}(Z) + I_{\nu+1}(Z)\, K_\nu(Z) = 1/Z$

For small values of X:

13. $I_0(X) = 1 + .25\, X^2 + .015625\, X^4 + \cdots$

14. $I_1(X) = .5X + .0625\, X^3 + .002604\, X^5 + \cdots$

15. $K_0(X) = -\left\{\gamma + \ln\left(\frac{X}{2}\right)\right\} I_0(X) + \frac{1}{4} X^2 + \frac{3}{128} X^4 + \cdots\Big\}$

16. $K_1(X) = \left\{\gamma + \ln\left(\frac{X}{2}\right)\right\} I_1(X) + \frac{1}{X} - \frac{1}{4} X - \frac{5}{64} X^3 + \cdots\Big\}$

$$\gamma = .5772 \ldots \text{ (Euler's constant)}$$

For large values of X:

17. $I_0(X) \sim \frac{e^X}{(2\pi X)^{1/2}} \left\{1 + \frac{.125}{X} + \frac{.0703125}{X^2} + \frac{.073242}{X^3} + \cdots\right\}$

18. $$I_1(X) \sim \frac{e^X}{(2\pi X)^{1/2}}\left\{1 - \frac{.375}{X} - \frac{.1171875}{X^2} - \frac{.102539}{X^3} - \cdots\right\}$$

19. $$K_0(X) \sim \left(\frac{\pi}{2X}\right)^{1/2} e^{-X}\left\{1 - \frac{.125}{X} + \frac{.0703125}{X^2} - \frac{.073242}{X^3} + \cdots\right\}$$

20. $$K_1(X) \sim \left(\frac{\pi}{2X}\right)^{1/2} e^{-X}\left\{1 + \frac{.375}{X} - \frac{.1171875}{X^2} + \frac{.102539}{X^3} - \cdots\right\}.$$

Fig. A1.1 shows $I_0(X)$ (solid line) and the first two terms of 13 and the first term of 17 (dashed lines).

Fig. A1.2 shows $I_1(X)$ (solid line) and the first term of 14 and the first term of 18 (dashed lines).

Fig. A1.3 shows $K_0(X)$ (solid line) and $-\left\{\gamma + \ln\left(\frac{X}{2}\right)\right\} I_0(X)$ and the first term of 19 (dashed lines).

Fig. A1.4 shows $K_1(X)$ (solid line) and $\left\{\gamma + \ln\left(\frac{X}{2}\right)\right\} I_1(X) + 1/X$ and the first term of 20 (dashed lines).

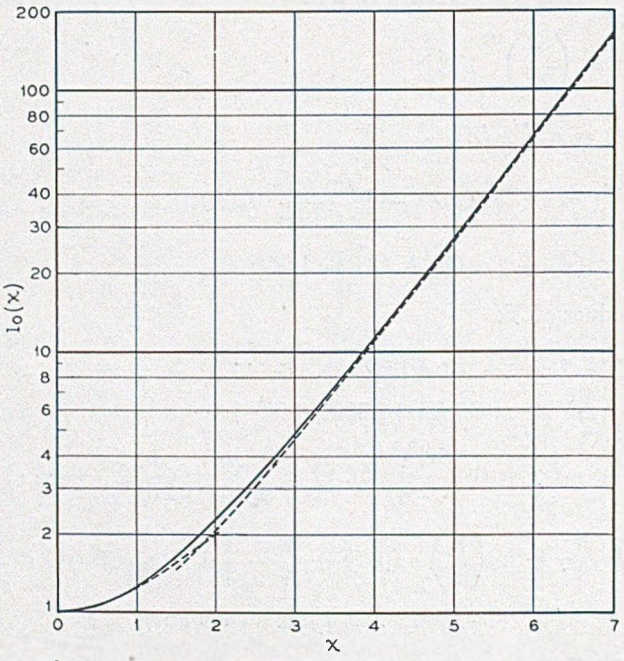

Fig. A1.1—The correct value of $I_0(X)$ (solid line), the first two terms of the series expansion 13 (dashed line from origin), and the first term of the asymptotic series 17 (dashed line to right).

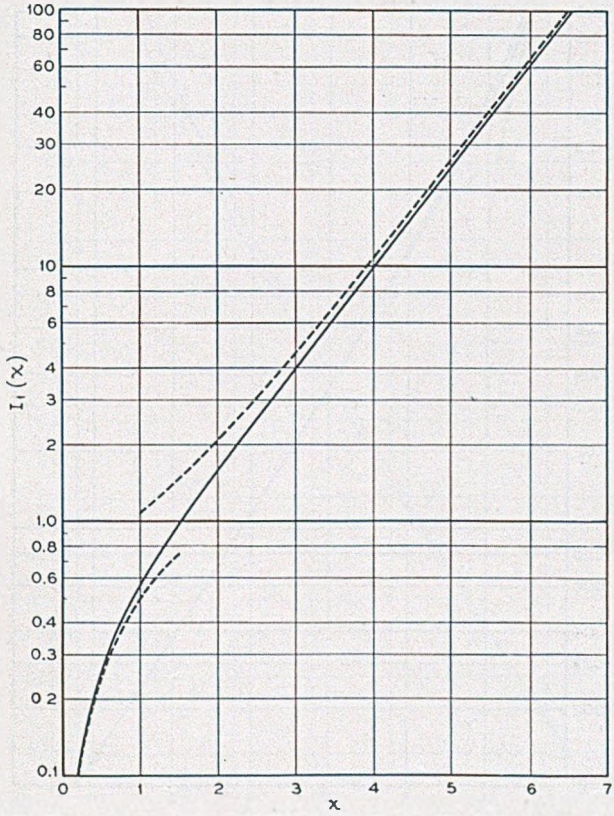

Fig. A1.2—The correct value of $I_1(X)$ (solid line), the first term of the series expansion 14 (lower dashed line), and the first term of the asymptotic series 18 (upper dashed line).

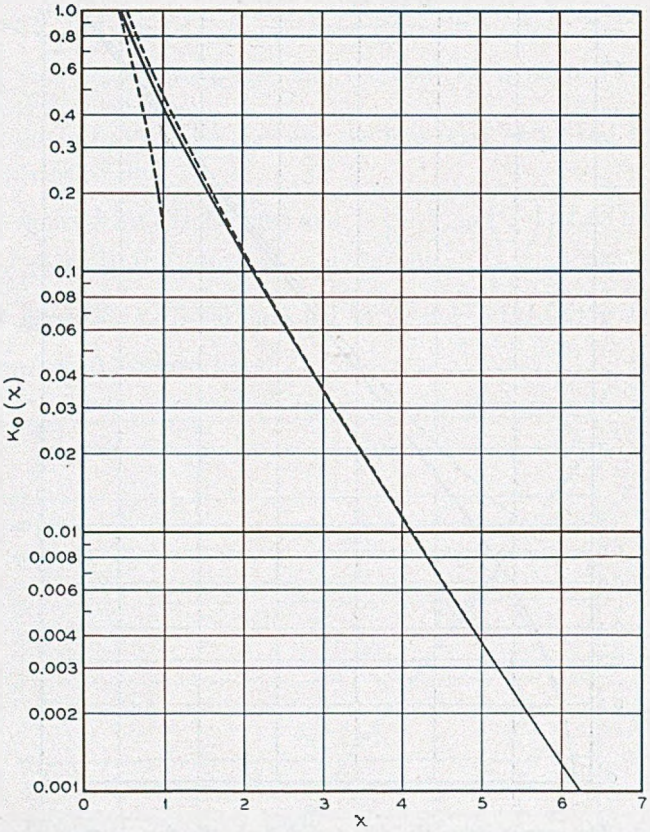

Fig. A1.3—The correct value of $K_0(X)$ (solid line), $-\left\{\gamma + \ln\left(\frac{X}{2}\right)\right\} I_0(X)$ from the series expansion 15 (left dashed line), and the first term of the asymptotic series 19 (right dashed line).

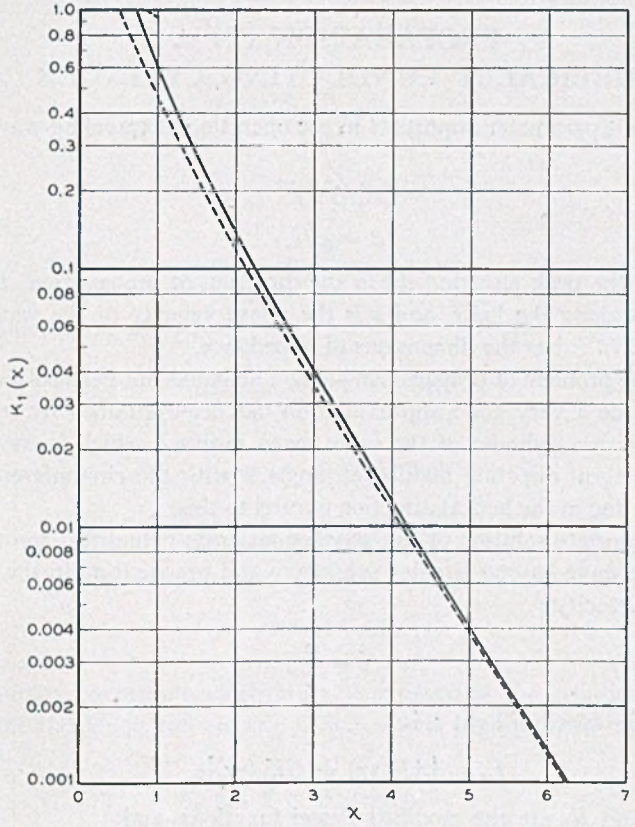

Fig. A1.4—The correct value of $K_1(X)$ (solid line), $\left\{\gamma + \ln\left(\frac{X}{2}\right)\right\} I_1(X)$ from the series expansion 16 (upper dashed line), and the first term of the asymptotic series 20 (lower dashed line).

APPENDIX II

PROPAGATION ON A HELICALLY CONDUCTING CYLINDER

The circuit parameter important in the operation of traveling-wave tubes is:

$$(E_z^2/\beta^2 P)^{1/3} \tag{1}$$

$$\beta = \omega/v. \tag{2}$$

Here E_z is the peak electric field in the direction of propagation, P is the power flow along the helix, and v is the phase velocity of the wave. The quantity $E_z^2/\beta^2 P$ has the dimensions of impedance.

While the problem of propagation along a helix has not been solved, what appears to be a very good approximation has been obtained by replacing the helix with a cylinder of the same mean radius a which is conducting only in a helical direction making an angle Ψ with the circumference, and nonconducting in the helical direction normal to this.

An appropriate solution of the wave equation in cylindrical co-ordinates for a plane wave having circular symmetry and propagating in the z direction with velocity

$$v = \frac{\omega}{\beta}, \tag{3}$$

less than the speed of light c, is

$$E_z = [AI_0(\gamma r) + BK_0(\gamma r)]e^{j(\omega t - \beta z)} \tag{4}$$

where I_0 and K_0 are the modified Bessel functions, and

$$\gamma^2 = \beta^2 - \left(\frac{\omega}{c}\right)^2 = \beta^2 - \beta_0^2. \tag{5}$$

The form of the z (longitudinal) components of an electromagnetic field varying as $e^{j(\omega t - \beta z)}$ and remaining everywhere finite might therefore be

$$H_{z1} = B_1 I_0(\gamma r)e^{j(\omega t - \beta z)} \tag{6}$$

$$E_{z3} = B_3 I_0(\gamma r)e^{j(\omega t - \beta z)} \tag{7}$$

inside radius a, and

$$H_{z2} = B_2 K_0(\gamma r)e^{j(\omega t - \beta z)} \tag{8}$$

$$E_{z4} = B_4 K_0(\gamma r) e^{j(\omega t - \beta z)} \tag{9}$$

outside radius α. Omitting the factor $e^{j(\omega t-\beta z)}$ the radial and circumferential components associated with these, obtained by applying the curl equation, are, inside radius α,

$$H_{\phi 3} = B_3 \frac{j\omega\epsilon}{\gamma} I_1(\gamma r) \tag{10}$$

$$H_{r1} = B_1 \frac{j\beta}{\gamma} I_1(\gamma r) \tag{11}$$

$$E_{\phi 1} = -B_1 \frac{j\omega\mu}{\gamma} I_1(\gamma r) \tag{12}$$

$$E_{r3} = B_3 \frac{j\beta}{\gamma} I_1(\gamma r) \tag{13}$$

and outside radius α

$$H_{\phi 4} = -B_4 \frac{j\omega\epsilon}{\gamma} K_1(\gamma r) \tag{14}$$

$$H_{r2} = -B_2 \frac{j\beta}{\gamma} K_1(\gamma r) \tag{15}$$

$$E_{\phi 2} = B_2 \frac{j\omega\mu}{\gamma} K_1(\gamma r) \tag{16}$$

$$E_{r4} = -B_4 \frac{j\beta}{\gamma} K_1(\gamma r). \tag{17}$$

The boundary conditions which must be satisfied at the cylinder of radius α are that the tangential electric field must be perpendicular to the helix direction

$$E_{z3} \sin \Psi + E_{\phi 1} \cos \Psi = 0 \tag{18}$$

$$E_{z4} \sin \Psi + E_{\phi 2} \cos \Psi = 0, \tag{19}$$

the tangential electric field must be continuous across the cylinder

$$E_{z3} = E_{z4} \text{ (and } E_{\phi 1} = E_{\phi 2}), \tag{20}$$

and the tangential component of magnetic field parallel to the helix direction must be continuous across the cylinder, since there can be no current in the surface perpendicular to this direction.

$$H_{z1} \sin \Psi + H_{\phi 3} \cos \Psi = H_{z2} \sin \Psi + H_{\phi 4} \cos \Psi. \tag{21}$$

These equations serve to determine the ratios of the B's and to determine γ through

$$(\gamma\alpha)^2 \frac{I_0(\gamma\alpha)K_0(\gamma\alpha)}{I_1(\gamma\alpha)K_1(\gamma\alpha)} = (\beta_0 \alpha \cot \Psi)^2. \tag{22}$$

We can easily express the various field components listed in (6) through (17) in terms of a common amplitude factor. As such expressions are useful in understanding the nature of the field, it seems desirable to list them in an orderly fashion.

Inside the Helix:

$$E_z = BI_0(\gamma r)e^{j(\omega t-\beta z)} \tag{23}$$

$$E_r = j\beta \frac{\beta}{\gamma} I_1(\gamma r)e^{j(\omega t-\beta z)} \tag{24}$$

$$E_\Phi = -B \frac{I_0(\gamma a)}{I_1(\gamma a)} \frac{1}{\cot \psi} I_1(\gamma r)e^{j(\omega t-\beta z)} \tag{25}$$

$$H_z = -j \frac{B}{k} \frac{\gamma}{\beta_0} \frac{I(\gamma a)}{I_1(\gamma a)} \frac{1}{\cot \psi} I_0(\gamma r)e^{j(\omega t-\beta z)} \tag{26}$$

$$H_r = \frac{B}{k} \frac{\beta}{\beta_0} \frac{I_0(\gamma a)}{I_1(\gamma a)} \frac{1}{\cot \psi} I_1(\gamma r)e^{j(\omega t-\beta z)} \tag{27}$$

$$H_\Phi = j \frac{B}{k} \frac{\beta_0}{\gamma} I(\gamma r)e^{j(\omega t-\beta z)}. \tag{28}$$

Outside the Helix:

$$E_z = B \frac{I_0(\gamma a)}{K_0(\gamma a)} K_0(\gamma r)e^{j(\omega t-\beta z)} \tag{29}$$

$$E_r = -jB \frac{\beta}{\gamma} \frac{I_0(\gamma a)}{K_0(\gamma a)} K_1(\gamma r)e^{j(\omega t-\beta z)} \tag{30}$$

$$E_\Phi = -B \frac{I_0(\gamma a)}{K_1(\gamma a)} \frac{1}{\cot \psi} K_1(\gamma r)e^{j(\omega t-\beta z)} \tag{31}$$

$$H_z = j \frac{B}{k} \frac{\gamma}{\beta_0} \frac{I_0(\gamma a)}{K_1(\gamma a)} \frac{1}{\cot \psi} K_0(\gamma r)e^{j(\omega t-\beta z)} \tag{32}$$

$$H_r = \frac{B}{k} \frac{I_0(\gamma a)}{K_1(\gamma a)} \frac{1}{\cot \psi} K_1(\gamma r)e^{j(\omega t-\beta z)} \tag{33}$$

$$H_\Phi = -j \frac{B}{k} \frac{\beta_0}{\gamma} \frac{I_0(\gamma a)}{K_0(\gamma a)} K_1(\gamma r)e^{j(\omega t-\beta z)} \tag{34}$$

Here

$$k = \sqrt{\mu/\epsilon} = 120\,\pi \text{ ohms} \tag{35}$$

The power associated with the propagation is given by

$$P = \tfrac{1}{2} \operatorname{Re} \int E \times H^* \, d\tau \tag{36}$$

taken over a plane normal to the axis of propagation. This is

$$P = \pi \operatorname{Re} \left[\int_0^a (E_r H_\Phi^* - E_\Phi H_r^*) r \, dr + \int_a^\infty (E_r H_\Phi^* - E_\Phi H_r^*) r \, dr \right] \tag{37}$$

or

$$\begin{aligned} P &= \pi E_z^2(0) \frac{\beta \beta_0^2}{\gamma^2 \omega \mu} \left[\left(1 + c \frac{I_0 K_1}{I_1 K_0} \right) \int_0^a I_1^2(\gamma r) r \, dr \right. \\ &\qquad \left. + \left(\frac{I_0}{K_0} \right)^2 \left(1 + \frac{I_1 K_0}{I_0 K_1} \right) \int_a^\infty K_1^2(\gamma r) r \, dr \right] \\ &= E_z^2(0) \frac{\pi}{2k} \frac{\beta \beta_0 \alpha^2}{\gamma^2} \left[\left(1 + \frac{I_0 K_1}{I_1 K_0} \right) (I_1^2 - I_0 I_2) \right. \\ &\qquad \left. + \left(\frac{I_0}{K_0} \right)^2 \left(1 + \frac{I_1 K_0}{I_0 K_1} \right) (K_0 K_2 - K_1^2) \right]. \end{aligned} \tag{38}$$

where $k = 120 \pi$ ohms.
Let us now write

$$(E_z^2/\beta^2 P)^{1/3} = (\beta/\beta_0)^{1/3} (\gamma/\beta)^{4/3} F(\gamma a) \tag{39}$$

where

$$\begin{aligned} F(\gamma\alpha) = \left\{ \left(\frac{(\gamma\alpha)^2}{240} \right) \left[(I_1^2 - I_0 I_2) \left(1 + \frac{I_0 K_1}{I_1 K_0} \right) \right. \right. \\ \left. \left. + \left(\frac{I_0}{K_0} \right)^2 (K_0 K_2 - K_1^2) \left(1 + \frac{I_1 K_0}{K_1 I_0} \right) \right] \right\}^{-1/3}. \end{aligned} \tag{40}$$

We can rewrite the expression for $F(\gamma\alpha)$ by using relations, Appendix I:

$$F(\gamma\alpha) = \left(\frac{\gamma\alpha}{240} \frac{I_0}{K_0} \left[\left(\frac{I_1}{I_0} - \frac{I_0}{I_1} \right) + \left(\frac{K_0}{K_1} - \frac{K_1}{K_0} \right) + \frac{4}{\gamma\alpha} \right] \right)^{-1/3}. \tag{41}$$

Communication in the Presence of Noise—Probability of Error for Two Encoding Schemes

By S. O. RICE

Recent work by C. E. Shannon and others has led to an expression for the maximum rate at which information can be transmitted in the presence of random noise. Here two encoding schemes are described in which the ideal rate is approached when the signal length is increased. Both schemes are based upon drawing random numbers from a normal universe, an idea suggested by Shannon's observation that in an efficient encoding system the typical signal will resemble random noise. In choosing these schemes two requirements were kept in mind: (1) the ideal rate must be approached, and (2) the problem of computing the probability of error must be tractable. Although both schemes meet both requirements, considerable work has been required to put the expression for the probability of error into manageable form.

1. Introduction

In recent work concerning the theory of communication it has been shown that the maximum or ideal rate of signaling which may be achieved in the presence of noise is (1, 2, 3, 4, 5)

$$R_I = F \log_2 (1 + W_S/W_N) \text{ bits/sec.} \tag{1-1}$$

In this expression F is the width of the frequency band used for signaling (which we suppose to extend from 0 to F cps), W_S is the average signaling power and W_N the average power of the noise. The noise is assumed to be random and to have a constant power spectrum of W_N/F watts per cps over the frequency band $(0, F)$.

This ideal rate is achieved only by the most efficient encoding schemes in which, as Shannon (1, 2) states, the typical signal has many of the properties of random noise. Here we shall study two different encoding schemes, both of them referring to a bandwidth F and a time interval T. By making the product FT large enough the ideal rate of signaling may be approached in either case* and we are interested in the probability of error for rates of signaling a little below the rate (1-1). The work given here is closely associated with Section 7 of Shannon's second paper (2).

In the first encoding scheme the signal corresponding to a given message lasts exactly T seconds, but (because the signal is zero outside this assigned interval of duration) the power spectrum of the signal is not exactly zero for frequencies exceeding F. In the second encoding scheme, the signal

* A recent analysis by M. J. E. Golay (*Proc. I. R. E.*, Sept. 1949, p. 1031) indicates that the ideal rate of signaling may also be approached by quantized PPM under suitable conditions.

power spectrum is limited to the band $(0, F)$ but the signal, regarded as a function of time, is not exactly zero outside its allotted interval of length T.

It turns out that both schemes lead to the same mathematical problem which may be stated as follows: Given two universes of random numbers both distributed normally about zero with standard deviations σ and ν, respectively. Let the first universe be called the σ (signal) universe and the second the ν (noise) universe. Draw $2N + 1$ numbers $A_{-N}^{(0)}, A_{-N+1}^{(0)}, \cdots, A_0^{(0)}, \cdots, A_N^{(0)}$ at random from the σ universe. These $2N + 1$ numbers may be regarded as the rectangular coordinates of a point P_0 in $2N + 1$-dimensional space. Draw $2N + 1$ numbers $B_{-N}, \cdots, B_0, \cdots, B_N$ at random from the ν universe and imagine a (hyper-) sphere S of radius $x_0^{1/2} = P_0Q$, where

$$x_0 = \sum_{n=-N}^{N} B_n^2 = \overline{P_0Q^2}, \tag{1-2}$$

centered on the point Q whose coordinates are $A_n^{(0)} + B_n$, $n = -N, \cdots, 0, \cdots, N$. Return to the σ universe, draw out K sets of $2N + 1$ numbers each, denote the kth set by $A_{-N}^{(k)}, \cdots, A_0^{(k)}, \cdots, A_N^{(k)}$ and the associated point by P_k.

What is the probability that none of the K points $P_1, \cdots, P_K$ lie within the sphere S? In other words what is the probability, which will be denoted by "Prob. $(P_1Q, \cdots, P_KQ > P_0Q)$," that the K distances $P_1Q, \cdots, P_KQ$ will all exceed the radius P_0Q? In terms of the A_n's and B_n's we ask for the probability that all K of the numbers $x_1, x_2, \cdots, x_K$ exceed x_0 where

$$x_k = \sum_{n=-N}^{N} (A_n^{(k)} - A_n^{(0)} - B_n)^2 = \overline{P_kQ^2} \tag{1-3}$$

Expression (1-2) for x_0 is seen to be a special case of (1-3). The relationship between the points P_0, Q, P_1, $P_2, \cdots, P_k, \cdots, P_K$ is indicated in Fig. 1.

The answer to this problem is given by the rather complicated expression (4-12) which, when written out, involves Bessel functions of imaginary argument and of order $N - 1/2$. When N and K become very large the work of Section 5 shows that the probability in question is given by

$$\text{Prob. } (P_1Q, \cdots, P_KQ > P_0Q) = (1 + \operatorname{erf} H)/2 + 0(1/K) + 0(N^{-1/2} \log^{3/2} N) \tag{1-4}$$

where, with $r = \nu^2/\sigma^2$,

$$H = \left(\frac{1 + r}{4N}\right)^{1/2} \left[(N + 1/2) \log_e (1 + 1/r) - \log_e (K + 1) + \frac{1}{2} \log_e \frac{2\pi N(1 + 2r)}{(1 + r)^2} \right] \tag{1-5}$$

The symbol $0(N^{-1/2} \log^{3/2} N)$ stands for a term of order $N^{-1/2} \log^{3/2} N$, i.e., a positive constant C and a value N_0 can be found such that the absolute value of the term in question is less than $CN^{-1/2} \log^{3/2} N$ when $N > N_0$. In order to obtain actual numerical values for C and N_0, considerably more work than is given here would be required. The term $0(1/K)$ is of the same nature. The "order of" terms have been carried along in the work of Section 5 in order to guard against error in the many approximations which are made in the derivation of (1-4).

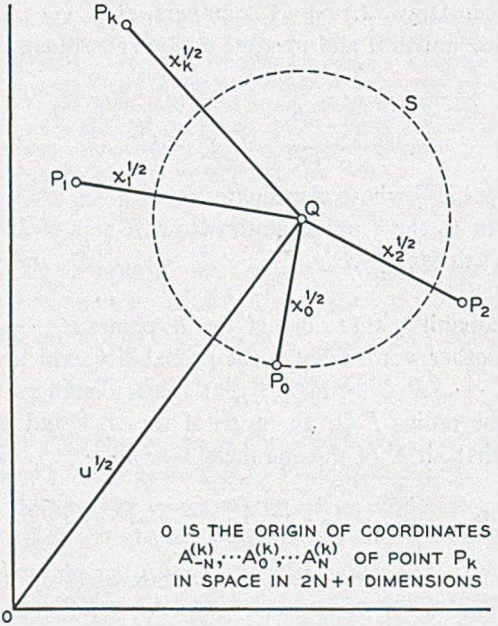

Fig. 1—Diagram indicating relationship between points P_0, Q, and P_k corresponding to signal, signal plus noise, and k^{th} signal not sent ($k > 0$), respectively.

The last term within the bracket in (1-5) has been retained even though it gives terms of order $N^{-1/2} \log N$ when (1-5) is put in (1-4) and could thus be included in $0(N^{-1/2} \log^{3/2} N)$. As shown by the table in the next paragraph, inclusion of this term considerably improves the agreement between (1-4) and values of Prob. $(P_1Q, \cdots, P_KQ > P_0Q)$ obtained by integrating the exact expression (4-12) numerically. This suggests that the term $0(N^{-1/2} \log^{3/2} N)$ in (1-4) is unnecessarily large.

Although the "order of" terms in (1-4) give us some idea of the accuracy of the approximation expressed by (1-4) and (1-5), a better one is desirable. With this in mind the lengthy task of computing the exact expression (4-12) for Prob. $(P_1Q, \cdots, P_KQ > P_0Q)$ by numerical integration was undertaken.

The values obtained in this way are listed in the second column of the following table. The values of Prob. $(P_1Q, \cdots, P_KQ > P_0Q)$ obtained from (1-4) (in which the "order of" terms are ignored) and (1-5) are given in the third column. Column IV lists values obtained from (1-4) and a simplified form of (1-5) obtained by omitting the last term in (1-5). These values are less accurate than those in the third column. The values in Column V are computed from (1-5) and a modified form of (1-4) obtained by adding the correction term shown in equation (5-53) (with $B = H$). The values in Column V are presumably the best that can be done with the approximations made in Section V of this paper, although the first entry renders this a little doubtful.

Prob. $(P_1Q, \cdots, P_KQ > P_0Q)$ for $N = 99.5$ & $r = 1$

$K+1$	*Numerical Integration*	(1-4) & (1-5)	*Col. IV*	*Col. V*
$2^{100}e^{-30}$	.994	.9995	.9987	1.0001
$2^{100}e^{-15}$	.962	.9650	.9337	.9710
2^{100}	.603	.621	.5000	.605
$2^{100}e^{15}$	.1196	.1159	.0663	.1176
$2^{100}e^{30}$	.0065	.00347	.0013	.00586

It will become apparent later that the value $K + 1 = 2^{100}$ corresponds to the ideal rate of signaling. The non-integer value of 99.5 for N is explained by the fact that the calculations were started before the present version of the theory was worked out. It will be noticed that for $K + 1 = 2^{100}e^{-30}$ all of the approximate values exceed the .994 obtained by numerical integration. I am in doubt as to whether the major part of the discrepancy is due to errors in numerical integration (due to the considerable difficulty encountered) or to errors in the approximations.

In both encoding schemes, the point P_0 corresponds to the transmitted signal, Q to the transmitted signal plus noise, and P_1, P_2, $\cdots$ P_K to K other possible signals. The average signal power turns out to be $(N + 1/2)\sigma^2$ and the average noise power to be $(N + 1/2)\nu^2$. Furthermore,

x_0 = twice the average power in the noise.
x_k = " " " " " " " plus the kth signal.

Prob. $(P_1Q, \cdots P_KQ > P_0Q)$ = Probability that none of the K other signals will be mistaken for the signal sent, i.e., the probability of no error.

The random numbers $A_n^{(k)}$ are taken to be distributed normally instead of some other way because this choice makes the encoding signals (in our two schemes) resemble random noise, a condition which seems to be necessary for efficient encoding (1, 2).

Both of the encoding schemes are concerned with sending, in an interval of duration T, one of $K + 1$ different messages. According to communication theory (1, 2, 3) this corresponds to sending at the rate of $T^{-1} \log_2 (K + 1)$ bits per second. However, instead of discussing the rate of transmission, it is more convenient, from the standpoint of (1-4), to deal with the total number of bits of information sent in time T. Thus, selecting and sending one of the $K + 1$ possible messages is equivalent to sending

$$M = \log_2(K + 1) \tag{1-6}$$

bits of information. M, or one of the adjacent integers if M is not an integer, is the number of "yes or no" questions required to select the sent message from the $K + 1$ possible messages (divide the $K + 1$ messages into two equal, or nearly equal, groups; select the group containing the sent message by asking the person who knows, "Is the sent message in the first group?"; proceed in this way until the last subgroup consists of only the sent message). The amount of information which would be sent in time T at the ideal rate R_I defined by (1-1) is

$$M_I = TR_I = FT \log_2 (1 + 1/r) = (N + 1/2) \log_2 (1 + 1/r) \tag{1-7}$$

where use has been made of $W_N/W_S = \nu^2/\sigma^2 = r$, and the relation $N < FT < N + 1$ (which turns out to be common to both encoding schemes) has been approximated by $N + 1/2 = FT$.

When (1-6) and (1-7) are used to eliminate N and K from (1-5) the result is an expression for the actual amount M of information sent (in time T) in terms of (1) the amount M_I which is sent by transmitting at the ideal rate (1-1) for a time T, (2) the ratio r of the noise power to the signal power, and (3) the probability of no error in sending M bits of information in time T, this probability being given as $(1 + \text{erf } H)/2$:

$$M = M_I - aM_I^{1/2}H + b \tag{1-8}$$

where

$$a = 2\left[\frac{\log_2 e}{(1 + r) \log_e (1 + 1/r)}\right]^{1/2},$$
$$b = \frac{1}{2} \log_2 \left[\frac{2\pi(1 + 2r)M_I}{(1 + r)^2 \log_2 (1 + 1/r)}\right] \tag{1-9}$$

Here the "order of" terms in (1-4) have been neglected together with similar terms which arise when $N + 1/2$ is used for N in computing a and b. The term b is usually small compared to $aM_I^{1/2}H$.

The more slowly we send, the less chance there is of error. The relationship between M, M_I and the probability of no error, as computed from

(1–8), is shown in the following table. The probability of no error is denoted by p and the terms are given in the same order as on the right of (1–8) in order to show their relative importance. The ratio $M/M_I(=R/R_I)$ for $r = 0.1$ is shown as a function of M in Fig. 2.

For $r = W_N/W_S = 0.1$

M_I bits	M for $p = .5$	M for $p = .99$	M for $p = .99999$
10^2	$M_I - 0 + 3.75$	$M_I - 24.3 + 3.75$	$M_I - 44.6 + 3.75$
10^4	" " $+ 7.07$	" $- 243 + 7.07$	" $- 446 + 7.07$
10^6	" " $+ 10.38$	" $- 2430 + 10.38$	" $- 4460 + 10.38$

For $r = W_N/W_S = 1$

10^2	$M_I - 0 + 4.44$	$M_I - 33.4 + 4.44$	$M_I - 61.2 + 4.44$
10^4	" " $+ 7.76$	" $- 334 + 7.76$	" $- 612 + 7.76$
10^6	" " $+ 11.08$	" $- 3340 + 11.08$	" $- 6120 + 11.08$

There may be some question as to the accuracy of the values for $p = .99999$, especially for $M_I = 100$, since this corresponds to points on the tail of the probability distribution where the "order of" terms in (1-4) become relatively important.

Of course, for a given bandwidth, the ideal rate of signaling R_I (given by (1-1)) for $r = .1$ exceeds that for $r = 1$ in the ratio $(\log_2 11)/(\log_2 2) = 3.46$.

The above results agree with the statement that, by efficient encoding, the rate of signaling R can be made to approach the ideal rate $R_I = M_I/T$ given by (1-1). As applied to our two schemes, the term "efficient encoding" means using a very large value of FT or N. To see this, divide both sides of (1-8) by M_I and rearrange the terms:

$$1 - M/M_I = aH\, M_I^{-1/2} + 0(M_I^{-1} \log M_I) \qquad (1\text{-}10)$$

When M_I is replaced by $R_I T$ in M/M_I, the fraction M/T occurs. We shall set $R = M/T$ and call R the rate of signaling corresponding to some fixed probability of error (which determines H). Thus, when (1-7) and the definition (1-9) for a are used, (1-10) goes into

$$\frac{(R_I - R)}{R_I} = \frac{2H}{[(1 + r)FT]^{1/2} \log_e (1 + 1/r)} + 0((\log FT)/FT) \qquad (1\text{-}11)$$

Equation (1-11) shows that when r and H are fixed (i.e. when the noise power/signal power and the probability of error are fixed) R/R_I approaches unity as $FT \to \infty$. This is shown in Fig. 2 for the case $r = 0.1$. Since $R/R_I = M/M_I$, M/M_I must approach unity and consequently M as well as M_I in-

creases linearly with FT. Thus, for efficient encoding M is large and, from (1-6), so is K.

It should be remembered that equation (1-8) has been established only for the two encoding schemes of this article. The question of how much faster M/T approaches R_I for the more efficient encoding schemes mentioned at the end of Section 2 still remains unanswered.

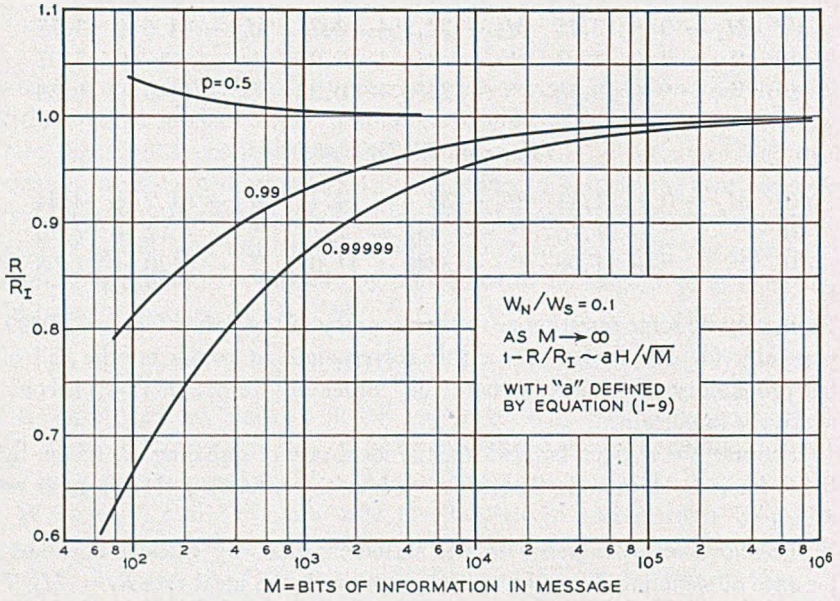

Fig. 2—Curves showing the approach of R/R_I ($= M/M_I$) to unity as the message length increases and the probability of no error remains fixed. R is the rate of signaling at which the probability of no error is p and R_I is the ideal rate.

It gives me pleasure to acknowledge the help I have received in the preparation of this memorandum from conversations with Messrs. H. Nyquist, John Riordan, C. E. Shannon, and M. K. Zinn. I am also indebted to Miss M. Darville for computing the tables shown above and for checking a number of the equations numerically.

2. The First Encoding Scheme

Suppose that we have $K + 1$ different messages any one of which is to be transmitted over a uniform frequency band extending from zero to the nominal cut-off frequency F in a time interval of length T. The adjective "nominal" is used because the sudden starting and stopping of the signals given by the first encoding scheme produces frequency components higher

than F. A shortcoming of this nature must be accepted since it is impossible to have a signal possessing both finite duration and finite bandwidth.

The first step of the encoding process is to compute the integer N given by

$$N < FT < N + 1 \tag{2-1}$$

We assume that FT is not an integer in order to avoid borderline cases. Let W_S be the average signal power available for transmission and define the standard deviation σ of the σ universe introduced in Section 1 by $(N + 1/2)\sigma^2 = W_S$. To encode the first message, draw $2N + 1$ numbers $A_{-N}^{(0)}, \cdots, A_0^{(0)}, \cdots A_N^{(0)}$ at random from the σ universe. The signal corresponding to the first message is then taken to be

$$I_0(t) = 2^{-1/2}A_0^{(0)} + \sum_{n=1}^{N} (A_n^{(0)} \cos 2\pi nt/T + A_{-n}^{(0)} \sin 2\pi nt/T) \tag{2-2}$$

The remaining K messages are encoded in the same way, the signal representing the kth message being

$$I_k(t) = 2^{-1/2}A_0^{(k)} + \sum_{n=1}^{N} (A_n^{(k)} \cos 2\pi nt/T + A_{-n}^{(k)} \sin 2\pi nt/T). \tag{2-3}$$

It is apparent that each signal consists of a d-c term plus terms corresponding to N discrete frequencies, the highest being $N/T < F$, and that the average power (assuming $I_k(t)$ to flow through a unit resistance) in the kth signal is

$$T^{-1} \int_{-T/2}^{T/2} I_k^2(t)\, dt = 2^{-1}(A_0^{(k)})^2 + \sum_{n=1}^{N} 2^{-1}[(A_n^{(k)})^2 + (A_{-n}^{(k)})^2] \tag{2-4}$$

Since the A's were drawn from a universe of standard deviation σ, the expected value of the right hand side is $(2N + 1)\sigma^2/2$ which is equal to the average signal power W_S, as required.

We pick one of the $K + 1$ messages at random and send the corresponding signal over a transmission system subject to noise. We choose our notation so that the sent signal is represented by $I_0(t)$ as given by (2-2). Let the noise be given by

$$J(t) = 2^{-1/2}B_0 + \sum_{n=1}^{N} (B_n \cos 2\pi nt/T + B_{-n} \sin 2\pi nt/T) \tag{2-5}$$

where $B_{-N}, \cdots, B_0, \cdots, B_N$ are $(2N + 1)$ numbers drawn at random from the normally distributed ν universe mentioned in the introduction. The standard deviation ν of the universe is given by $(N + 1/2)\nu^2 = W_N$, W_N being the average noise power. We call $J(t)$ simply "noise" rather than

"random noise" to emphasize that (2-5) does not represent a random noise current unless N and T approach infinity.

The input to the receiver is $I_0(t) + J(t)$. Let the process of reception consist of computing the $K + 1$ integrals

$$x_k = 2T^{-1} \int_{-T/2}^{T/2} [I_k(t) - I_0(t) - J(t)]^2 \, dt, \qquad k = 0, 1, \cdots, K \tag{2-6}$$

and selecting the smallest one (all of the $K + 1$ encodings have been carried to the receiver beforehand). If the value of k corresponding to the smallest integral happens to be 0, as it will be if the noise $J(t)$ is small, no error is made. In any other case the receiver picks out the wrong message.

When the representations (2-2), (2-3), and (2-5) are put in (2-6) and the integrations performed, it is found that

$$x_k = \sum_{n=-N}^{N} (A_n^{(k)} - A_n^{(0)} - B_n)^2, \qquad x_0 = \sum_{n=-N}^{N} B_n^2 \tag{2-7}$$

which have already appeared in equations (1-2) and (1-3). If, as in Section 1, P_k is interpreted as a point in $2N + 1$ — dimensional Euclidean space with coordinates $A_{-N}^{(k)}, \cdots, A_0^{(k)}, \cdots, A_N^{(k)}$ and Q is the point $A_{-N}^{(0)} + B_{-N}, \cdots, A_0^{(0)} + B_0, \ldots, A_N^{(0)} + B_N$, then x_k is the square of the distance between points P_k and Q. Point P_0 corresponds to the signal actually sent, points $P_1, \cdots, P_K$ to the remaining signals, and point Q to the signal plus noise at the receiver. The expected distance between the origin and P_k is $\sigma(2N + 1)^{1/2} = (2W_S)^{1/2}$, that between P_0 and Q is $\nu(2N + 1)^{1/2} = (2W_N)^{1/2}$, and that between the origin and Q is

$$(\sigma^2 + \nu^2)^{1/2}(2N + 1)^{1/2} = (2W_N + 2W_S)^{1/2}$$

No error is made when x_0 is less than every one of $x_1, x_2, \cdots, x_K$, i.e., when none of the points $P_1, \cdots, P_K$ lies within the sphere S of radius $x_0^{1/2}$ centered on Q and passing through P_0. Therefore the probability of obtaining no error when the first encoding scheme is used is equal to the probability denoted by Prob. $(P_1Q, \cdots, P_KQ > P_0Q)$ in the mathematical problem of Section 1.

One might wonder why probability theory has played such a prominent part in the encoding scheme just described. It is used because we do not know the best method of encoding. In fact, it would not be used if we knew how to solve the following problem:* Arrange $K + 1$ points $P_0, \cdots P_K$ on the hyper-surface of the $2N + 1$ — dimensional sphere of radius $(2W_S)^{1/2}$

* C. E. Shannon has commented that although the solution of this problem leads to a good code, it may not be the best possible, i.e., it is not obvious that the code obtained in this way is the same as the one obtained by choosing a set of points so as to minimize the probability of error (calculated from the given set of points and some given W_N) averaged over all $K + 1$ points.

in such a way that the smallest of the $K(K+1)/2$ distances P_kP_ℓ, $k, \ell = 0, 1, \cdots, K, k \neq l$, has the largest possible value. This would maximize the difference (as measured by the distance between their representative points) between the two (or more) most similar encoding signals.†

In this paper we have been forced to rely on the randomness of probability theory to secure a more or less uniform scattering of the points $P_0, \cdots, P_K$. In our work they do not lie exactly on a sphere of radius $(2W_S)^{1/2}$ but this causes us no trouble.

3. The Second Encoding Scheme

The second of the two encoding schemes is suggested by one of Shannon's (2) proofs of the fundamental result (1-1). In this scheme the $K+1$ messages are to be sent over a transmission system having a frequency band extending from zero to F cycles per second, and are to be sent during a time interval of nominal length T.

The first few steps in the encoding process are just the same as in the first scheme. N is still given by (2-1) and σ by $(N+1/2)\sigma^2 = W_S$. After drawing $K+1$ sets of A's, with $2N+1$ in each set, the $K+1$ messages are encoded so that the signal corresponding to the kth message, $k = 0, 1, \cdots, K$, is

$$I_k(t) = (FT)^{1/2} \sum_{n=-N}^{N} A_n^{(k)} \frac{\sin \pi(2Ft - n)}{\pi(2Ft - n)} \tag{3-1}$$

From (3-1), the value of $I_k(t)$ at $t = n/(2F)$ is zero if the integer n exceeds N in absolute value. If the integer n is such that $|n| \leq N$, the corresponding value of $I_k(t)$ is $(FT)^{1/2}A_n^{(k)}$. The energy in the kth signal is obtained by squaring both sides of (3-1) and integrating with respect to t. Thus

$$\int_{-\infty}^{\infty} I_k^2(t)\, dt = 2^{-1}T \sum_{n=-N}^{N} A_n^{(k)2} \tag{3-2}$$

which has the expected value $(N+1/2)\sigma^2T$. The average power developed when this amount of energy is expended during the nominal signal length T is $(N+1/2)\sigma^2$ which is equal to W_S, as it should be.

The noise introduced by the transmission system is taken to be

$$J(t) = (FT)^{1/2} \sum_{n=-N}^{N} B_n \frac{\sin \pi(2Ft - n)}{\pi(2Ft - n)} \tag{3-3}$$

† Possibly if $K+1$ discrete unit charges of electricity were allowed to move freely on the sphere, their mutual repulsion would separate them in the required manner. In $2N+1$ dimensions this leads to the problem of minimizing the mutual potential energy

$$\tfrac{1}{2}\Sigma(\overline{P_kP_\ell})^{-2N+1}$$

where $N \geq 1$ and the summation extends over $k, \ell = 0, 1, \ldots K$ with $k \neq \ell$. However, this problem also appears to be difficult.

where the ν universe from which the B's are drawn has, as before, standard deviation ν given by $(N + 1/2)\nu^2 = W_N$. When the signal $I_0(t)$ is sent, the input to the receiver is $I_0(t) + J(t)$ and the process of reception consists of selecting the smallest of the $K + 1$ x_k's

$$x_k = 2T^{-1} \int_{-\infty}^{\infty} [I_k(t) - I_0(t) - J(t)]^2 \, dt \tag{3-4}$$

$$= \sum_{n=-N}^{N} (A_n^{(k)} - A_n^{(o)} - B_n)^2$$

The second expression for x_k is the same as the one given by (2-7) for the first encoding scheme, and the discussion in Section 2 following (2-7) may also be applied to the second encoding scheme. In particular, the probability of obtaining no error in transmitting a signal through noise is the same in both systems of encoding, and is given by the Prob. $(P_1Q, \cdots, P_KQ > P_0Q)$ of the mathematical problem of Section 1.

4. Solution of the Mathematical Problem

We shall simplify the work of solving the mathematical problem stated in Section 1 by taking $\sigma = 1$ and $\nu^2/\sigma^2 = r$. First regard the $4N + 2$ numbers $A_n^{(0)}$, B_n, $n = -N, \cdots, N$ as fixed or given beforehand. Geometrically, this corresponds to having the points P_0 and Q given. Select a typical set of random variables $A_n^{(k)}$, $n = -N, \cdots, N$, $k > 0$ and consider the associated set of variables

$$y_n = A_n^{(k)} - A_n^{(0)} - B_n = A_n^{(k)} + \bar{y}_n. \tag{4-1}$$

y_n is a random variable distributed normally about its average value

$$\bar{y}_n = -A_n^{(0)} - B_n \tag{4-2}$$

with standard deviation $\sigma = 1$. The quantity x_k, defined by (1-3) and representing the square of the distance between P_k and Q, may be written as

$$x_k = \sum_{n=-N}^{N} y_n^2 \tag{4-3}$$

Thus x_k is the sum of the squares of $2N + 1$ independent and normally distributed variates, having the same standard deviation but different average values. The probability density of such a sum is remarkable in that it does not depend upon the $\bar{y}_n$'s individually but only on the smu of their squares which we denote by

$$u = \sum_{n=-N}^{n} \bar{y}_n^2 = \sum_{n=-N}^{n} (A_n^{(0)} + B_n)^2$$

$$= 2T^{-1}\left[\begin{matrix}\text{Energy in sent signal} + \text{Energy} \\ \text{in noise}\end{matrix}\right] \tag{4-4}$$

This behavior follows from the fact that the probability density of P_k has spherical symmetry about the origin (because all the $A_n^{(k)}$'s have the same σ). For the probability that x_k is less than some given value x is the probability that P_k lies within a sphere of radius $x^{1/2}$ centered on Q, and this, because of the symmetry, depends only on x and the distance $u^{1/2}$ of Q from the origin. Accordingly, we write $p(x, u)dx$ for the probability that $x < x_k < x + dx$ when the $\bar{y}_n'$'s (and hence u) are fixed.

The probability density $p(x, u)$ may be obtained from its characteristic function:

$$p(x, u) = (2\pi)^{-1} \int_{-\infty}^{\infty} e^{-izx} [\text{ave. } e^{izx}]\, dz$$

$$\text{ave. } e^{izx} = \text{ave. exp} \left[iz \sum_{n=-N}^{N} y_n^2 \right] \tag{4-5}$$

$$= \prod_{n=-N}^{N} \text{ave. exp } [izy_n^2] = (1 - 2iz)^{-N-1/2} \exp [iuz(1 - 2iz)^{-1}]$$

where we have used (4-3) and, since y_n is distributed normally about $\bar{y}_n$,

$$\text{ave. exp } [izy_n^2] = (2\pi)^{-1/2} \int_{-\infty}^{\infty} e^{izy_n^2 - (y_n - \bar{y}_n)^2/2}\, dy_n$$

$$= (1 - 2iz)^{-1/2} \exp [\bar{y}_n^2\, iz(1 - 2iz)^{-1}]$$

Hence

$$p(x, u) = (2\pi)^{-1} \int_{-\infty}^{\infty} (1 - 2iz)^{-N-1/2} \exp [izu(1 - 2iz)^{-1} - izx]\, dz \tag{4-6}$$

$$= 2^{-1}(x/u)^{N/2-1/4} I_{N-1/2}[(ux)^{1/2}]\, e^{-(u+x)/2}$$

where it is to be understood that x is never negative. The Bessel function of imaginary argument appears when we change the variable of integration from z to t by means of $1 - 2iz = 2t/x$, and bend the path of integration to the left in the t plane (6). This expression for the probability density of the sum of the squares of a number of normal variates having the same standard deviation but different averages has been given by R. A. Fisher (7).

We are now in a position to solve the following problem which is somewhat simpler than the one stated in Section 1: Given the $2N + 1$ coordinates $A_n^{(0)}$ of the point P_0 and the $2N + 1$ numbers B_n so that the coordinates $A_n^{(0)} + B_n$ of the point Q are given. What is the probability that none of the K points $P_1, P_2, \cdots, P_K$, whose coordinates $A_n^{(k)}$ are drawn at random from a universe distributed normally about zero with standard deviation $\sigma = 1$, be inside the sphere centered on the given point Q and passing through the other given point P_0? In other words, what is the probability that all K of the

independent random variables $x_1, x_2, \cdots, x_K$ will exceed the given value x_0 when u has the value defined by (4-4) together with the given values of the $A_n^{(0)}$'s and B_n's? The variables $x_1, x_2, \cdots, x_K$ have the probability density $p(x, u)$ shown in (4-6) and x_0 is defined by (1-2) and the given values of the B_n's.

The answer to the above problem follows at once when we note that the probability of any one of $x_1, \cdots, x_K$, say x_1 for example, being less than x_0 is

$$P(x_0, u) = \int_0^{x_0} p(x, u)\, dx. \tag{4-7}$$

The probability of x_1 exceeding x_0 is then $1 - P(x_0, u)$ and the probability of all K of $x_1, \cdots, x_K$ exceeding x_0 is

$$[1 - P(x_0, u)]^K \tag{4-8}$$

Instead of being assigned quantities, x_0 and u are actually random variables when we consider the problem of Section 1. Now we take up the problem of finding the probability density of u when x_0 is fixed. Thus, from (4-4), we wish to find the probability density of

$$u = \sum_{n=-N}^{N} (A_n^{(0)} + B_n)^2 \tag{4-9}$$

in which the $2N + 1$ numbers $A_n^{(0)}$ are drawn at random from a universe distributed normally about zero with standard deviation $\sigma = 1$ and the numbers $B_{-N}, \cdots, B_0, \cdots, B_N$ are given. It is seen that u is the sum of the squares of $2N + 1$ normal variates all having the standard deviation $\sigma = 1$. The nth variate, $A_n^{(0)} + B_n$, has the average value B_n. This is just the problem which was encountered at the beginning of this section. Equation (4-9) is of the same form as (4-3) and we have the following correspondence:

Equation (4-3)	*Equation (4-9)*
x_k	u
y_n	$A_n^{(0)} + B_n$
$\bar{y}_n$	B_n
$u = \sum \bar{y}_n^2$	$x_0 = \sum B_n^2$

The probability that u lies in the interval $u, u + du$ when x_0 is given is therefore $p(u, x_0)\, du$ where $p(u, x_0)$ is obtained by putting u for x and x_0 for u in the probability density $p(x, u)$.

Until now x_0 has been fixed. At this stage we regard $B_{-N}, \cdots, B_0, \cdots, B_N$ as random variables drawn from a normal universe of average zero and standard deviation $\nu = \sigma r^{1/2} = r^{1/2}$. If the standard deviation were unity,

the probability density of x_0 could be obtained directly from $p(x, u)$ by letting $u \to 0$ in (4-6). As it is, the x's appearing in the resulting expression must be divided by r to obtain the correct expression. Thus, the probability of finding x_0 between x_0 and $x_0 + dx_0$ is

$$p_0(x_0) = \frac{[x_0/2r]^{N-1/2}}{2r\Gamma(N + 1/2)} \cdot e^{-x_0/2r} \tag{4-10}$$

which is of the χ^2 type frequently encountered in statistical theory.

It follows that the probability of finding u in $(u, u + du)$ and x_0 in $(x_0, x_0 + dx_0)$ at the same time is $p_0(u, x_0)\, du\, dx_0$ where

$$\begin{aligned} p_0(u, x_0) &= p(u, x_0)p_0(x_0) \\ &= \frac{1}{4r\Gamma(N + 1/2)} \left(\frac{ux_0}{4r^2}\right)^{N/2-1/4} I_{N-1/2}[(x_0 u)^{1/2}]\, e^{-[u+x_0(1+1/r)]/2} \end{aligned} \tag{4-11}$$

The replacement of (x, u) in (4-6) by (u, x_0) should be noted.

Now that we have the probability density of u and x_0 we may combine it with the probability (4-8) that all K of $x_1, \cdots, x_K$ exceed x_0 when x_0 and u are fixed. The result is the answer to the problem stated in Section 1:

$$\begin{aligned} &\text{Prob. } (P_1Q, \cdots, P_KQ > P_0Q) \\ &\quad = \int_0^\infty du \int_0^\infty dx_0\, p_0(u, x_0)[1 - P(x_0, u)]^K \end{aligned} \tag{4-12}$$

This result is more complicated than it seems, for $p_0(u, x_0)$ is given by (4-11) and $P(x_0, u)$ is obtained by integrating $p(x, u)$ of (4-6) from $x = 0$ to $x = x_0$ in accordance with (4-7). The remaining portion of the paper is concerned with obtaining an approximation to (4-12) which holds when N and K are very large numbers.

5. Behavior of Prob. $(P_1Q, \cdots, P_KQ > P_0Q)$ as N and K Become Large

In this section we introduce a number of approximations which lead to a manageable expression for Prob. $(P_1Q, \cdots, P_KQ > P_0Q)$ when N and K become large.

Since u and x_0 are sums of independent random variables, namely

$$\begin{aligned} u &= \sum_{n=-N}^{N} (A_n^{(0)} + B_n)^2 \\ x_0 &= \sum_{n=-N}^{N} B_n^2, \end{aligned} \tag{5-1}$$

the central limit theorem tells us that the probability density $p_0(u, x_0)$ approaches a two-dimensional normal distribution centered on the average

values

$$\bar{u} = \sum_{n=-N}^{N} \text{ave.}\,[A_n^{(0)2} + B_n^2] = (2N + 1)(1 + r)$$
$$\bar{x}_0 = \sum_{n=-N}^{N} \text{ave.}\, B_n^2 = (2N + 1)r \tag{5-2}$$

Here we keep the convention $\sigma = 1$, $v^2/\sigma^2 = r$ used in Section 4. The same sort of reasoning as used to establish (5-2) shows that the spread about these average values is given by

$$\begin{aligned} \text{ave.}\,(u - \bar{u})^2 &= (4N + 2)(1 + r)^2 \\ \text{ave.}\,(x_0 - \bar{x}_0)^2 &= (4N + 2)r^2 \\ \text{ave.}\,(u - \bar{u})(x_0 - \bar{x}_0) &= (4N + 2)r^2 \end{aligned} \tag{5-3}$$

If the parameters N, K, and r in the integral (4-12) are such that its value is appreciably different from zero, most of the contribution comes from the region around $\bar{u}$ and $\bar{x}_0$ where $p_0(u, x_0)$ is appreciably different from zero. However, instead of taking $\bar{u}$ and $\bar{x}_0$ as reference values, we take the nearby values

$$\begin{aligned} u_2 &= \bar{u} - 2 - 2r = (2N - 1)(1 + r) = 2q(1 + r) \\ x_2 &= \bar{x}_0 - 2r = (2N - 1)r = 2qr \end{aligned} \tag{5-4}$$

as these turn out to be better representatives of the center of the distribution. We have introduced the number

$$q = N - 1/2 \tag{5-5}$$

in order to simplify the writing of later equations. We assume $q > 1$.

First, we shall show that

$$\begin{aligned} &\text{Prob.}\,(P_1Q, \cdots, P_KQ > P_0Q) \\ &\quad = \int_{u_2-a}^{u_2+a} du \int_{x_2-b}^{x_2+b} dx_0\, p_0(u, x_0)[1 - P(x_0, u)]^K + R_1 \end{aligned} \tag{5-6}$$

where $a = 2(1 + r)(2q \log q)^{1/2}$, $b = 2r(2q \log q)^{1/2}$ and R_1 is of order $1/q$ (denoted by $0(1/q)$), i.e. a constant C and a value q_0 can be found such that $|R_1| < C/q$ when $q > q_0$. From (4-12) it is seen that R_1 is positive and less than

$$\begin{aligned} &\left[\int_0^{u_2-a} du + \int_{u_2+a}^{\infty} du\right] \int_0^{\infty} dx_0\, p_0(u, x_0) \\ &\qquad + \left[\int_0^{x_2-b} dx_0 + \int_{x_2+b}^{\infty} dx_0\right] \int_0^{\infty} du p_0(u, x_0) \end{aligned} \tag{5-7}$$

Since $p_0(u, x_0)$ is the joint probability density of u and x_0, the integration with respect to x_0 in the first part of (5-7) yields the probability density of u, and the integration with respect to u in the second part gives the probability density $p_0(x_0)$ (stated in (4-10)) of x_0. Thus (8)

$$\begin{aligned} \int_0^\infty dx_0\, p_0(u, x_0) &= \frac{[u/2(1+r)]^q\, e^{-u/2(1+r)}}{2(1+r)\Gamma(q+1)} \\ \int_0^\infty du p_0(u, x_0) &= \frac{[x_0/2r]^q\, e^{-x_0/2r}}{2r\Gamma(q+1)} \end{aligned} \tag{5-8}$$

Setting (5-8) in (5-7) and putting $u = 2(1+r)y$ and $x_0 = 2ry$ in the two parts of (5-7) reduces them to the same form. Thus (5-7) is equal to

$$2 - \frac{2}{\Gamma(q+1)} \int_{q-\ell}^{q+\ell} y^q e^{-y}\, dy \tag{5-9}$$

with $\ell = (2q \log q)^{1/2}$. In order to show that (5-9) is $0(1/q)$ we use the expansion

$$-y + q \log y = -q + q \log q - (y-q)^2/(2q) + (y-q)^3/(3q^2) - (y-q)^4 q[q + (y-q)\theta]^{-4}/4$$

where $0 \leqslant \theta \leqslant 1$. Let v represent the sum of the $(y-q)^3$ and $(y-q)^4$ terms, and expand $\exp v$ as $1 + v$ plus a remainder term. The integral of $\exp -(y-q)^2/(2q)$, taken between the limits $q \pm \ell$, can be shown to be of the form $1 - 0(1/q)$ by integrating by parts as in obtaining the asymptotic expansion for the error function. The term in $(y-q)^3$ vanishes upon integration and the remainder terms may be shown to be of $0(1/q)$. In all of this work a square root of q comes in through the fact that

$$1 > (2\pi q)^{1/2} q^q e^{-q}/\Gamma(q+1) > \exp[-1/(12q)] \tag{5-10}$$

We have just shown that the error introduced by restricting the region of integration as indicated by (5-6) introduces an error of order $1/q$ which vanishes as $q \to \infty$. The normal law approximation to $p_0(u, x_0)$ predicted by the central limit theorem holds over this restricted region. However, instead of appealing to the central limit theorem to determine the accuracy of the approximation, we prefer to deal directly with the functions involved.

Consideration of (5-4) and the behavior of $p_0(u, x_0)$ suggests the substitution

$$\begin{aligned} x_0 &= 2r(q+\alpha) \\ u &= 2(1+r)(q+\beta) \end{aligned} \tag{5-11}$$

where α and β are new variables whose absolute values never exceed $(2\ q\ \log\ q)^{1/2}$ in the restricted region of integration of (5-6). From (4-11)

$$p_0(u, x_0)\ du\ dx_0 = \frac{(1 + r)}{\Gamma(q + 1)} \left(\frac{z}{4r^2}\right)^{q/2} I_q(z^{1/2}) e^{-(1+r)(2q+\alpha+\beta)}\ d\alpha\ d\beta \tag{5-12}$$

in which

$$z = ux_0 = 4r(1 + r)(q + \alpha)(q + \beta) \tag{5-13}$$

In Appendix II it is shown that

$$I_q(z^{1/2}) = \frac{q^{q+1/2}\ e^{-q}\ z^{q/2} \exp\ [(q^2 + z)^{1/2} + V]}{\Gamma(q + 1)(q^2 + z)^{1/4}[q + (q^2 + z)^{1/2}]^q} \tag{5-14}$$

where $|\ V\ | < 1/(2q - 1)$ when $q > 1$. Upon using (5-10) and (5-14) the right hand side of (5-12) may be written as

$$d\alpha\ d\beta(2\pi)^{-1/2}(1 + r)(2r)^{-q}(q^2 + z)^{-1/4} \exp\ [-(1 + r)(2q + \alpha + \beta) + f(z) - \log\ \Gamma(q + 1) + 0(1/q)] \tag{5-15}$$

with

$$f(z) = q\ \log\ z - q\ \log\ [q + (q^2 + z)^{1/2}] + (q^2 + z)^{1/2} \tag{5-16}$$

The value z_2 of z corresponding to the central point (u_2, x_2) of $p_0(u, x_0)$ is obtained by putting $\alpha = \beta = 0$ in (5-13):

$$\begin{aligned} z_2 &= 4r(1 + r)q^2 \\ z - z_2 &= 4r(1 + r)[q(\alpha + \beta) + \alpha\beta]. \end{aligned} \tag{5-17}$$

Since we are interested in the form of $p_0(u, x_0)$ in the restricted region of integration of (5-6) we expand $f(z)$ about $z = z_2$ in a Taylor's series plus a remainder term.

$$\begin{aligned} f(z) &= q\ \log\ 2rq + q(1 + 2r) + (z - z_2)/(4rq) \\ &\quad - \frac{(z - z_2)^2}{32r^2q^3(1 + 2r)} + \frac{(z - z_2)^3}{3!}\left[\frac{(\xi_3 + q)^3(3\xi_3 - q)}{8\ z_3^3\ \xi_3^3}\right] \end{aligned} \tag{5-18}$$

In the last term $z_3 = z_2 + (z - z_2)\theta$, $0 \leqslant \theta \leqslant 1$, $\xi_3^2 = q^2 + z_3$. The work of obtaining this expansion is simplified if $(q^2 + z)^{1/2}$ is replaced by ξ in (5-16) before differentiating. For example, by using $2\xi'\xi = 1$, it can be shown that $f'(z)$ is simply $(q + \xi)/(2z)$. When the extreme values of α and β are put in (5-17), it is seen that $z - z_2$ does not exceed $0(q^{3/2}\ \log^{1/2}\ q)$ in the restricted region of integration. In the last term of (5-18) z_3 is $0(q^2)$, ξ_3 is $0(q)$ and consequently the last term itself is $0(q^{-1/2}\ \log^{3/2}\ q)$.

When the expression (5-17) for $(z - z_2)$ is put in (5-18) an expression for $f(z)$ is obtained. This expression, together with

$$\log \Gamma(q + 1) = (q + 1/2) \log q - q + (1/2) \log 2\pi + 0(1/q),$$

enables us to write the argument of the exponential function in (5-15) as $q \log 2r - (1/2) \log 2\pi q - Q(\alpha, \beta) + 0(q^{-1/2} \log^{3/2} q)$ where $Q(\alpha, \beta)$ denotes the quadratic function

$$\begin{aligned} Q(\alpha, \beta) &= [(1 + r)^2(\alpha^2 + \beta^2) - 2r(1 + r)\alpha\beta]D \\ D &= 1/[2q(1 + 2r)] \end{aligned} \tag{5-19}$$

Similar considerations show that

$$(q^2 + z)^{-1/4} = q^{-1/2}(1 + 2r)^{-1/2}[1 + 0(q^{-1/2} \log^{1/2} q)] \tag{5-20}$$

When the above results are gathered together it is found that (5-12) may be written as

$$p_0(u, x_0)\, du\, dx_0 = D_1 \exp [-Q(\alpha, \beta) + 0(q^{-1/2} \log^{3/2} q)]\, d\alpha\, d\beta \tag{5-21}$$

where

$$D_1 = \frac{1 + r}{2\pi q(1 + 2r)^{1/2}} \tag{5-22}$$

Expression (5-21) is valid as long as $|\alpha|$ and $|\beta|$ do not exceed

$$(2q \log q)^{1/2}.$$

Expression (5-21) differs from the one predicted by the central limit theorem (and (5-2) and (5-3)) in that it is not quite centered on the average values $\bar{x}_0$, $\bar{u}$, which correspond to $\alpha = 1$, $\beta = 1$, respectively. Also, q enters in place of $q + 1$. However, these differences amount to $0(q^{1/2} \log^{1/2} q)$ at most, as may be seen by putting $\alpha - 1$ and $\beta - 1$ for α and β in (5-19).

By using relations (5-6) and (5-21), it may be shown that

$$\begin{aligned} &\text{Prob. } (P_1Q, \cdots, P_KQ > P_0Q) \\ &= \int_{-q}^{\infty} d\alpha \int_{-c}^{\infty} d\beta\, D_1 e^{-Q(\alpha,\beta)}[1 - P(x_0, u)]^K + 0(q^{-1/2} \log^{3/2} q) \end{aligned} \tag{5-23}$$

where it is understood that x_0 and u in $P(x_0, u)$ depend on α and β through (5-11). The term $0(q^{-1/2} \log^{3/2} q)$ in (5-23) represents the sum of three contributions. The first is R_1 in (5-6) which is $0(1/q)$. The second arises from the fact that when the factor $\exp [0(q^{-1/2} \log^{3/2} q)]$ in (5-21) is neglected in integrating (5-21) over $-\ell < \alpha < \ell$, $-\ell < \beta < \ell$, where $\ell = (2q \log q)^{1/2}$, the resulting integral is in error by $0(q^{-1/2} \log^{3/2} q)$. The third is due to the contributions of the integral from the region $|\alpha| > \ell$, $|\beta| > \ell$.

By introducing polar coordinates $\alpha = \rho \cos\theta$, $\beta = \rho \sin\theta$ it can be shown that the region $\rho > \ell$ more than covers the region in question and that

$$Q(\alpha, \beta) \geqslant (1 + r)\rho^2 D \tag{5-24}$$

Upon integrating with respect to ρ and setting in the lower limit ℓ, it is seen that the third contribution is $0(q^{-1/2})$.

We now assume K to be large. Since $0 \leqslant P(x_0, u) \leqslant 1$ we have

$$0 \leqslant e^{-KP} - (1 - P)^K \leqslant KP^2 e^{-KP} < 1/K \tag{5-25}$$

The last inequality follows from $x^2 \exp(-x) < 1$ for $x \geqslant 0$. A proof of the remaining portions will be found in "Modern Analysis" by Whittaker and Watson, Cambridge University Press, Fourth Edition (1927), page 242. When we observe that replacing $[1 - P(x_0, u)]^K$ by $1/K$ in the right hand side of (5-23) gives an integral whose value is less than $1/K$, we see that

$$\text{Prob.}\,(P_1 Q, \cdots, P_K Q > P_0 Q) \tag{5-26}$$

$$= \int_{-q}^{\infty} d\alpha \int_{-q}^{\infty} d\beta\, D_1\, e^{-Q(\alpha,\beta) - KP(x_0,u)} + 0(1/K) + 0(q^{-1/2} \log^{3/2} q)$$

We now take up the problem of expressing the cumulative probability density $P(x_0, u)$ in terms of α and β. When x_0 and u lie in the restricted region of integration shown in (5-6) they are near their average values $\bar{x}_0 = (2N + 1)r$ and $\bar{u} = (2N + 1)(1 + r)$. On the other hand the average value $\bar{x}$ of x and the mean square value σ_x^2 of $(x - \bar{x})^2$ as computed from (4-6), or directly, are $2N + 1 + u$ and $4N + 2 + 4u$, respectively. Thus we see that $\bar{x} - x_0$ is of the same magnitude as $4N$ and becomes much larger than σ_x as $N \to \infty$. The asymptotic development of Appendix I may therefore be used. In Appendix I (equations (A1-27) and (A1-29)) it is shown that when $M(= 2m = 2N + 1)$ is a large number and $1 << (\bar{x} - x_0)/\sigma_x$

$$P(x_0, u) = (4\pi m b_2)^{-1/2}\,(1 + 0(1/m))\,\exp\,[m\mathrm{F}(v_1)] \tag{5-27}$$

where we have introduced the number $m = N + 1/2 = q + 1$ to save writing $N + 1/2$ or $q + 1$ repeatedly and where

$$\begin{aligned} 2b_2 &= (1 - 1/v_1)^2(1 + 4st)^{1/2} \\ v_1 &= [1 + (1 + 4st)^{1/2}]/2s \\ F(v_1) &= (1 + 4st)^{1/2} - s - t - \log v_1 \\ x_0 &= 2ms = (2N + 1)s, \qquad u = 2mt = (2N + 1)t \end{aligned} \tag{5-28}$$

Comparison of the last line in (5-28) with (5-11) shows that ms and mt are equal to $r(q + \alpha) = r(m + \alpha - 1)$ and

$$(1 + r)(q + \beta) = (1 + r)(m + \beta - 1),$$

respectively. It is convenient to introduce the notation

$$\gamma = \alpha - 1, \qquad \delta = \beta - 1$$
$$s = r(1 + \gamma/m), \qquad t = (1 + r)(1 + \delta/m). \tag{5-29}$$

It is seen that for the restricted region in which $|\alpha|$ and $|\beta|$ are less than $\ell = (2q \log q)^{1/2}$, $|\gamma|$ and $|\delta|$ are at most

$$0(q^{1/2} \log^{1/2} q) = 0(m^{1/2} \log^{1/2} m).$$

Hence s, t, $(1 + 4st)^{1/2}$, v_1 differ at most from r, $1 + r$, $1 + 2r$, $1 + 1/r$, respectively, by terms of order $m^{-1/2} \log^{1/2} m$. Similar considerations show that

$$(4\pi m b_2)^{-1/2} = (2\pi q)^{1/2} D_1[1 + 0(m^{-1/2} \log^{1/2} m)] \tag{5-30}$$

The argument of the exponential function in (5-27) must be expanded in powers of γ and δ. It turns out that when γ and δ lie in the restricted region, powers above the second may be neglected. For the sake of convenience we rewrite (5-13) and introduce z_1:

$$\begin{aligned} z &= x_0 u = 4m^2 st = 4r(1 + r)(m + \gamma)(m + \delta) \\ z_1 &= 4r(1 + r)m^2 \\ z - z_1 &= 4r(1 + r)[m(\gamma + \delta) + \gamma\delta] \end{aligned} \tag{5-31}$$

so that $z - z_1$ is $0(m^{3/2} \log^{1/2} m)$. Then

$$\begin{aligned} (1 + 4st)^{1/2} &= (1 + z/m^2)^{1/2} \\ &= (1 + z_1/m^2)^{1/2} + (z - z_1)(1 + z_1/m^2)^{-1/2}/(2m^2) \\ &\quad - (z - z_1)^2(1 + z_1/m^2)^{-3/2}/(8m^4) + R_2 \end{aligned} \tag{5-32}$$

where R_2 is of the same order as $(z - z_1)^3/m^6$, or $m^{-3/2} \log^{3/2} m$. It follows that

$$\begin{aligned} (1 + 4st)^{1/2} &= 1 + 2r + \frac{2r(1 + r)}{1 + 2r}\left[\frac{\gamma + \delta}{m} + \frac{\gamma\delta}{m^2}\right] \\ &\quad - \frac{2r^2(1 + r)^2}{(1 + 2r)^3}\frac{(\gamma + \delta)^2}{m^2} + 0(m^{-3/2} \log^{3/2} m) \\ v_1 &= \frac{(1 + r)}{r(1 + \gamma/m)}\left\{1 + \frac{r}{1 + 2r}\left[\frac{\gamma + \delta}{m} + \frac{\gamma\delta}{m^2}\right]\right. \\ &\quad \left. - \frac{r^2(1 + r)(\gamma + \delta)^2}{m^2(1 + 2r)^2} + 0(m^{-3/2} \log^{3/2} m)\right\}. \end{aligned} \tag{5-33}$$

Combining these and a similar expression for $\log v_1$ leads to

$$\begin{aligned} mF(v_1) &= -m \log (1 + 1/r) + \gamma - \delta \\ &\quad -[(1 + r)\gamma - r\delta]^2/[2m(1 + 2r)] + 0(m^{-1/2} \log^{3/2} m) \\ &= -(q + 1) \log (1 + 1/r) + \alpha - \beta - [(1 + r)\alpha - r\beta]^2 D \\ &\qquad + 0(q^{-1/2} \log^{3/2} q) \end{aligned} \tag{5-34}$$

Substitution of (5-30) and (5-34) in (5-27) gives the result we seek:

$$\begin{aligned} P(x_0, u) &= (1 + 1/r)^{-q-1}(2\pi q)^{1/2} D_1 \\ &\qquad \exp (\alpha - \beta - [(1 + r)\alpha - r\beta]^2 D + 0(q^{-1/2} \log^{3/2} q)) \end{aligned} \tag{5-35}$$

Since $P(x_0, u)$ occurs only in the product $KP(x_0, u)$ in (5-26) we set, in view of (5-35),

$$KP(x_0, u) = A\lambda(\alpha, \beta) \exp S(\alpha, \beta) \tag{5-36}$$

where $\lambda(\alpha, \beta)$ stands for the terms denoted by $\exp [0(q^{-1/2} \log^{3/2} q)]$ in (5-35) and

$$\begin{aligned} A &= K(1 + 1/r)^{-q-1}(2\pi q)^{1/2} D_1 \\ S(\alpha, \beta) &= \alpha - \beta - [(1 + r)\alpha - r\beta]^2 D \end{aligned} \tag{5-37}$$

As long as $|\alpha| < \ell$ and $|\beta| < \ell$, $\lambda(\alpha, \beta)$ is nearly unity and we write

$$\begin{aligned} &\lambda_1 < \lambda(\alpha, \beta) < \lambda_2 \\ &\lambda_1 = 1 - \epsilon, \lambda_2 = 1 + \epsilon, \epsilon = Cq^{-1/2} \log^{3/2} q \end{aligned} \tag{5-38}$$

where C is a positive constant large enough to make ϵ dominate the terms of order $q^{-1/2} \log^{3/2} q$ in (5-35). q is supposed to be so large that ϵ is very small in comparison with unity.

Setting (5-36) in (5-26) gives

$$\text{Prob. } (P_1Q, \cdots, P_KQ > P_0Q) = I + 0(1/K) + 0(q^{-1/2} \log^{3/2} q) \tag{5-39}$$

where the contribution of the region outside $|\alpha| < \ell$, $|\beta| < \ell$ has been returned to the terms denoted by $0(q^{-1/2} \log^{3/2} q)$ (we could have stayed in the region $|\alpha| < \ell$, $|\beta| < \ell$ from (5-23) onward, but didn't do so because we wanted to show that the results coming from (5-25) were not restricted to this region) and

$$I = \int_{-\ell}^{\ell} d\alpha \int_{-\ell}^{\ell} d\beta \, D_1 \exp [-Q(\alpha, \beta) - A\lambda(\alpha, \beta) e^{S(\alpha,\beta)}] \tag{5-40}$$

Let $L(\lambda)$ denote the integral obtained by replacing the function $\lambda(\alpha, \beta)$ in I by the positive constant λ (which we shall take to be either λ_1 or λ_2 defined

by (5-38)). Then, since $A \exp S(\alpha, \beta)$ is positive, it follows from (5-40) that

$$L(\lambda_1) > I > L(\lambda_2) \tag{5-41}$$

Also since $\exp [-A\lambda \exp S(\alpha, \beta)]$ lies between 0 and 1 for all real values of α and β it may be shown from (5-24) that $L(\lambda)$ is equal to $J(\lambda) + 0(q^{-1/2})$ where

$$J(\lambda) = \int_{-\infty}^{\infty} d\alpha \int_{-\infty}^{\infty} d\beta \, D_1 \exp [- Q(\alpha, \beta) - A\lambda e^{S(\alpha,\beta)}] \tag{5-42}$$

Here λ is a constant and $Q(\alpha, \beta)$, A, $S(\alpha, \beta)$ are defined by (5-19) and (5-37). From (5-39) and (5-41) we obtain

$$\text{Prob.} \, (P_1 Q, \cdots, P_K Q > P_0 Q) = J(1) + \theta[J(\lambda_1) - J(1)] \tag{5-43}$$
$$+ (1 - \theta)[J(\lambda_2) - J(1)] + 0(1/K) + 0(q^{-1/2} \log^{3/2} q)$$

where $0 < \theta < 1$. It will be shown later that $J(\lambda_1)$ and $J(\lambda_2)$ differ from $J(1)$ by terms which are certainly not larger than $0(q^{-1/2})$.

The problem now is to evaluate the integral (5-42) for $J(\lambda)$. It turns out that $\exp [-A\lambda \exp S(\alpha, \beta)]$ acts somewhat like a discontinuous factor which is unity when $S(\alpha, \beta) + \log A\lambda$ is negative and zero when it is positive. In order to investigate this behavior we make the change of variable

$$\begin{aligned} \alpha - \beta &= w \qquad \alpha = y - rw \\ (1 + r)\alpha - r\beta &= y \qquad \beta = y - (1 + r)w \\ d\alpha \, d\beta &= dw \, dy \end{aligned} \tag{5-44}$$

From (5-19), (5-37), and (5-42)

$$\begin{aligned} Q(\alpha, \beta) &= [y^2 + (1 + 2r)\beta^2]D = y^2 D + \beta^2/2q \\ S(\alpha, \beta) &= w - y^2 D \end{aligned} \tag{5-45}$$
$$J(\lambda) = \int_{-\infty}^{\infty} dy \int_{-\infty}^{\infty} dw \, D_1 \exp [- y^2 D - \beta^2/2q - A\lambda e^{w - y^2 D}]$$

Here and in the following work β is to be regarded as a function of w and y.

Split the interval of integration with respect to w into the two subintervals $(-\infty, w_0)$ and (w_0, ∞) where

$$w_0 = y^2 D - \log A\lambda \tag{5-46}$$

and y is temporarily regarded as constant. In the first interval

$$\begin{aligned} &\int_{-\infty}^{w_0} \exp [- \beta^2/2q - e^{w - w_0}] \, dw \\ &= \int_{-\infty}^{w_0} e^{-\beta^2/2q} \, dw - \int_{-\infty}^{w_0} (1 - \exp [- e^{w - w_0}]) e^{-\beta^2/2q} \, dw \end{aligned} \tag{5-47}$$

Splitting the interval of integration $(-\infty, w_0)$ into $(-\infty, -\log A\lambda)$ and $(-\log A\lambda, w_0)$ in the first integral on the right of (5-47) shows that its contribution to $J(\lambda)$ is

$$D_1 \int_{-\infty}^{\infty} dy \int_{-\infty}^{-\log A\lambda} dw\, e^{-y^2 D - \beta^2/2q} + D_1 \int_{-\infty}^{\infty} dy \int_{\log A\lambda}^{w_0} dw\, e^{-y^2 D - \beta^2/2q} \tag{5-48}$$

Integrating with respect to y, after inverting the order of integration, shows that the value of the first integral is

$$\pi^{-1/2} \int_{-\infty}^{B} e^{-t^2}\, dt = (1 + \operatorname{erf} B)/2 \tag{5-49}$$

where, from (5-37) and the definition (5-22) of D_1,

$$\begin{aligned} B &= -\tfrac{1}{2}(1 + r)^{1/2} q^{-1/2} \log A\lambda \\ &= -\tfrac{1}{2}(1 + r)^{1/2}\, q^{-1/2} \log \frac{\lambda K r (1 + 1/r)^{-q}}{[2\pi q(1 + 2r)]^{1/2}} \end{aligned} \tag{5-50}$$

That the value of $J(\lambda)$ differs from (5-49) by $0(q^{-1/2})$ may be seen as follows. Since $0 < \exp[-\beta^2/2q] < 1$, the integral over (w_0, ∞) (mentioned just above (5-46) and obtained by taking the limits of integration to be w_0 and ∞ in the left side of (5-47)) is positive and less than

$$\int_{w_0}^{\infty} \exp[-e^{w-w_0}]\, dw = \int_{1}^{\infty} e^{-x}\, dx/x = .219\ldots \tag{5-51}$$

Likewise, the second integral on the right side of (5-47) is less than

$$\int_{-\infty}^{w_0} (1 - \exp[-e^{w-w_0}])\, dw = \int_{0}^{1} (1 - e^{-x})\, dx/x = .796\ldots \tag{5-52}$$

Therefore the contribution of the first integral on the right of (5-47) differs from $J(\lambda)$ by a quantity less than

$$\int_{-\infty}^{\infty} D_1 e^{-y^2 D}(.219 + .796)\, dy = 0(q^{-1/2})$$

in absolute value. The contribution of the first integral on the right of (5-47) differs from (5-49) by the second integral in (5-48) which is $0(q^{-1/2})$ because it is less than

$$\int_{-\infty}^{\infty} D_1(y^2 D) e^{-y^2 D}\, dy$$

The factor $(y^2 D)$ arises from $w_0 - (-\log A\lambda)$ when the mean value theorem is applied to the integral in w. Hence $J(\lambda)$ differs from (5-49) by $0(q^{-1/2})$.

Although (5-49) is a sufficiently accurate expression of $J(\lambda)$ for our pur-

poses, it seems worthwhile to set down approximate expressions for the terms which have been dismissed as $0(q^{-1/2})$. From the above work,

$$J(\lambda) = (1 + \operatorname{erf} B)/2 + D_1 \int_{-\infty}^{\infty} dy\, e^{-y^2 D} \left\{ \int_{w_0}^{\infty} e^{-\beta^2/2q} \exp\left[- e^{w-w_0}\right] dw \right.$$

$$- \int_{-\infty}^{w_0} e^{-\beta^2/2q} (1 - \exp\left[- e^{w-w_0}\right]) \, dw$$

$$\left. + \int_{-\log A\lambda}^{w_0} e^{-\beta^2/2q}\, dw \right\} \tag{5-53}$$

$$\approx (1 + \operatorname{erf} B)/2 + D_1 \int_{-\infty}^{\infty} dy\, e^{-y^2 D} \{-.577.. + y^2 D\} e^{-\beta_1^2/2q}$$

$$= (1 + \operatorname{erf} B)/2 + \left(\frac{1+r}{4\pi q}\right)^{1/2} [- .577 \cdots +$$

$$4^{-1}(1 + r)^{-1}\{1 + (2 + 4r)B^2\}] e^{-B^2}$$

where $\beta_1 = y + (1 + r) \log A\lambda$ and we have made use of the fact that $\beta^2/2q$ changes relatively slowly in comparison with w when q is large.

Since $J(\lambda)$ differs from $(1 + \operatorname{erf} B)/2$ by $0(q^{-1/2})$, and since the three B's for λ equal to λ_1, 1, and λ_2 differ by not more than $0(q^{-1/2} \log (\lambda_2/\lambda_1)) = 0(q^{-1} \log^{3/2} q)$, from (5-50) and (5-38), it follows that the terms involving $J(\lambda_1)$ and $J(\lambda_2)$ in (5-43) may be included in the term $0(q^{-1/2} \log^{3/2} q)$. In using our result it is more convenient to deal with N and $K + 1$ instead of $q = N - 1/2$ and K. Hence instead of B we deal with H defined by

$$H = -\frac{1}{2} \frac{(1 + r)^{1/2}}{(q + 1/2)^{1/2}} \log \frac{(K + 1)(1 + 1/r)^{-q-1}(1 + r)}{[2\pi(q + 1/2)(1 + 2r)]^{1/2}}. \tag{5-54}$$

The difference $B - H$, with $\lambda = 1$ and H finite, may be shown to be (with considerable margin) $0(1/K) + 0(q^{-1/2})$. From (5-43), as amended by the first sentence in this paragraph, it follows that

$$\text{Prob.}\,(P_1 Q, \cdots, P_K Q > P_0 Q) = (1 + \operatorname{erf} H)/2 + 0(1/K) + 0(q^{-1/2} \log^{3/2} q) \tag{1-4}$$

where the difference between erf B and erf H has been absorbed by the "order of" terms. When $q + 1/2$ is replaced by N in (5-54) the result is expression (1-5) for H.

APPENDIX I

Cumulative Distribution Function for a Sum of Squares of Normal Variates

Let x be a random variable defined by

$$x = \sum_{n=1}^{M} y_n^2 \tag{A1-1}$$

where y_n is a random variable distributed normally about its average value $\bar{y}_n$ with unit standard deviation. In writing $(A1 - 1)$ we have been guided by (4-3), where $M = 2N + 1$, but here we shall let M be any positive integer. In much of the following work $M/2$ occurs and for convenience we put

$$m = M/2 \tag{A1-2}$$

From the work of Section 4 it follows that the probability density $p(x, u)$ of x is given by Fisher's expression

$$p(x, u) = 2^{-1}(x/u)^{m/2-1/2} I_{m-1}[(ux)^{1/2}]e^{-(u+x)/2} \tag{A1-3}$$

where u is the constant

$$u = \sum_{n=1}^{M} \bar{y}_n^2 \tag{A1-4}$$

Here we are interested in the cumulative distribution function, i.e., the probability that x is less than some given value x_0,

$$P(x_0, u) = \int_0^{x_0} p(x, u)\, dx \tag{A1-5}$$

as M becomes large. In this case the central limit theorem tells us that $p(x, u)$ approaches a normal law with average $\bar{x} = M + u$ and variance = ave. $(x - \bar{x})^2 = 2M + 4u$. The function $P(x_0, u)$ has been studied by J. I. Marcum in some unpublished work, and by P. K. Bose(9). In particular, Marcum has used the Gram-Charlier series to obtain values for $P(x_0, u)$ in the vicinity of $\bar{x}$ for large values of M. However, since I have not been able to find any previous work covering the case of interest here, namely values of $P(x_0, u)$ when x_0 is appreciably less than $\bar{x}$, a separate investigation is necessary and will be given here.

Integrating the general expression (4-5) with respect to x between $-X$ and x_0, letting $X \to \infty$, and discarding the portions of the integrand which oscillate with infinite rapidity gives

$$P(x_0, u) = -\frac{1}{2\pi i}\int_{-\infty,\text{ above }0}^{\infty} z^{-1}e^{-izx_0}[\text{ave. } e^{izx}]\,dz$$
$$= 1 - \frac{1}{2\pi i}\int_{-\infty,\text{ below }0}^{\infty} z^{-1}e^{-izx_0}[\text{ave. } e^{izx}]\,dz \tag{A1-6}$$

where the subscripts "above 0" and "below 0" indicate that the path of integration is indented so as to pass above or below, respectively, the pole at $z = 0$. The value of ave. exp (izx) may be obtained by setting $N + 1/2 = m$ in (4-5). The new notation

$$x_0 = Ms = 2ms, \qquad u = 2mt, \qquad 2z = \zeta \tag{A1-7}$$

enables us to write

$$P(x_0, u) = -\frac{1}{2\pi i}\int_{-\infty,\text{ above }0}^{\infty} \zeta^{-1}\exp m[-is\zeta - \log(1 - i\zeta) - t + t(1 - i\zeta)^{-1}]\,d\zeta. \tag{A1-8}$$

The further change of variable

$$1 - i\zeta = v \tag{A1-9}$$

carries (A1-8) into

$$P(x_0, u) = \frac{1}{2\pi i}\int_K (1 - v)^{-1}\exp[mF(v)]\,dv \tag{A1-10}$$

where the path of integration K is the straight line in the complex v plane running from $1 + i\infty$ to $1 - i\infty$ with an indentation to the right of $v = 1$, and

$$F(v) = sv - \log v + t/v - s - t. \tag{A1-11}$$

The K used here should not be confused with the K denoting the number of messages in the body of the paper. We have run out of suitable symbols.

An asymptotic expression for (A1-10) will now be obtained by the method of "steepest descents." The saddle points are obtained by setting the derivative

$$F'(v) = s - 1/v - t/v^2 \tag{A1-12}$$

to zero and are at

$$v_1 = [1 + (1 + 4st)^{1/2}]/2s$$
$$v_2 = [1 - (1 + 4st)^{1/2}]/2s \tag{A1-13}$$

As x_0 and s increase from 0 to ∞, u and t of course being fixed, we have the following behavior:

$$\begin{array}{lll} x_0 = 0 & \bar{x} & \infty \\ s = 0 & 1 + t & \infty \\ v_1 = \infty & 1 & 0 \\ v_2 = -t & -t/(1+t) & 0 \end{array} \tag{A1-14}$$

It is seen that $v_1 \geqslant 0$ and $v_2 \leqslant 0$.

Putting aside for the moment the factor $(1 - v)^{-1}$ in (A1-10), the path of steepest descent through the saddle point v_1 is one of the two curves specified by equating the imaginary part of $F(v)$ to zero. Introducing polar coordinates gives

$$\begin{aligned} v &= \rho e^{i\theta} \\ \text{Real } F(v) &= (s\rho + t/\rho)\cos\theta - \log\rho - s - t \\ \text{Imag. } F(v) &= (s\rho - t/\rho)\sin\theta - \theta \end{aligned} \tag{A1-15}$$

At v_1, $\theta = 0$, $\rho = v_1$. Imag. $F(v_1) = 0$ and, from (A1-12),

$$\begin{aligned} \text{Real } F(v_1) &= (2sv_1 - 1) - \log v_1 - s - t \\ &= (1 + 4st)^{1/2} - \log v_1 - s - t \end{aligned} \tag{A1-16}$$

The path of steepest descent through v_1 may be obtained in polar form by solving

$$(s\rho - t/\rho) = \theta/\sin\theta \tag{A1-17}$$

for ρ as a function of θ. Setting $\varphi = \theta \csc\theta$ and taking the positive value of ρ leads to

$$\rho = [\varphi + (\varphi^2 + 4st)^{1/2}]/2s \tag{A1-18}$$

As θ increases from 0 to π, φ increases from 1 to ∞, and ρ starts from v_1 (as it should) and ends at ∞. Thus, the path of steepest descent through v_1 comes in from $v = -\infty + i\pi/s$ (when θ is nearly π, $\rho \approx \varphi/s$, $\varphi \approx \pi/(\pi - \theta)$ and $\rho(\pi - \theta) \approx \pi/s$), crosses the positive imaginary v axis and bends down to cut the real positive v axis (at right angles) at v_1, and then goes out to $v = -\infty - i\pi/s$ along a similar path in the lower part of the plane. It thus avoids the branch cut (which we take to run from $-\infty$ to 0) in the v plane necessitated by the term $\log v$ in $F(v)$. Since m and s are positive the path of integration K in (A1-10) may be made to coincide with the path of steepest descent when $v_1 > 1$. This corresponds to the case in which $x_0 < \bar{x}$ as (A1-14)

shows. When $0 < v_1 < 1$, i.e., $\infty > x_0 > \bar{x}$, the two paths may still be made to coincide but it is necessary to add the contribution of the pole at $v = 1$ as K is pulled over it. This is equivalent to passing from the first to the second of equations (A1-6). The path $\theta = 0$ which makes Imag. $F(v)$ of (A1-15) zero turns out to be the curve of "steepest ascent" and hence need not be considered. As (A1-13) shows, the saddle point v_2 does not enter into our considerations because it lies on the negative real v axis and the path of integration K in (A1-10) cannot be made to pass through it without trouble from the singularity of $F(v)$ at $v = 0$.

We now suppose $x_0 < \bar{x}$ so that s and t are such as to make $v_1 > 1$. In order to remove the factor $(1 - v)$ from the denominator of the integrand in (A1-10), we change the variable of integration from v to w:

$$v - 1 = e^w, \qquad (1 - v)^{-1} dv = -dw$$
$$P(x_0, u) = -\frac{1}{2\pi i} \int_L \exp\left[mF(1 + e^w)\right] dw \tag{A1-19}$$

As v comes in along the path of steepest descent, the path of integration L for w comes in from $w = \infty + i\pi$ and dips down towards the real w axis as arg v decreases from π. L crosses the real w axis perpendicularly at the point

$$w_1 = \log (v_1 - 1) \tag{A1-20}$$

and then runs out to $w = \infty - i\pi$ along a curve which tends to become parallel to the real w axis. w_1 may be either positive or negative. When x_0 is almost as large as $\bar{x}$, w_1 is large and negative.

Since $F(v)$ is real along the path of steepest descent, $F(1 + e^w)$ is real along L. This real value is $-\infty$ at the ends of L and attains its maximum value $F(v_1)$, given by (A1-16), at $w = w_1$. w_1 is a saddle point in the complex w plane because

$$\frac{d}{dw} F(1 + e^w) = F'(1 + e^w)e^w = F'(v)e^w \tag{A1-21}$$

vanishes at $w = w_1$.

Instead of $F(1 + e^w)$ itself we shall be concerned with

$$\tau = F(1 + e^{w_1}) - F(1 + e^w) \tag{A1-22}$$

so that (A1-19) may be written as

$$P(x_0, u) = -\frac{\exp\left[mF(1 + e^{w_1})\right]}{2\pi i} \int_L e^{-m\tau} dw. \tag{A1-23}$$

The variable τ is real on the path of integration L, is zero at w_1, and increases to $+\infty$ as we follow L out to $w = \infty \pm i\pi$. It is convenient to split

K into two parts (10). The first part connects $\infty + i\pi$ to w_1 and the second part connects w_1 to $\infty - i\pi$. The values of w on these two parts will be denoted by w_I and w_{II}, respectively. Corresponding to each value of τ there is a value w_I and a value w_{II} (in fact it turns out that w_{II} is the conjugate complex of w_I). Changing the variable of integration in (A1-23) from w to τ, and remembering that K starts at $\infty + i\pi$, gives

$$P(x_0, u) = \frac{\exp [mF(1 + e^{w_1})]}{2\pi i} \int_0^\infty e^{-m\tau} \left[\frac{d}{d\tau} w_I - \frac{d}{d\tau} w_{II} \right] d\tau \quad \text{(A1-24)}$$

Since m is large, most of the contribution to the value of the integral comes from around $\tau = 0$ or $w = w_1$. In order to obtain an expression for the integrand in this region we note that, because $F'(v_1) = 0$, the Taylor series for (A1-22) is of the form

$$\tau = -b_2(w - w_1)^2 - b_3(w - w_1)^3 - b_4(w - w_1)^4 - \cdots \quad \text{(A1-25)}$$

The circle of convergence of this series is centered on w_1 and extends out to $w = \pm i\pi$, these points being the nearest singularities of $F(1 + e^w)$ as may be seen by setting $v = 1 + e^w$ in (A1-11) and observing that the singularities of $\log v - t/v$ in the finite portion of the w plane occur at odd multiples of $\pm i\pi$. We imagine the branch cuts associated with $\log v$ to run out to the right from these points along lines parallel to the real w axis. Since (A1-25) has a non-zero radius of convergence, the same is true of the two series obtained from it by inversion, namely

$$\begin{aligned} w_I - w_1 = {} & ib_2^{-1/2}\tau^{1/2} + b_3\tau/2b_2^2 \\ & + i[b_2^{-2}b_4 - 5b_2^{-3}b_3^2/4]\tau^{3/2}/2b_2^{1/2} + \cdots \end{aligned} \quad \text{(A1-26)}$$

and the series for $w_{II} - w_1$ obtained from (A1-26) by changing the sign of i. Differentiation of these two series gives a series for $d(w_I - w_{II})/d\tau$ which also converges for sufficiently small $|\tau|$ (putting aside the term in $\tau^{-1/2}$), and which, when put in (A1-24), leads to

$$P(x_0, u) \sim \frac{e^{mF(v_1)}}{(4\pi m b_2)^{1/2}} \left\{ 1 + \frac{3}{4m} [b_2^{-2}b_4 - 5b_2^{-3}b_3^2/4] + \cdots \right\} \quad \text{(A1-27)}$$

That this is an asymptotic expansion holding for large values of m follows from a lemma given by Watson (11). The conditions of the lemma hold since we have already shown that the series for $d(w_I - w_{II})/d\tau$ converges for $|\tau|$ small enough. Furthermore, $d(w_I - w_{II})/d\tau$ is bounded for $a \leqslant \tau$ where τ is real and $0 < a \leqslant$ the radius of convergence of (A1-26). This follows the fact that

$$\frac{dw}{d\tau} = \left[\frac{d\tau}{dw} \right]^{-1} = [-F'(1 + e^w)e^w]^{-1}$$

is bounded except near $w = w_1$ (i.e., $\tau = 0$) and, indeed, decreases to zero like $-e^{-w}/s$ as $w \to \infty \pm i\pi$ (i.e., $\tau \to \infty$).

The values of b_2, b_3, b_4 obtained by expanding (A1-22) and comparing the result with (A1-25) are

$$\begin{aligned} b_2 &= F''(v_1)e^{2w_1}/2 \\ b_3 &= [F'''(v_1)e^{3w_1} + 3F''(v_1)e^{2w_1}]/6 \\ b_4 &= [F''''(v_1)e^{4w_1} + 6F'''(v_1)e^{3w_1} + 7F''(v_1)e^{2w_1}]/24 \end{aligned} \tag{A1-28}$$

$$F''(v) = v^{-2} + 2tv^{-3}, \quad F'''(v) = -2v^{-3} - 6tv^{-4}, \quad F''''(v) = 6v^{-4} + 24tv^{-5}$$

Our asymptotic expression for $P(x_0, u)$, when $x_0 < \bar{x}$, is given by (A1-28) and (A1-27). Only the leading term of (A1-27) is used in the paper. Sometimes the following expressions are more convenient than the ones which have already been given.

$$\begin{aligned} b_2 &= v_1^{-3}(v_1 + 2t)e^{2w_1}/2 = v_1^{-3}(v_1 + 2t)(v_1 - 1)^2/2 \\ &= (1 - 1/v_1)^2(1 + 4st)^{1/2}/2 \end{aligned} \tag{A1-29}$$

$$F(v_1) = (1 + 4st)^{1/2} - s - t - \log v_1.$$

In all of these formulas v_1 is given in terms of s and t by (A1-13) and s and t in terms of x_0 and u by (A1-7).

When $x_0 > \bar{x}$, the saddle point v_1 lies between 0 and 1 in the v plane. As v follows the path of steepest descent (discussed just below equation (A1-18)) arg $(v - 1)$ now stays close to π. From (A1-19) Imag. w stays close to π on the new path of steepest descent in the w plane, and the saddle point w_1 now lies on the negative real portion of the line Imag. $w = \pi$. The new path starts at $w = \infty + i\pi$, swings down a little as it comes in, swerves up to pass through w_1 and then goes out to $w = \infty + i\pi$ above the branch cut joining $w = i\pi$ to $w = \infty + i\pi$. The analysis goes along much as for $v_1 > 1$ except that instead of being 0 the imaginary part of w_1 is $i\pi$. This causes the terms in b_3 and b_4 containing exp $(3w_1)$ to change sign. The numerical values of b_2 and $F(v_1)$ are computed by the formulas (A1-29) as before. The fact that b_2 contains the factor exp $(i2\pi)$ shows up only in changing the sign of $b_2^{1/2}$ to give the minus sign in the leading term:

$$P(x_0, u) \sim 1 - (4\pi m|\, b_2\,|)^{-1/2} \exp\,[mF(v_1)]$$

which holds for $x_0 > \bar{x}$. The one arises from the pole at $v = 1$ and is the same as the one in the second of equations (A1-6).

In order to see how (A1-27) breaks down near $x_0 = \bar{x}$, we set $x_0 - \bar{x} = 2m(s - 1 - t) = -2m\epsilon$ or $s = 1 + t - \epsilon$ where ϵ is a small positive number

Using $\sigma_x^2 \equiv$ ave. $(x - \bar{x})^2 = 4(m + u) = 4m(1 + 2l)$ it is found that

$$v_1 = 1 + \epsilon/(1 + 2l) = 1 - 2(x_0 - \bar{x})\sigma_x^2$$

$$mF(v_1) = -m\epsilon^2/(2 + 4l) = -(x_0 - \bar{x})^2/2\sigma_x^2$$

$$2mb_2 = m(v_1 - 1)^2(1 + 2l) = (x_0 - \bar{x})^2/\sigma_x^2$$

and that, since $w_1 \to -\infty$, $b_3 \to b_2$ and $b_4 \to 7b_2/12$. When these values are put in (A1-27) the leading term becomes

$$P(x_0, u) \sim (2\pi)^{-1/2}(\sigma_x/z) \exp [-z^2/2\sigma_x^2]$$

and the term within the braces in (A1-27) reduces to $1 - \sigma_x^2/z^2$ where $z = \bar{x} - x_0 > 0$. Since the asymptotic expansion is useful only in the region where the second term within the braces is small in comparison with the first term, which is unity, $\bar{x} - x_0$ must be several times as large as σ_x before we can use (A1-27). It will be noticed that the above expression for $P(x_0, u)$ is closely related to the asymptotic expansion of the error function.

APPENDIX II

An Approximation for $I_N(x)$

When z in the Bessel function $J_q(qz)$ is imaginary a formula given by Meissel (12) becomes

$$I_q(qy) = \frac{(qy)^q \exp (qw + V)}{e^q \Gamma(q + 1) w^{1/2}(1 + w)^q} \tag{A2-1}$$

where $w = (1 + y^2)^{1/2}$ and V is a function of y and q which, when q is large, has the formal expansion

$$V = \frac{1}{24q}\left\{2 - \frac{2 - 3y^2}{w^3}\right\} + \frac{y^4 - 4y^2}{16q^2w^6} - \frac{1}{5760q^3}\left\{16 - \frac{16 + 1512y^2 - 3654y^4 + 375y^6}{w^9}\right\} + \cdots \tag{A2-2}$$

Here we shall show that for $y \geqslant 0$ and $q > 1$

$$| V | < 1/(2q - 1) \tag{A2-3}$$

Consideration of (A2-2) and also of the method used to establish (A2-3) indicates that the inequality is very rough. It doubtlessly can be greatly improved (but not beyond the $1/(12q)$ obtained by letting y and $q \to \infty$ in (A2-2)). Incidentally, it may be shown that the constant terms which remain in (A2-2) when $y = \infty$ are associated with the asymptotic expansion of $\log \Gamma(q + 1)$.

When (A2-1) is substituted in Bessel's differential equation, which we write as

$$y^2 \frac{d^2}{dy^2} I_q(qy) + y \frac{d}{dy} I_q(qy) - q^2(1 + y^2) I_q(qy) = 0,$$

we obtain a differential equation for V:

$$V'' = (4 - y^2)w^{-4}/4 - (2qw + w^{-2})y^{-1}V' - V'^2 \qquad \text{(A2-4)}$$

Here the primes denote differentiation with respect to y. The constants of integration associated with (A2-4) are to be chosen so that

$$V \to y^2/(4q + 4) \text{ as } y \to 0. \qquad \text{(A2-5)}$$

This condition is obtained by comparing the limiting form of (A2-1), in which $w \to 1 + y^2/2$, with

$$I_q(qy) \to \frac{(qy/2)^q}{\Gamma(q + 1)} \left[1 + \frac{(qy/2)^2}{q + 1}\right] \to \frac{(qy/2)^q}{\Gamma(q + 1)} \exp\left[\frac{q^2y^2}{4(q + 1)}\right]$$

Condition (A2-5) completely determines V since substitution of the assumed solution

$$V = 4^{-1}(q + 1)^{-1}y^2 + c_1y^4 + c_2y^6 + \cdots$$

in (A2-4) leads to relations which determine $c_1, c_2, \cdots$ successively.

Let $V' = v$. Then (A2-4) becomes

$$v' = c - 2bv - v^2 \qquad \text{(A2-6)}$$

where c and b are known functions of y defined by

$$c = (4 - y^2)w^{-4}/4, \qquad b = (qw + w^{-2}/2)y^{-1} \qquad \text{(A2-7)}$$

From (A2-5), $v \to y/(2q + 2)$ as $y \to 0$ and therefore

$$V = \int_0^y v\, dy \qquad \text{(A2-8)}$$

We first show that $|v| < 1/(2q - 1)$ when $q > 1$. The (y, v) plane may be divided into regions according to the sign of v'. The equations of the dividing lines between these regions are obtained by setting $v' = 0$ in (A2-6). Thus, for a given value of y, v' is positive if $v_2 < v < v_1$ and negative if $v > v_1$ or $v < v_2$ where

$$\begin{aligned} v_1 &= -b + (b^2 + c)^{1/2} = c/[b + (b^2 + c)^{1/2}] \\ v_2 &= -b + (b^2 + c)^{1/2} \end{aligned} \qquad \text{(A2-9)}$$

When $y > 0$ we have $b \geqslant q$. A plot of c versus y shows that $|c| \leqslant 1$. Hence,

when $q > 1$,

$$b^2 + c \geqslant q^2 - 1 > (q-1)^2$$
$$|v_1| < 1/(2q-1) \tag{A2-10}$$
$$v_2 < -2q + 1$$

The curve obtained by plotting v_1 as a function of y plays an important role because, as we shall show, the maxima and minima of the curve for v lie on it. Therefore, the maximum value of $|v|$ cannot exceed the maximum value of $|v_1|$. The maxima and minima must lie on either the v_1 or the v_2 curve since v' vanishes only on these curves. In order to show that it is the v_1 curve we note from (A2-9) that, near $y = 0$, v_1 behaves like $y/(2q+1)$. Consequently both the v_1 and v curves start from $v = 0$ at $y = 0$ but for a while v_1 lies above v which behaves like $y/(2q+2)$. Here v lies in a $v' > 0$ region and continues to increase until it intersects v_1 (as it must do before y reaches 2 because $v_1 \leqslant 0$ at $y = 2$) at which point $v' = 0$, $v_1' \leqslant 0$, and v has a maximum which is less than the maximum of $|v_1|$ so $v < 1/(2q-1)$ when $q > 1$. Upon passing through v_1, v enters a $v' < 0$ region and decreases steadily until it either again intersects the v_1 curve or else approaches some limit as $y \to \infty$. In either case $|v|$ does not exceed $1/(2q-1)$, since, in the first case v would have a minimum at the intersection and in the second $v_1 \to 0$ as $y \to \infty$. The same reasoning may be applied to the remaining points of intersection, if any, of the v and v_1 curves.

In order to obtain an inequality for V itself we rewrite (A2-6) as

$$v' = c - (2b + v)v \tag{A2-11}$$

The solution of this equation which behaves like $y/(2q+2)$ as $y \to 0$ also satisfies the relation

$$v(y) = \int_0^y c(x) \exp\left[-\int_x^y [2b(\xi) + v(\xi)]\, d\xi\right] dx.$$

as may be verified by making use of the relations $c(x) \to 1$ as $x \to 0$ and $2b(\xi) \to (2q+1)/\xi$, $v(\xi) \to \xi/(2q+2)$ as $\xi \to 0$. For then

$$-\int_x^y [2b(\xi) + v(\xi)]\, d\xi \to (2q+1) \log x/y$$

$$v(y) \to \int_0^y (x/y)^{2q+1}\, dx = y/(2q+2)$$

Hence, from (A2-8)

$$V(y_1) = \int_0^{y_1} dy \int_0^y c(x) \exp\left[-\int_x^y [2b(\xi) + v(\xi)]\, d\xi\right] dx$$

and

$$|V(y_1)| \leq \int_0^{y_1} dy \int_0^{y} |c(x)| \exp\left[-\int_x^{y} [2b(\xi) - |v(\xi)|]\, d\xi\right] dx.$$

From $b \geqslant q$ and $|v| < 1/(2q-1)$ it follows that $2b(\xi) - |v(\xi)| > 2q - 1$ when $q > 1$. This and $|c(x)| \leqslant (4 + x^2)(1 + x^2)^{-2}/4$ gives

$$|V(y_1)| < \int_0^{\infty} dy \int_0^{y} (4 + x^2)(1 + x^2)^{-2} 4^{-1} \exp[-(2q-1)(y-x)]\, dx$$

$$= \frac{5\pi}{16(2q-1)} < \frac{1}{2q-1}$$

which is the result we set out to establish. The double integral may be reduced to a single integral by inverting the order of integration and integrating with respect to y. Incidentally, most of the roughness of our result is due to the use of the inequality for $|c(x)|$.

References

1. C. E. Shannon, A Mathematical Theory of Communication, *Bell Sys. Tech. Jour.*, 27, 379–423, 623–656 (1948) See especially Section 24.
2. C. E. Shannon, Communication in the Presence of Noise *Proc. I.R.E.*, 37, 10–21 (1949).
3. W. G. Tuller, Theoretical Limitations on the Rate of Transmission of Information *Proc. I.R.E.*, 37, 468–478 (1949).
4. N. Wiener, Cybernetics, John Wiley and Sons (1948).
5. S. Goldman, Some Fundamental Considerations Concerning Noise Reduction and Range in Radar and Communication, *Proc. I.R.E.*, 36, 584–594 (1948).
6. G. N. Watson, Theory of Bessel Functions, Cambridge University Press (1944), equation (1) p. 181.
7. R. A. Fisher, The General Sampling Distribution of the Multiple Correlation Coefficient. *Proc. Roy. Soc. of London* (A) Vol. 121, 654–673 (1928). See in particular pages 669–670.
8. Reference (6), equation (4) p. 394.
9. P. K. Bose, On Recursion Formulae, Tables and Bessel Function Populations Associated with the Distribution of Classical D^2—Statistic, Sankhyā, 8, 235–248 (1947).
10. Compare with §8.4 of reference (6).
11. Reference (6), p. 236.
12. Reference (6), p. 227.

Realization of a Constant Phase Difference

By SIDNEY DARLINGTON

This paper bears on the problem of splitting a signal into two parts of like amplitudes but different phases. Constant phase differences are utilized in such circuits as Hartley single sideband modulators. The networks considered here are pairs of constant-resistance phase-shifting networks connected in parallel at one end. The first part of the paper shows how to compute the best approximation to a constant phase difference obtainable over a prescribed frequency range with a network of prescribed complexity. The latter part shows how to design networks producing the best approximation.

A PERENNIAL problem is that of designing a circuit to split a signal into two parts which are the same in amplitude but which differ in phase by a constant amount. A 90-degree phase difference is needed, for example, in the single sideband modulation system due to R. V. L. Hartley.[1] It is well known that it is not possible to obtain exactly equal amplitudes and exactly constant phase differences at all frequencies except in the trivial special case of a 180-degree phase difference. Various methods have been devised, however, for approximating these characteristics over finite frequency ranges. The most obvious method is to use a pair of constant resistance phase shifting sections in parallel at one end and with separate terminations at the other end[2] as indicated in Fig. 1.

This paper is devoted to the problem of obtaining approximately constant phase differences under the specific assumption that pairs of constant resistance phase shifting networks are to be used. The paper has been written with two objects in mind. The first is the development of a method for determining the best approximation to a constant phase difference which can be obtained over a prescribed frequency range with a pair of phase shifting networks of a prescribed total complexity. The second object is the description of a straightforward design procedure by means of which the networks can be designed to give this best possible approximation.

The problem under consideration is typical of those usually described as problems in network synthesis. In other words, a network of a prescribed general type is to be designed to approximate as closely as possible an ideal operating characteristic of a prescribed form. The same procedure will be followed as that appropriate for most such problems. The procedure begins with the development of a mathematical expression representing the most

[1] *U. S. Patent* 1,666,206, 4/17/28, Modulation System.

[2] Another common method uses reactance shunt branches between effectively infinite impedances, such as the plate and grid impedances of screen grid tubes.

general characteristics which can be obtained with the prescribed type of network. This is followed by the determination of particular choices of the arbitrary constants in the expression, which will lead to the best approximation to the prescribed ideal characteristic. The next step is to determine formulae for the degree of approximation to the ideal, which will be

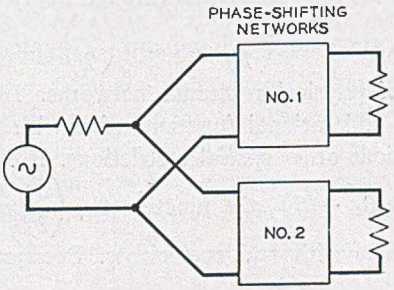

Fig. 1—Phase-shifting networks for approximation to a constant phase difference.

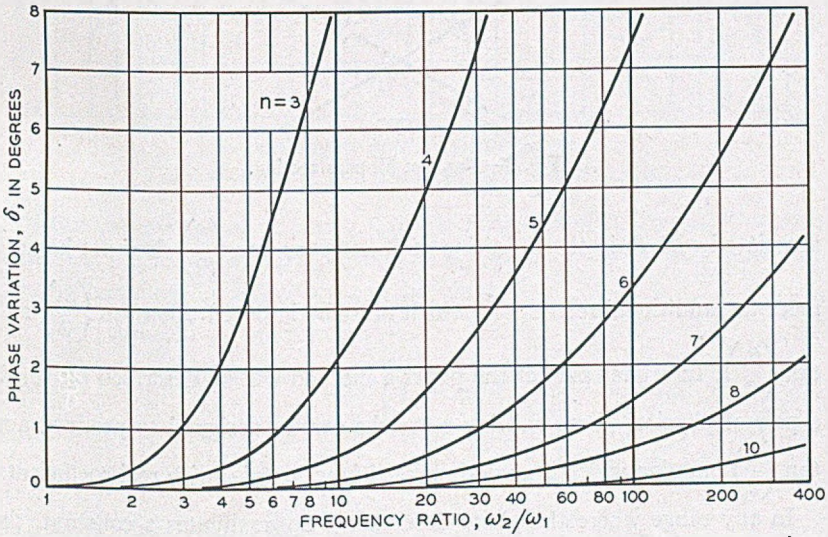

Fig. 2—Variation in phase difference, when average is 90°, with a network of n sections.

obtained with those particular values of the constants. The final step is the development of a method for determining corresponding actual networks.

From the optimum choice of constants, curves can be calculated which show what can be done with a network of any given complexity (Fig. 2). Then the complexity needed for any particular application can be read directly from the curves. The special choice of constants also leads to special

formulae for element values of corresponding networks, using tandem sections of the simplest all-pass type (Fig. 3).

Form of the $\tan\left(\frac{\beta}{2}\right)$ Function

If β_1 and β_2 represent the phase shifts through the two constant resistance networks of Fig. 1, then $\tan\left(\frac{\beta_1}{2}\right)$ and $\tan\left(\frac{\beta_2}{2}\right)$ must both be realizable as the reactances of physical reactance networks. In other words, these quantities must be odd rational functions of ω with real coefficients and must also meet various other special restrictions. If β is used to represent the phase difference $\beta_2 - \beta_1$, the function $\tan\left(\frac{\beta}{2}\right)$ must also be an odd rational function of ω with real coefficients. Because of the minus sign

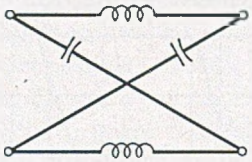

Fig. 3—Simplest all-pass section.

associated with β_1 in the definition of β, however, $\tan\left(\frac{\beta}{2}\right)$ does not have to meet the additional restrictions which must be imposed upon $\tan\left(\frac{\beta_1}{2}\right)$ and $\tan\left(\frac{\beta_2}{2}\right)$. In a later part of the paper a method will be described by which a pair of physical phase shifting networks can be designed to produce any $\tan\left(\frac{\beta}{2}\right)$ function which is an odd rational function of ω with real coefficients.

In any range where the phase difference β approximates a constant, the function $\tan\left(\frac{\beta}{2}\right)$ will also approximate a constant. Hence, the present problem is really that of approximating a constant over a given frequency range with an odd rational function of ω with real coefficients. In this problem, the degree of the function must be assumed to be prescribed as well as the frequency range in which a good approximation is to be obtained, for the degree of the function determines the complexity of the corresponding network.

W. Cauer shows how functions of certain types can be designed to approx-

imate unity in prescribed frequency ranges.[3] These functions, however, are not odd rational functions of frequency but are irrational functions appropriate to represent filter image impedances or the hyperbolic tangents or cotangents of filter transfer constants. It turns out, however, that they can be transformed into odd rational functions of the desired type by a simple transformation of the variable.

Each of Cauer's functions is said to approximate a constant in the Tchebycheff sense, which means that in the prescribed range of good approximation the maximum departure from the approximated constant is as small as is permitted by the specifications on the frequency range and the degree of the function. Each function also has the property of exhibiting series of equal maxima and equal minima in the range of good approximation, such as those indicated in the illustrative β curve[4] of Fig. 4.

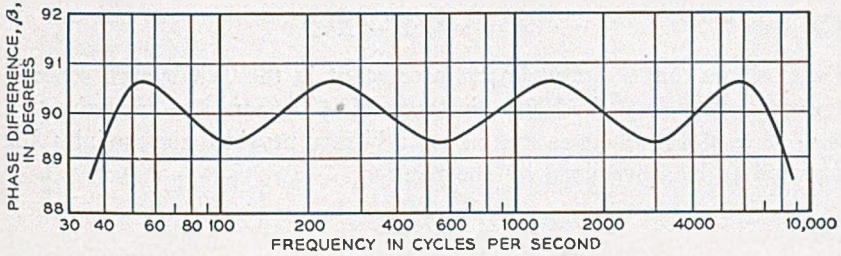

Fig. 4—Example of a phase difference characteristic.

Of the various forms in which Cauer's Tchebycheff functions F can be expressed, the following form is the one appropriate for showing how odd rational functions of frequency can be obtained:

(1)
$$F = \begin{cases} \text{When } n \text{ is odd} \\ \quad U\sqrt{1-X^2}\prod_{s=1}^{s=\frac{n-1}{2}} \dfrac{\left[1 - sn^2\left(\dfrac{2s-1}{n}K, k\right)X^2\right]}{\left[1 - sn^2\left(\dfrac{2s}{n}K, k\right)X^2\right]}. \\ \text{When } n \text{ is even} \\ \quad F = \dfrac{U}{\sqrt{1-X^2}} \dfrac{\prod_{s=1}^{s=\frac{n}{2}}\left[1 - sn^2\left(\dfrac{2s-1}{n}K, k\right)X^2\right]}{\prod_{s=1}^{s=\frac{n}{2}-1}\left[1 - sn^2\left(\dfrac{2s}{n}K, k\right)X^2\right]}. \end{cases}$$

[3] "Ein Interpolationsproblem mit Funktionen mit Positivem Realteil," *Mathematische Zeitschrift*, 38, 1–44 (1933).

[4] The data for the illustrative curve were obtained from a trial design carried out by P. W. Rounds.

In these equations, the symbol *sn* indicates an elliptic sine, of modulus k, while K represents the corresponding complete elliptic integral. U is merely a constant scale factor, while n is an integer measuring the complexity of corresponding networks. In the case of phase-difference networks, n represents the total number of sections of the type indicated in Fig. 3, which are included in the two phase-shifting networks or their tandem section equivalents.

In Cauer's filter theory, the variable X represents a rational function of ω which permits F to be an image impedance or a $\coth\left(\frac{\theta}{2}\right)$ function. In order that F may be an odd rational function of ω, however, as is required when it is to represent $\tan\left(\frac{\beta}{2}\right)$, X must be defined by the relation

$$\omega = \omega_2\sqrt{1 - X^2}. \tag{2}$$

Cauer shows that F approximates a constant in the Tchebycheff sense in the range $0 < X < k$. Hence, in terms of ω, the range of approximation is $\omega_1 < \omega < \omega_2$, where ω_1 and ω_2 are arbitrary provided the modulus k is assumed to be determined by the relation

$$k = \frac{\sqrt{\omega_2^2 - \omega_1^2}}{\omega_2}. \tag{3}$$

Alternative Expression for the $\tan\left(\frac{\beta}{2}\right)$ Function

While equations (1) are the most convenient form of F to use in deriving the transformation of the variable, an alternative more compact form is more suitable for determining the degree of approximation to a constant phase difference and the element values of corresponding networks. When F represents $\tan\left(\frac{\beta}{2}\right)$ and hence ω and X are related as in (2), the equivalent expression is as follows:[5]

$$\tan\left(\frac{\beta}{2}\right) = U\, dn\left(nu\,\frac{K_1}{K}, k_1\right) \tag{4}$$

$$\omega = \omega_2\, dn(u, k).$$

In this expression, *dn* represents a so-called "*dn*" function, the third type of Jacobian elliptic function usually associated with the elliptic sine, or *sn* function, and the elliptic cosine, or *cn* function. The symbol u represents

[5] This expression depends on a so called modular transformation of elliptic functions not found in the usual elliptic function text. The transformation theory may be found in "An Elementary Treatise on Elliptic Functions," Arthur Cayley, G. Bell & Sons, London, 1895.

a "parametric variable" which would be eliminated on forming a single equation from the two simultaneous equations indicated. The modulus k_1, of the *dn* function corresponding to $\tan\left(\frac{\beta}{2}\right)$ is related to the modulus k, of the *dn* function corresponding to ω, in the manner indicated below. The constant K_1, of course, represents the complete integral of modulus k_1, just as K represents the complete integral of modulus k.

Corresponding to any modulus k there is a so-called modular constant q. Using q_1 to represent the corresponding modular constant of modulus k_1, it is here required that

$$q_1 = q^n. \tag{5}$$

One modulus can be computed from the other by means of this relationship and tabulations of $\log_{10} q$ vs $\sin^{-1} k$ which are included in most elliptic function tables.[6]

Degree of Approximation to a Constant Phase Difference

When u is real and varies from zero to infinity, the corresponding value of ω as determined by (4) merely oscillates back and forth between the values ω_1 and ω_2. In other words, it merely crosses back and forth across the range in which $\tan\left(\frac{\beta}{2}\right)$ approximates a constant. Similarly, when u is real and increases from zero to infinity, $\tan\left(\frac{\beta}{2}\right)$ oscillates between $U\sqrt{1-k_1^2}$ and U. The *equal ripple* property of the curve illustrated in Fig. 4 is explained by the fact that the period of oscillation of $\tan\left(\frac{\beta}{2}\right)$ with respect to u is merely a fraction of that of ω, so that $\tan\left(\frac{\beta}{2}\right)$ passes through several ripples while the value of ω moves from ω_1 to ω_2.

Combining the formulae for the maximum and minimum values of $\tan\left(\frac{\beta}{2}\right)$ gives the relation

$$\tan\left(\frac{\delta}{2}\right) = \frac{U(1-\sqrt{1-k_1^2})}{1+U^2\sqrt{1-k_1^2}} \tag{6}$$

[6] When k is extremely close to unity, it may be easier to obtain accurate computations by using the additional relation

$$\log_{10}(q)\,\log_{10}(q') = \left(\frac{\pi}{\log_e(10)}\right)^2$$

where q' is the modular constant of modulus $\sqrt{1-k^2} = \frac{\omega_1}{\omega_2}$.

in which δ represents the total variation of the phase difference β in the approximation range. Similarly, the average value β_a of β in the approximation range is given by[7]

$$\tan(\beta_a) = \frac{U(1 + \sqrt{1 - k_1^2})}{1 - U^2\sqrt{1 - k_1^2}}. \tag{7}$$

If the phase variation δ is reasonably small, (6) and (7) can be replaced by the approximate relationships

$$\delta = \frac{\sin(\beta_a)}{2} k_1^2 \quad \text{radians}$$
$$\tan\left(\frac{\beta_a}{2}\right) = U\sqrt[4]{1 - k_1^2}.^{8} \tag{8}$$

A still further modification is obtained by replacing k_1^2 by the quantity $16q_1$, which is an approximate equivalent when k_1^2 is small, and by then replacing q_1 by the equivalent q^n of (5). This gives

$$\delta = 8 \sin(\beta_a) q^n \tag{9}$$
$$\tan\left(\frac{\beta_a}{2}\right) = U\sqrt[4]{1 - 16q^n}.$$

When combined with (3) and tabulations of $\sin^{-1}(k)$ vs $\log_{10}(q)$, these formulae can be used to compute δ when the parameters ω_1, ω_2, β_a and n are prescribed. Curves of δ are plotted against ω_2/ω_1 in Fig. 2, assuming β_a to be 90 degrees.

Determination of a Network Corresponding to a General Phase Difference Function

Since $\tan\left(\frac{\beta}{2}\right)$ must be an odd rational function of ω, it can be expressed in the form

$$\tan\left(\frac{\beta}{2}\right) = \frac{\omega B}{A} \tag{10}$$

in which A and B are even polynomials in ω. This requires

$$\frac{\beta}{2} = \arg(A + i\omega B). \tag{11}$$

[7] More exactly, β_a is the average of the maximum and minimum values of β occurring in the range of approximation.

[8] In the important special case in which the average phase difference β_a is 90°, this expression for $\tan\left(\frac{\beta_a}{2}\right)$ is exact rather than approximate.

Similarly, if attention is focused on the phase shifts of the individual phase-shifting networks rather than on the phase difference, the following odd rational functions can be introduced:

$$\tan\left(\frac{\beta_1}{2}\right) = \frac{\omega B_1}{A_1}$$
$$\tan\left(\frac{\beta_2}{2}\right) = \frac{\omega B_2}{A_2} \tag{12}$$

in which A_1, B_1, A_2, and B_2 are additional even polynomials in ω. This requires

$$\frac{\beta_1}{2} = \arg(A_1 + i\omega B_1)$$
$$\frac{\beta_2}{2} = \arg(A_2 + i\omega\beta_2). \tag{13}$$

It also requires

$$-\frac{\beta_1}{2} = \arg(A_1 - i\omega B_1). \tag{14}$$

Since the argument of a product is the sum of the arguments of the separate factors, (13) and (14) require

$$\frac{\beta}{2} = \frac{\beta_2 - \beta_1}{2} = \arg(A_2 + i\omega B_2)(A_1 - i\omega B_1). \tag{15}$$

This permits us to write

$$(A_2 + i\omega B_2)(A_1 - i\omega B_1) = H(A + i\omega B) \tag{16}$$

in which H is a real constant.

When $\tan\left(\frac{\beta}{2}\right)$ is prescribed, a corresponding polynomial of the form $(A + i\omega B)$ can readily be derived. The problem is then to factor it into the product of two polynomials $(A_2 + i\omega B_2)$ and $(A_1 - i\omega B_1)$ such that A_1, B_1, A_2, and B_2 determine physically realizable phase shifts through (12). Two factors of the general form $(A_2 + i\omega B_2)$ and $(A_1 - i\omega B_1)$ can readily be obtained in a number of ways. The only question is how to obtain them in such a way that the corresponding phase characteristics will be physical. A procedure meeting this requirement is described below.

The variable ω is first replaced in $(A + i\omega B)$ by p representing $i\omega$. This leaves a polynomial in p with real coefficients, since A and B represent polynomials in ω^2, while p^2 represents $-\omega^2$. Suppose all the roots of the polynomial $A + pB$ are determined. Then this polynomial can be split into

two factors by assigning various of the roots to each of the two factors. It turns out that physically realizable phase characteristics will be obtained if all those roots with positive real parts are assigned to the factor $(A_1 - pB_1)$ which appears in (16) when $i\omega$ is replaced by p, all other roots being assigned to the factor $(A_2 + pB_2)$.

The physical realizability of the above division of the roots follows from a theorem which states that $\frac{pB_x}{A_x}$ is realizable as the impedance of a two-terminal reactance network whenever A_x and B_x are even polynomials in p with real coefficients such that $A_x + pB_x$ has no roots with positive real parts.[9] From this theorem and the fact that the evenness of A_x and B_x causes them to remain unchanged when p is reversed in sign, it follows that $\frac{pB_x}{A_x}$ will also be the impedance of a physical two-terminal reactance network whenever $A_x - pB_x$ has no roots with *negative* real parts. Thus, by (12) the above division of the roots of $A + pB$ makes $\tan\left(\frac{\beta_1}{2}\right)$ and $\tan\left(\frac{\beta_2}{2}\right)$ realizable as the impedances of two-terminal reactance networks. These reactance networks and their inverses are merely the arms of unit impedance lattices producing the phase characteristics defined by (12).

The above argument merely shows that each of the two phase-shifting networks can at least be realized as a single lattice when $\tan\left(\frac{\beta_1}{2}\right)$ and $\tan\left(\frac{\beta_2}{2}\right)$ are determined by the method described. Actually, they can be broken into tandem sections directly as soon as the roots of $(A_1 - pB_1)$ and $(A_2 + pB_2)$ have been determined. From $(A_1 - pB_1)$, the quantity $(A_1 + pB_1)$ can be found by merely reversing the signs of the roots. Then by using the principle that the argument of a product is the sum of the arguments of the separate factors, phase-shifting networks can be designed corresponding to various factors or groups of factors as determined from the known roots of $(A_1 + pB_1)$ and $(A_2 + pB_2)$. There can be a separate section for each real root and each conjugate pair of complex roots.[10]

Determination of a Network Corresponding to a Tchebycheff Type of Phase Difference Characteristic

The procedure described above for determining a network corresponding to a general phase difference characteristic is complicated by the necessity

[9] See "Synthesis of Reactance 4-Poles which Produce Prescribed Insertion Loss Characteristics," *Journal of Mathematics and Physics*, Vol. XVIII, No. 4, September, 1939—page 276.

[10] See H. W. Bode, "Network Analysis and Feedback Amplifier Design," D. Van Nostrand Company, New York, 1945, Page 239, §11.6.

of determining the roots of the polynomial $A + pB$. In the case of the Tchebycheff type of characteristic described in the first part of the paper, the required roots can be determined by means of special relationships. In the first place, the roots of $A + pB$ are the roots of $\left(1 + i \tan\frac{\beta}{2}\right)$. In other words, by equation (4) they are the roots of $\left[1 + iU\, dn\left(nu\frac{K_1}{K}, k_1\right)\right]$. The values of u at the roots turn out to have an imaginary part iK', where K' is the complete elliptic integral of modulus $\sqrt{1 - k^2}$. If a new variable u' is defined by

$$u = u' + iK' \tag{17}$$

the roots can be shown to correspond to the values of u' determined by

$$\frac{sn\left(nu'\frac{K_1}{K}, k_1\right)}{cn\left(nu'\frac{K_1}{K}, k_1\right)} = -U. \tag{18}$$

If it is assumed that the phase variation is small in the range of approximation to a constant, it can be shown that one value of u' determined by the above relation is given approximately by

$$\frac{nu'\pi}{K} = -\beta_a \tag{19}$$

where β_a is the average phase difference for the range of approximation as before (in radians). After this value of u' has been computed, all the roots of $\left[1 + iU\, dn\left(nu\frac{K_1}{K}, k_1\right)\right]$ can be found by computing the values of ω corresponding to this value of u' and to those values obtained by adding integral multiples of the real period $\frac{2K}{n}$ of $dn\left(nu\frac{K_1}{K}, k_1\right)$. This gives the following formula for the roots in terms of $p = i\omega$.

$$p_\sigma = \omega_2 \frac{cn\left(\frac{2\sigma K}{n} + u_0'\right)}{sn\left(\frac{2\sigma K}{n} + u_0'\right)}, \qquad \sigma = 0, \cdots, (n-1) \tag{20}$$

in which u_0' is the value of u' determined by (19).

Finally, instead of using the above elliptic function formula directly, one may replace the elliptic functions by equivalent ratios of Fourier series expansions of θ functions. This gives

$$p_\sigma = \sqrt{\omega_1\omega_2}\, \frac{\cos(\lambda_\sigma) + q^2\cos(3\lambda_\sigma) + q^6\cos(5\lambda_\sigma) \cdots}{\sin(\lambda_\sigma) - q^2\sin(3\lambda_\sigma) + q^6\sin(5\lambda_\sigma) \cdots} \tag{21}$$

in which the angle λ_σ is defined by

$$\lambda_\sigma = \frac{\sigma \cdot 180^\circ - \frac{1}{2}\beta_a}{n} \text{ degrees}, \qquad \sigma = 0, \cdots, (n-1). \tag{22}$$

Because all the p_σ's are real in this Tchebycheff case, corresponding networks can be made up of sections of the simple type indicated in Fig. 3. In one of the two phase-shifting networks there will be one section for each positive p_σ, and it will be given by

$$L = \frac{R_0}{p_\sigma} \qquad C = \frac{1}{R_0 p_\sigma}$$

where R_0 is the image impedance. Similarly, in the second phase-shifting network there will be one section for each negative p_σ, and it will be given by

$$L = -\frac{R_0}{p_\sigma} \qquad C = \frac{-1}{R_0 p_\sigma}.$$

Conversion of Concentrated Loads on Wood Crossarms to Loads Distributed at Each Pin Position

By RICHARD C. EGGLESTON

ONE of the most important requisites in all fields of engineering endeavor is knowledge of the strength of materials. The development of testing machines and techniques to study the basic properties of metals, plastics and wood products to withstand breaking forces has been a distinctive achievement during the last half century. All materials, whether they be part of a bridge, a building, a shipping crate, a telephone pole or a crossarm on a telephone pole, break under an excessive stress. To have accurate knowledge of the strength of the millions of crossarms used to carry the regular load of wires, which are frequently subjected to the extra loads of wind and ice, is most important in electrical communication.

When strength tests of crossarms are made, the information most generally sought is how great a vertical load equally distributed at each insulator pin hole will the arms stand. In the past many crossarm tests have been made by the concentrated load method, where the arm is either supported at each end and loaded at the center, or supported at the center and loaded at the ends until failure occurs (Fig. 1, a and b). Some have been made by the distributed load method by placing, manually and simultaneously, 50-pound weights in wire baskets suspended from each pin hole, and continuing such load applications until the arm fails. The method is objectionable chiefly because, in many of the tests, the loading is inadvertently carried past the maximum loads the arms will support. This objection was overcome in recent tests made by the Bell Telephone Laboratories[1], where the loads were also distributed at each pin position. However, instead of subjecting the 10-pin test arms to sudden 500-pound load increments (viz. 50 pounds at each of the 10 pin holes), the loads were applied gradually by a hydraulic testing machine (Fig. 1, c). But, in spite of the advantages of this machine method of distributed load application, it is probable that, because of the less elaborate apparatus involved in simple beam tests, there will continue to be tests made by the concentrated load method.

Where tests have been made by the concentrated load method, the question arises how can the results be converted to a load-per-pin basis? A conversion is needed before a fair comparison can be made of all test results, and also to furnish the information generally most wanted, which is, as

[1]Bell System Monograph No. B-1563, Strength Tests of Wood Crossarms.

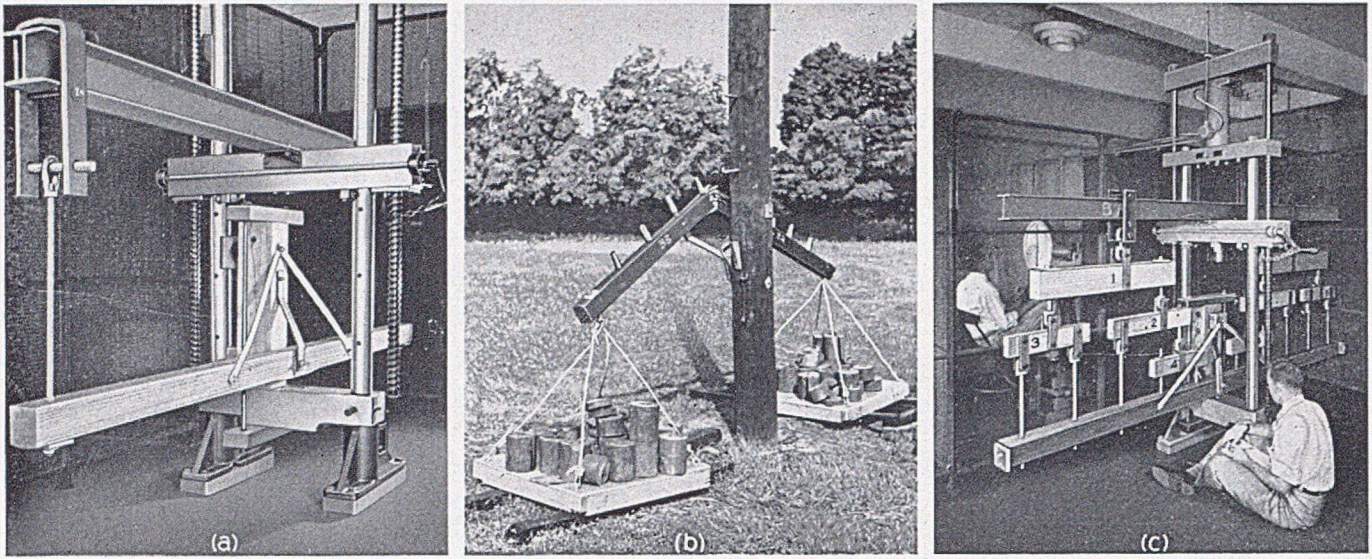

Fig. 1—Photographs of crossarm tests:
a—Arm supported at center in testing machine ready for application of load at end pin holes.
b—Arm supported at center on a pole. This roofed 10A arm was loaded manually at end pin holes and failed at a pole pin hole (critical) section.
c—Arm supported at center in testing machine ready for application of load at each pin position.

previously stated, what load per pin will the arm support? There are more than twenty million crossarms in the pole lines of the Bell System and each year about a million arms are added. A complete understanding of every problem associated with this important item of outside plant material is manifestly worth while. This paper is intended to contribute to that end. It presents a solution of the problem of converting concentrated vertical loads to comparable loads distributed at each insulator pin position.

The location of the critical section in crossarms is a basic factor in a study of the problem. The critical section of a crossarm is the section at which the fiber stress is greatest when the arm is loaded. It is the section where the arm may be expected to break if overloaded. To determine its location, the bending moment at various sections along the arm is divided by the section modulus of the respective sections. The quotient in each instance is the fiber stress for each section investigated. The location showing the greatest fiber stress is the critical section. Since horizontal shear is not the controlling stress in crossarm failures under loads distributed at each pin hole, bending stresses only were considered in this analysis.

Because of the differences in arm shape and in the spacing of pin holes, the location of the critical section is not the same in all arms. It is estimated that at least three fourths of the arms in the Bell System are 10A and 10B crossarms.[2] Both are 10 feet long and 3.25″ x 4.25″ in cross section. In the 10A arm (Fig. 3), the space between the pin holes is 12 inches, except between the pole pin holes, where the space is 16 inches. In the 10B (Fig. 4) the pin hole spacing is 10 inches with a 32-inch space between the pole pins. Both types are bored for wood pins. Most of the arms now in the plant are "roofed", that is, the top surface of the arm, except the center foot of length, is rounded on a radius of about 4.25 inches. Under the current design, however, the top surface of Bell System arms is flat, except for the edges, which are beveled.

Previous studies of both roofed and beveled arms of various types have shown that the critical section of clear arms under vertical loads is either at the center or at the pole pin hole sections. This study is confined to those sections of clear 10A and 10B crossarms of nominal dimensions, both roofed and beveled. Moreover, it was assumed for the purpose of load analysis, that the crossarms are supported at the center only; since, under loads on each side of the pole, the standard crossarm braces provide no significant support when the loads are sufficient to break the arm.

Roofed 10A Arm

Let it be assumed that the breaking load concentrated in each end pin hole of a roofed 10A arm is 800 pounds. As shown in Calculation 1 in the

[2]10A and 10B crossarms were formerly known as Type A and Type B crossarms, respectively.

appendix, the bending moment at the center of the arm from the assumed loads would be 44,800 pound-inches, and the fiber stress at the center would be 4600 psi. That calculation also shows that the bending moment at the pole pin holes would be 38,400 pound-inches, and the fiber stress at the pole pin holes 7515 psi. Since the stress at the pole pin holes is greater than that at the center, the critical section of a roofed 10A arm is at the pole pin holes when the arm is subjected to a breaking load at each end pin hole.

The information wanted, however, is what load at each of the ten pin positions would have produced the same moment and same fiber stress at the critical section? A *tentative* answer is found by dividing the 38,400 bending moment by the "total-per-pin" lever arm[3], 120″ (see Calculation 1) or 320 pounds. Checking to determine whether the location of the critical section changes under loads of 320 pounds at each pin position, Calculation 1 shows that the fiber stress at the pole pin holes and at the center would be 7515 psi and 5257 psi, respectively. Since the stress at the pole pin holes is greater, it is clear that the critical section is there also under equal loads at each pin position; and the 320-pound load per pin is comparable to the concentrated load of 800 pounds at each end of the arm.

If a similar investigation were made of a roofed 10B arm and of a beveled 10A arm, it would be found that the pole pin hole section is the critical section of these arms; and that the load per pin comparable to concentrated loads at the arm ends would, like the roofed 10A arm, be equal to the bending moment at the pole pin hole section due to the concentrated load divided by the total per pin lever arm to that section. Figure 1b shows a roofed 10A arm that broke under test at a pole pin hole (critical) section from concentrated loads at the ends of the arm.

Beveled 10B Arm

For the investigation of this arm, let a breaking load of 1000 pounds at each end pin hole be assumed. Incidentally, it should be noted that so far as this analysis is concerned, the magnitude of the assumed concentrated loads is of no importance. However, since both computations and tests show the 10B arm to be stronger than the 10A, it seemed appropriate to assume a larger concentrated load for the 10B arm.

As shown in Calculation 2 of the appendix, the bending moment at the center due to the 1000-pound load would be 56,000 pound-inches and the fiber stress 5882 psi, while at the pole pin holes the bending moment would be 40,000 pound-inches and the fiber stress 6885 psi. Here again, under concentrated loads at each end pin hole, the critical section is at the pole pin holes.

[3]By total-per-pin lever arm is meant the summation of the distances from each pin position to the section concerned—in this instance to the pole pin hole section.

Calculating the load for each of the 10 pin positions in the same manner as for the roofed 10A arm, we have, tentatively, a load per pin of 400 pounds. However, in checking to determine whether the location of the critical section changes under loads of 400 pounds at each pin position, we obtain results quite different from those in Calculation 1; for Calculation 2 indicates a fiber stress of 6885 psi at the pole pin holes, but a higher stress (7563 psi) at the center, which shows that the location of the critical section does change. Moreover, this change would occur whether the loads were 400 pounds per pin or 4 pounds per pin. But let us now consider the 400-pound load.

If a concentrated load of 1000 pounds results in a fiber stress at the pole pin hole section of 6885 psi and causes failure, that stress is the *maximum* ultimate fiber stress for the arm. It is, therefore, not reasonable to suppose that the same arm would have endured a higher stress (7563 psi) at the center if it had been loaded at each pin position. If 6885 psi is the maximum stress for the arm, the maximum moment it would endure at its center would be 65,500 pound-inches (viz. 6885 multiplied by 9.52, the section modulus of the center section). The maximum load per pin would be 364 pounds (viz. 65,500 divided by 180, the total-per-pin lever arm to the center); and this load of 364 pounds, not 400 pounds, distributed at the 10 pin positions is comparable to the 1000-pound concentrated load. Thus, while the critical section of a beveled 10B arm is at the pole pin holes when the load is concentrated at the arm ends, it shifts to the center when the load is distributed at each pin position; and, moreover, the load is less than the load per pin tentatively computed.

A graphic illustration of this shift of the critical section is shown in Fig. 2. Graph 1 in this figure is the graph of the resisting moments of a clear, straight-grained beveled 10B arm, 3.25″ x 4.25″ in cross-section, and having an assumed ultimate fiber strength in bending of 6000 psi. Each point in the graph is equal to the section modulus of the section under consideration multiplied by 6000 psi. Graph 2, which is the graph of a concentrated load at the end pin position, was drawn from the zero moment under the end pin to the point of greatest moment possible without intersecting resisting moment Graph 1. Since the point of coincidence between Graphs 1 and 2 is the pole pin hole section, that section is the critical section for a concentrated load at the end pin. The magnitude of this concentrated load is equal to the resisting moment at the pole pin hole, 34,860 pound-inches (viz. 5.81 inches^3 x 6000 psi) divided by the 40″ lever arm, or 871.5 pounds. The load per pin, *tentatively figured*, would be 34,860 pound-inches divided by 100 inches or 348.6 pounds. Graph 3 is the graph of a load (P) of 348.6 pounds at each pin hole. Under such loading, however, the bending moment at the center of the crossarm would be 62,748 pound-

inches (viz. 348.6 x 180), which exceeds the 57,120 pound-inches resisting moment at the center (viz. 9.52 inches^3 x 6000 psi). This means that the

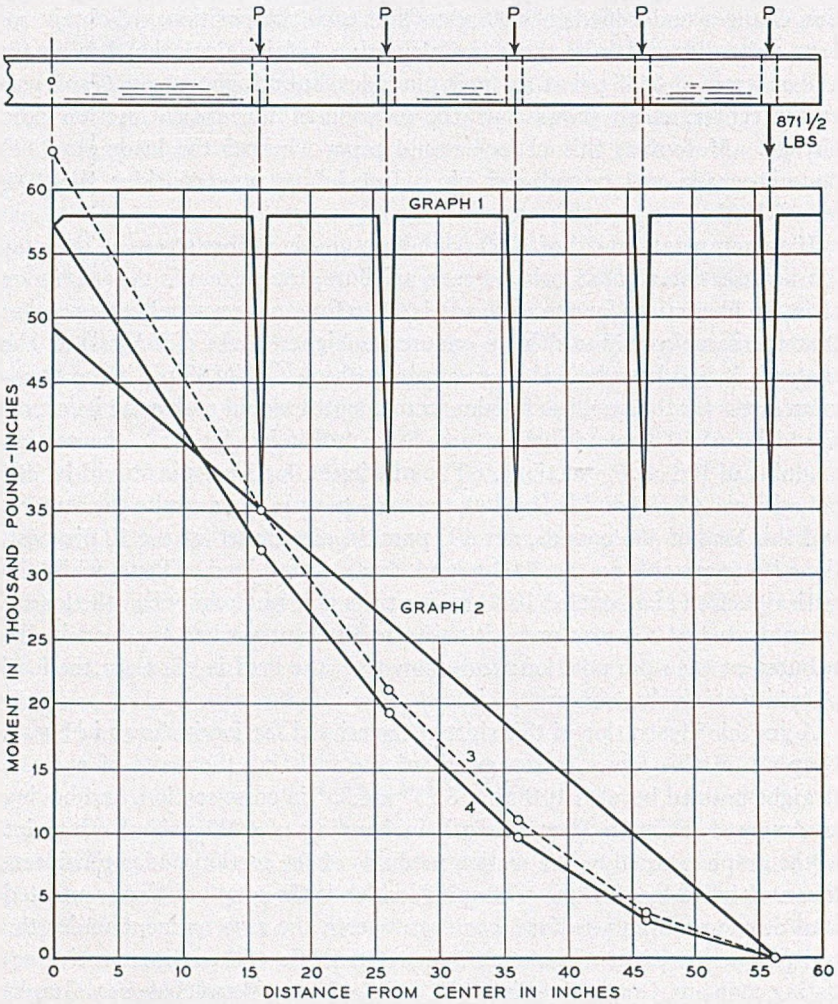

Fig. 2—Moment diagrams for a beveled 10B crossarm:
Graph 1—Resisting moments of a clear, straight grained, 3.25″ x 4.25″ arm. Fiber stress assumed to be 6000 psi;
Graph 2—Bending moments from a concentrated load of 871.5 pounds at end pin hole;
Graph 3—Bending moments from a load of 348.6 pounds at each pin hole; and
Graph 4—Bending moments from a load of 317.3 pounds at each pin hole.

arm would fail under such loading; and that the critical section of the arm under loads distributed at each pin hole is not at the pole pin holes but at the center of the arm. The maximum load per pin that the arm would

endure is the resisting moment at the center divided by the total-per-pin lever arm, or 57,120 pound-inches divided by 180 inches or 317.3 pounds. Graph 4 is the bending moment graph of this 317.3-pound maximum load per pin.

SUMMARY

Let W = Concentrated load,
P = Load per pin,
Mp = Bending moment at pole pin hole section,
fc = Fiber stress at center section,
fp = Fiber stress at pole pin hole section,
Sc = Section modulus of center section, and
Sp = Section modulus of pole pin hole section.

Using this notation, the results of the analyses may be summarized as follows:

For 10A arms both roofed and beveled:

$$Mp = 48W \quad \text{(for concentrated loads), and}$$

$$Mp = 120P \quad \text{(for pin loads). Therefore,}$$

$$P = \frac{48W}{120} = 0.4W$$

For 10B arms-roofed:

$$Mp = 40W \quad \text{(for concentrated loads), and}$$

$$Mp = 100P \quad \text{(for pin loads). Therefore,}$$

$$P = \frac{40W}{100} = 0.4W$$

For the beveled 10B arm, however, where the critical section is at the center, the value P = 0.4W does not apply. The value of P would be such as to produce the same fiber stress at the center section as the fiber stress resulting from the concentrated load (W) at the pole pin hole section. Thus

$$fc = \frac{180P}{Sc} \quad \text{and}$$

$$fp = \frac{40W}{Sp}$$

Equating these, we have

$$\frac{180P}{Sc} = \frac{40W}{Sp} \quad \text{and}$$

$$P = \frac{40W}{Sp} \times \frac{Sc}{180} = \frac{2ScW}{9Sp} = \frac{2 \times 9.52W}{9 \times 5.81} = 0.364W$$

Therefore, under the conditions assumed, and only under such conditions, we may say that the loads per pin (P) comparable to the assumed concentrated loads (W) would be

$$P = 0.4W \text{ for } \begin{cases} \text{10A arms—roofed} \\ \text{10A arms—beveled} \\ \text{10B arms—roofed} \end{cases}$$

and

$$P = 0.364W \text{ for 10B arms—beveled}$$

While these results are restricted to the four arm types listed, the same principles followed in arriving at these results may be applied to other types and sizes of arms, and to other conditions of loading. Whether the conversion of single concentrated loads to loads per pin is performed by the method illustrated in Calculations 1 and 2 of the appendix, or is done by a moment diagram, as in Fig. 2, the procedure recommended is as follows:

Step 1. Determine the critical section under the concentrated load.

Step 2. Divide the bending moment at the critical section by the total-per-pin lever arm to the critical section to determine the load per pin.

Step 3. Check the fiber stress (under such loads per pin) at various sections to see whether the *location* of the critical section differs under load per pin.

Step 4. If it does differ, proceed as shown for the beveled 10B arm (viz., the comparable load per pin is equal to the resisting moment of the *critical section* divided by the total-per-pin lever arm to the critical section). If it does not differ, the load per pin as determined in Step 2 is the comparable load per pin sought.

Conclusions

(1) The location of the critical section under loads distributed at each pin position must be determined before undertaking the conversion of concentrated loads to distributed loads.

(2) The location of the critical section of a crossarm under a given condition of loading may or may not be the same under a different condition of loading.

(3) The load per pin comparable with a given concentrated load is equal to the resisting moment of the *critical* section divided by the total-per-pin lever arm to the critical section.

(4) While the results shown are confined to the conversion of concentrated vertical loads to distributed loads for 10A and 10B arms only, the principles of the study may be applied to other types and sizes of arms and to other conditions of loading.

APPENDIX

Calculation 1. Bending Moments and Fiber Stresses in a Roofed 10A Crossarm—(See Figure 3)

Notation:

W = 800 pounds concentrated load
P = Load per pin
Mc = Bending moment at arm center
Mp = Bending moment at pole pin hole
fc = Fiber stress at center
fp = Fiber stress at pole pin hole
Sc = Section modulus of center section[4]
Sp = Section modulus of pole pin hole section[4]

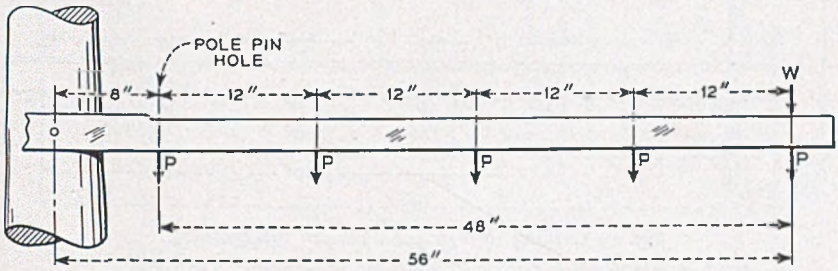

Fig. 3—Loading diagram for a roofed 10A crossarm.

Concentrated Load:

$Mc = W \times 56 = 800 \times 56 = 44{,}800$ pound-inches
$Mp = W \times 48 = 800 \times 48 = 38{,}400$ pound-inches
$fc = Mc \div Sc = 44{,}800 \div 9.74 = 4600$ psi
$fp = Mp \div Sp = 38{,}400 \div 5.11 = 7515$ psi

Load per Pin:

$Mc = 56P + 44P + 32P + 20P + 8P = 160P$
$Mp = 48P + 36P + 24P + 12P = 120P$

(Note: The total-per-pin lever arms are 160″ to center and 120″ to the pole pin hole).

Since under W load f is maximum at pole pin hole, the P load that would result in same f is $P = 38{,}400 \div 120 = 320$ pounds. Thus

$fp = 120P \div Sp = (120 \times 320) \div 5.11 = 7515$ psi
$fc = 160P \div Sc = (160 \times 320) \div 9.74 = 5257$ psi

Conclusion:

Under both W loads and P loads, the critical section is the pole pin hole section.

[4] $Sc = 9.74$ and $Sp = 5.11$ for clear roofed 3.25″ x 4.25″ crossarms. (See Pages 27 and 28 of *Bell Sys. Tech. Jour.*, Jan. 1945).

Calculation 2. Bending Moments and Fiber Stresses in a Beveled 10B Crossarm—(See Figure 4)

Notation:

W = 1000 pounds concentrated load
P = Load per pin
Mc = Bending moment at arm center
Mp = Bending moment at pole pin hole
fc = Fiber stress at center
fp = Fiber stress at pole pin hole
Sc = Section modulus of center section[5]
Sp = Section modulus of pole pin hole section[5]

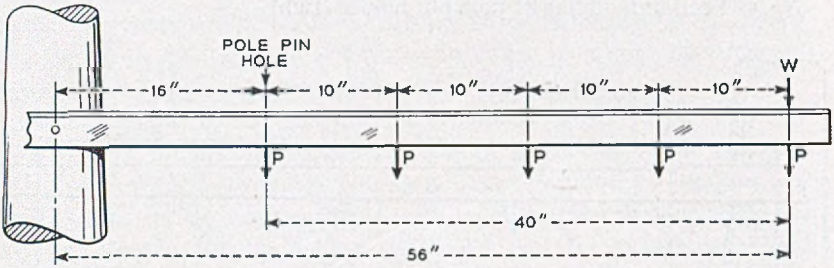

Fig. 4—Loading diagram for a beveled 10B crossarm.

Concentrated Load:

$Mc = W \times 56 = 1000 \times 56 = 56{,}000$ pound-inches
$Mp = W \times 40 = 1000 \times 40 = 40{,}000$ pound-inches
$fc = Mc \div Sc = 56{,}000 \div 9.52 = 5882$ psi
$fp = Mp \div Sp = 40{,}000 \div 5.81 = 6885$ psi

Load per Pin:

$Mc = 56P + 46P + 36P + 26P + 16P = 180P$
$Mp = 40P + 30P + 20P + 10P = 100P$
$P = 40{,}000 \div 100 = 400$ pounds

$$fp = \frac{100P}{Sp} = \frac{100 \times 400}{5.81} = 6885 \text{ psi}$$

$$fc = \frac{180}{Sc} = \frac{180 \times 400}{9.52} = 7563 \text{ psi}$$

Conclusion:

Critical section shifts under P loads, and arm will not support 400 pounds per pin.

[5] $Sc = 9.52$ and $Sp = 5.81$ for clear beveled 3.25" x 4.25" crossarms. (See Calculation 3 of this appendix.)

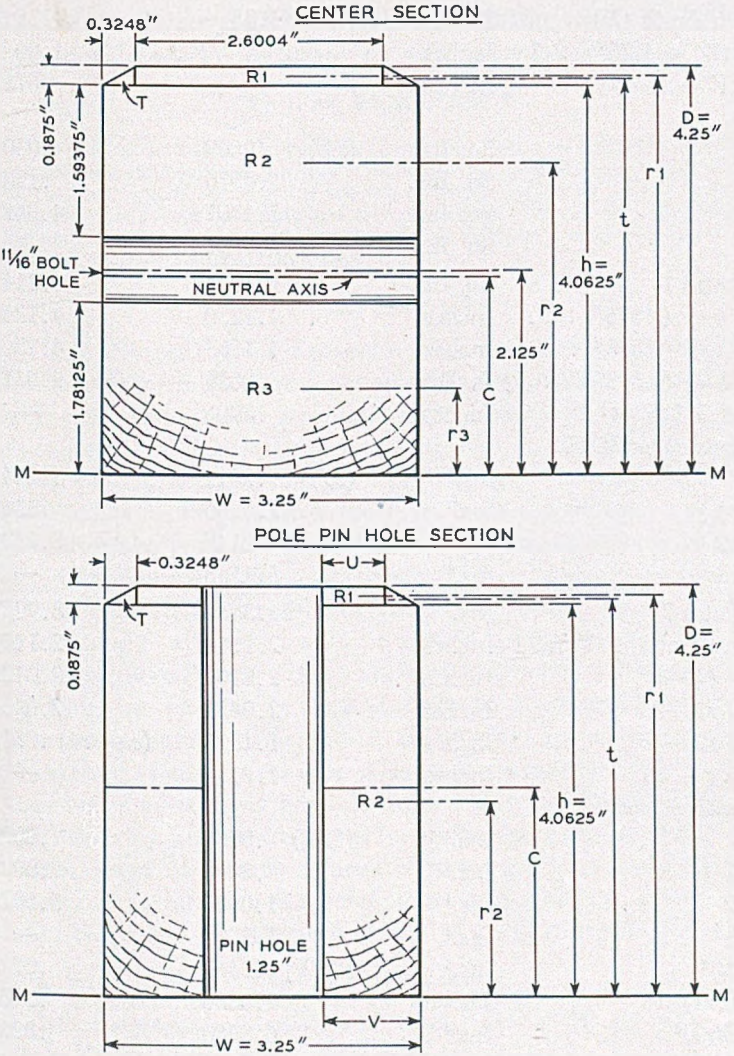

Fig. 5—Beveled crossarm sections showing significance of the notation used in Calculation 3 of this appendix.

Calculation 3. Section Modulus—Clear Beveled Sections
(The notation used in this calculation is shown in Fig. 5)

		Center Section		Pole Pin Hole Section
Section width (W)	Inches		3.25	3.25
Section depth (D)	Inches		4.25	4.25
$V = (W - 1.25'') \div 2$	Inches			1.00
$U = V - .3248''$	Inches			.6752
Areas:				
T	Sq. Ins.	$(2T)$	.0609	.0304
$R1$	Sq. Ins.		.4876	.1266
$R2$	Sq. Ins.		5.1797	4.0625
$R3$	Sq. Ins.		5.7891	—
Total 1	Sq. Ins.		11.5173	4.2145
$t = h + (.1875'' \div 3)$	Inches		4.1250	4.1250
$r1 = h + (.1875'' \div 2)$	Inches		4.1563	4.1563
$r2 = h - (1.59375'' \div 2)$	Inches		3.2656	$(\frac{1}{2}h)$ 2.0313
$r3 = 1.78125'' \div 2$	Inches		.8906	—
Moments about MM:				
Tt	Ins.^{3}	$(2Tt)$	.2512	.1254
$R1r1$	Ins.^{3}		2.0266	.5262
$R2r2$	Ins.^{3}		16.9148	8.2522
$R3r3$	Ins.^{3}		5.1558	—
Total 2	Ins.^{3}		24.3484	8.9038
c = Total 2 ÷ Total 1	Inches		2.1141	2.1127
$dt = t - c$	Inches		2.0109	2.0123
$dr1 = r1 - c$	Inches		2.0422	2.0436
$dr2 = r2 - c$	Inches		1.1515	$(c - r2)$ .0812
$dr3 = c - r3$	Inches		1.2151	—
Moments of Inertia:				
IT	Ins.^{4}	$(2IT)$	.0001	.00006
$IR1$	Ins.^{4}		.0014	.0003
$IR2$	Ins.^{4}		1.0964	5.5873
$IR3$	Ins.^{4}		1.5307	—
$T(dt)^2$	Ins.^{4}	$[2T(dt)^2]$	.2463	.0612
$R1(dr1)^2$	Ins.^{4}		2.0336	.5287
$R2(dr2)^2$	Ins.^{4}		6.8680	.0268
$R3(dr3)^2$	Ins.^{4}		8.5474	—
I	Ins.^{4}		20.3239	6.2044
$y = D - c$	Inches		2.1359	2.1373
Section Modulus:				
$S = I \div y$	Ins.^{3}		9.52	$(\frac{1}{2}S)$ 2.9029
				S = 5.81

The Linear Theory of Fluctuations Arising from Diffusional Mechanisms—An Attempt at a Theory of Contact Noise

By J. M. RICHARDSON

The spectral density is calculated for the electrical resistance when it is linearly coupled to a diffusing medium (particles or heat) undergoing thermally excited fluctuations. Specific forms of the spectral density are given for several types of coupling which are simple and physically reasonable. The principal objective is the understanding of the frequency dependence of the resistance fluctuations in contacts, rectifying crystals, thin films, etc.

1. Introduction

WHEN a direct current is passed through a granular resistance such as a carbon microphone or a metallic-film grid leak, or through a single contact, there is produced a voltage fluctuation possessing a component called contact noise which is differentiated from the familiar thermal noise component by the fact that its r.m.s. value in any frequency band is roughly proportional to the magnitude of the average applied voltage, and is differentiated from shot noise by the strong frequency dependence of its spectral density. One may regard this component of the voltage fluctuation as arising from the spontaneous resistance fluctuations of the element in question if one is willing to allow the resistance to have a slight voltage dependence. This effect has been the subject of numerous experimental investigations,[1–8] among which we mention in particular that of Christensen and Pearson[9] on granular resistance elements. These authors (henceforth abbreviated as CP) arrived at an empirical formula, to be discussed presently, connecting the contact noise power per unit frequency band with the applied voltage, the resistance, and the frequency for several types of granular resistance. Their measurements covered a range of frequency from 60 to 10,000 cps, and involved the variation of several other parameters, i.e., pressure. More recently, Wegel and Montgomery[10] have measured the noise power arising

[1] H. A. Frederick, *Bell Telephone Quarterly* **10**, 164 (1931).
[2] A. W. Hull and N. H. Williams, *Phys. Rev.* **25**, 173 (1925).
[3] R. Otto, *Hochfrequenztechnikund Elektroakustik* **45**, 187 (1935).
[4] G. W. Barnes, *Jour. Franklin Inst.* **219**, 100 (1935).
[5] Erwin Meyer and Heinz Thiede, *E. N. T.* **12**, 237 (1935).
[6] F. S. Goucher, *Jour. Franklin Inst.* **217**, 407 (1934). *Bell Sys. Tech. Jour.* **13**, 163 (1934).
[7] J. Bernamont, *Annales de Phys.*, **1937**, 71–140.
[8] M. Surdin, *R. G. E.*, **47**, 97–101 (1940).
[9] C. J. Christensen and G. L. Pearson, *Bell Sys. Tech. Jour.* **15**, 197–223 (1936).
[10] Private communication.

from single contacts and have obtained results in agreement with the CP empirical formula down to frequencies of the order of $10^{-1} - 10^{-2}$ cps.

Significant theoretical work upon this problem has not been attempted until recently. G. G. Macfarlane[11] has advanced a theory based upon a non-linear mechanism containing one degree of freedom which seems to be in agreement with the CP law. W. Miller[12] has worked out a general theory of noise in crystal rectifiers. His theory is linear, contains essentially an infinite number of degrees of freedom, and is equivalent in many respects to the theory discussed in this paper; however, he has not succeeded in obtaining agreement with the experimental data on crystal rectifiers (which satisfy approximately the CP law) for any of the specific models he used.

The purpose of this paper is the calculation of the spectral density of the fluctuations of the electrical resistance when it is linearly coupled to a diffusing medium (particles or heat), or, mathematically speaking, is equal to a linear function of the concentration deviations of this diffusing medium. This diffusing medium undergoes thermally excited fluctuations and thereby causes fluctuations in the resistance. The motive behind this investigation was the understanding of the frequency dependence of contact noise discussed in the following paragraphs, but at the present time it is apparent that this treatment in addition may apply to rectifying crystals, thin films, transistors, etc. The quantitative details of the coupling between the resistance and the diffusing medium are not considered here; in consequence of which, this work can hardly pretend to give a complete explanation of contact noise. However, important results are given concerning the relation between the spectral density of the resistance, on one hand, and the geometry of the coupling and the dimensionality of the diffusion field on the other.

Now let us consider the CP empirical formula in detail. Let $\bar{R}$ be the average resistance[13] of the contact (we will henceforth consider only contacts and will regard a granular resistance as a contact assemblage) and let $R_1(t)$ be the instantaneous deviation from the average. By theorems I-3 of Appendix I, we can express the m.s. value of R_1 as a sum of the m.s. values of R_1 in each frequency interval as follows:

$$\overline{R_1^2} = \int_0^\infty S(\omega)\, d\omega, \tag{1.1}$$

[11] G. G. Macfarlane, *Proc. Phys. Soc.* **59**, Pt. 3, 366–374 (1947).

[12] To be published.

[13] The resistance of a contact is composed of two parts: the "gap resistance" and the "spreading resistance." The term "gap resistance" is self-explanatory. The "spreading resistance" is the resistance involved in driving the electric current through the body of the contact material along paths converging near the area of lowest gap resistance. The measured contact resistance is the sum of these two parts. In some of the particular physical models considered in Section 5, $\bar{R}$ is taken to be the gap resistance necessitating ad hoc arguments relating gap resistance and total resistance.

where $S(\omega)$ is called the spectral density of R_1 and ω is the frequency in radians per second. Now in our notation the CP formula may be expressed

$$S(\omega) = KV^{a-2}\bar{R}^{b+2}/\omega, \tag{1.2}$$

where V is the applied d-c voltage across the contact, K is a constant depending upon the temperature and the nature of the contact, and a and b are constants having values of about 1.85 and 1.25 respectively. CP state that the constant K is equal to about 1.2×10^{-10} in the case of a single carbon contact at room temperature.

In this paper we will regard the nonvanishing of $a - 2$ as arising from a non-linear effect which should become negligible at a sufficiently low voltage, although this interpretation does not seem completely justified on the basis of the work of CP. Consequently we assume that $a \to 2$ as $V \to 0$ in such a way that $V^{a-2} \to 1$. This is in keeping with the idea that the resistance fluctuations are truly spontaneous—at least for small applied voltages.

Although Eq. (1.2) may represent the observations over a large range of frequency it must break down at very high and very low frequencies in order that the noise power be finite (or, in other words, in order that the integral (1.1) converge).

One has several clues to be considered in looking for an underlying mechanism of the resistance fluctuations. First of all, the mechanical action of the thermal vibrations in the solid electrodes of the contact seems to be unimportant because of the following reasons: (1) there are no resonance peaks in $S(\omega)$ at the lowest characteristic frequencies of mechanical vibration of the contact assembly; (2) $S(\omega)$ becomes very large far below the lowest characteristic frequency; and (3), according to CP, $\overline{R_1^2}$ is strictly proportional to V^2 when the fluctuations are produced by acoustic noise vibrating the contact, whereas $\overline{R_1^2}$ is proportional to V^{a-2}, $a \sim 1.85$, when the fluctuations arise from the dominant mechanism existing in the macroscopically unperturbed contact. One of the obvious mechanisms left is a diffusional mechanism. Such a mechanism does not violate any of the observations to date and, furthermore, possesses a sufficient density of long relaxation times to give large contributions to $S(\omega)$ near zero frequency.

Evidence that diffusion of atoms (or ions) can be important in modulating a current is provided by the "flicker effect" in which the emission of electrons from a heated cathode is caused to fluctuate by the fluctuations in concentration of an adsorbed layer. We might suppose that contact noise is a different manifestation of the basic mechanism involved in the flicker effect.

In view of these considerations it seems worthwhile to investigate in a

general way a large class of models involving resistance fluctuations arising from diffusional mechanisms. In the next section we propose a general mathematical model embracing a class of linear diffusional mechanisms. In Sections 3 and 4 the consequences of the general mathematical model are obtained by the "Fourier" and "Smoluchowski" methods, respectively, these alternative methods leading to identical results. In Section 5, the general results are specialized to several physical cases, some of which are introduced only for the purpose of providing some insight into the relations between the possible physical mechanisms and the resultant resistance fluctuations, and one of which along with its refinement is a successful[14] attempt to provide a theory of Eq. (1.2). Section 6. is a summary.

2. The General Mathematical Model

The physical models which we consider in this paper are concerned with the fluctuations of contact resistance arising from a diffusional process. We are consequently led to consider the following general mathematical model embracing a rather extensive class of the physical models as special cases: Let us consider the instantaneous contact resistance $R(t)$ to be related to the intensity $c(\mathbf{r}, t)$ of some diffusing quantity as follows[15]:

$$G(R(t)) = \int F(\mathbf{r}, c(\mathbf{r}, t))\, d\mathbf{r}, \tag{2.1}$$

where $\mathbf{r}$ is a vector in two or three dimensional space depending on whether the diffusion takes place on a surface or in a volume, and $d\mathbf{r}$ is correspondingly a differential area or volume. The intensity $c(\mathbf{r}, t)$ may be either a concentration (in the case of diffusion of material in two or three dimensions) or a temperature (in the case of heat flow in three dimensions). In writing Eq. (2.1) we have evidently assumed that the contact resistance $R(t)$ is independent of the applied voltage. Eq. (2.1) may of course allow a dependence on voltage through the quantity c; however, we will consider no processes involving a dependence of c on the voltage. These restrictions, strictly speaking, make the model applicable only in the limit of low applied voltages.

Before proceeding further let us limit the treatment to the case in which the deviations of R and c from their average values are sufficiently small for higher powers of these deviations to be neglected. Let

$$R(t) = \bar{R} + R_1(t), \tag{2.2}$$

$$c(\mathbf{r}, t) = \bar{c} + c_1(\mathbf{r}, t), \tag{2.3}$$

[14] That is, successful in so far as agreement with the form of Eq. (1.2) is concerned.

[15] A relation more general than $R(t) = SF(\mathbf{r}, c(\mathbf{r}, t))\, d\mathbf{r}$ is required as one can see from considering the special case of a total resistance composed of a parallel array of resistive elements.

where $\bar{R}$ and $\bar{c}$ are the average[16] values of $R(t)$ and $c(r, t)$ respectively. Evidently, $\overline{R_1(t)} = 0$, and $\overline{c_1(r, t)} = 0$. Introducing the expressions (2.2) and (2.3) into Eq. (2.1), expanding in terms of $c_1(r, t)$, and neglecting terms of the order of c_1^2, we get

$$R_1(t) = \int f(r)\, c_1(r, t)\, dr, \tag{2.4}$$

where

$$f(r) = \left[\frac{\partial F(r, c)}{\partial c}\right]_{c=\bar{c}} \Big/ \left[\frac{dG(R)}{dR}\right]_{R=\bar{R}}$$

The function $f(r)$ defines the linear coupling between R_1 and c_1 and depends upon the specific physical model used. The non-linear terms neglected in Eq. (2.4) may be of importance under some conditions; however, we will not consider them here. Nevertheless, non-linear effects in the behavior of c_1 itself are possibly important in determining the form of the power spectrum of $R_1(t)$ in the neighborhood of zero frequency.

3. The Fourier Series Method of Solution

In this section we consider the state of the diffusing system to be defined by the Fourier space-amplitudes $c_k(t)$ of $c_1(r, t)$. The time behavior of $c_k(t)$ will be described by an infinite set of ordinary differential equations containing random exciting forces according to the conventional theory of Brownian motion.[17] This method yields the spectral density of $R_1(t)$ directly.

Now the diffusion process is assumed to occur in a rectangular area $A_2 = L_1 \times L_2$ or in a rectangular parallelopiped of volume $A_3 = L_1 \times L_2 \times L_3$. In regions of the above types, if we apply periodic boundary conditions[18], $c_1(r_0 t)$ may be expanded in Fourier space-series as follows:

$$c_1(r, t) = \sum_k{}' c_k(t) e^{ik \cdot r} \tag{3.1}$$

where the components of k take the values

$$k_i = 2\pi n_i / L_i, \quad i = 1, \cdots, \nu, \tag{3.2}$$

in which n_i are integers and ν is the number of dimensions. The prime on the summation indicates that the term for $k = 0$ is to be omitted. This is required by the equivalence of the time and space averages of c_1 (true for A_ν sufficiently large) and by the vanishing of the time average of c_1 (by definition).

[16] The average values here may be considered as either time or ensemble averages but not space averages.

[17] See Wang and Uhlenbeck, *Rev. Mod. Phys.*, 17, 323–342 (1945).

[18] If the final results are given by integrals over k- space they will be insensitive to the boundary conditions.

Before proceeding to the solution itself let us consider what it is that we wish to know about $c_k(t)$. Expanding the function $f(r)$ of Eq. (2.4) in a Fourier space-series in the region A_ν,

$$f(r) = \sum_k f_k e^{ik\cdot r}, \tag{3.3}$$

we can write Eq. (2.4) in the form

$$R_1(t) = A_\nu \sum_k{}' f_k^* c_k(t) \tag{3.4}$$

where f_k^* is the conjugate of f_k.
The spectral density $S(\omega)$ of $R_1(t)$ is then

$$S(\omega) = A_\nu^2 \sum_{kk'}{}' C_{kk'}(\omega) f_k^* f_{k'}, \tag{3.5}$$

where $C_{kk'}(\omega)$ is the spectral density matrix for the set $c_k(t)$ given by

$$C_{kk'}(\omega) = 2\pi \operatorname*{Lim}_{\tau\to\infty} \frac{1}{\tau} [c_k(\omega, \tau) c_{k'}^*(\omega, \tau) + c_k(-\omega, \tau) c_{k'}^*(-\omega, \tau)] \tag{3.6}$$

in which

$$c_k(\omega, \tau) = \frac{1}{2\pi} \int_{-\tau/2}^{+\tau/2} c_k(t) e^{-i\omega t}\, dt. \tag{3.7}$$

For a full discussion of spectral densities and spectral density matrices see Appendix I. Consequently our objective in this section is the calculation of the maxtix $C_{kk'}(\omega)$ defined by Eq. (3.6).

Now we assume that $c_1(\mathbf{r}, t)$ satisfies the diffusion equation

$$\frac{\partial}{\partial t} c_1(\mathbf{r}, t) = D\overrightarrow{\nabla}^2 c_1(r, t) + g(r, t) \tag{3.8}$$

where D is a constant, ∇^2 is the Laplacian operator in two or three dimensions, and where $g(r, t)$ is a random source function, whose Fourier space-amplitudes $g_k(t)$ possess statistical properties to be discussed presently. The random source function g is required for exciting c_1 sufficiently to maintain the fluctuations given by equilibrium theory. In the case of material diffusion the random source function g may be discarded in favor of a random force term of the form $-D/\chi\ T\cdot\vec{\nabla}\cdot[f(\bar{c} + c_1)]$, where $\nabla\cdot f = div f$, χ is the Boltzmann constant, T is the temperature, and f is the random force; however, in the linear approximation these two procedures will give identical final results. In the case of heat flow it is understood that the diffusion constant is $D = K/\rho C$ where K is the thermal conductivity, ρ the density, and C the specific heat. Eq. (3.8) as written is valid only for D a constant and c_1 small.

Introducing the expansion (3.1) and the expansion

$$g(r, t) \sum_k{}' g_k(t) e^{ik \cdot r} \tag{3.9}$$

into Eq. (3.8) we obtain the infinite set of ordinary differential equations

$$\frac{d}{dt} c_k(t) = -Dk^2 c_k(t) + g_k(t), \tag{3.10}$$

$$k = | k |,$$

describing the time behavior of the Fourier space-amplitudes $c_k(t)$. The Fourier space-amplitudes $g_k(t)$ are assumed to be random functions of t possessing a white (flat) spectral density matrix C_{kk}, independent of frequency. Multiplying Eq. (3.10) by $\frac{1}{2\pi} e^{-i\omega t}$, integrating with respect to time from $-\frac{1}{2}\tau$ to $+\frac{1}{2}\tau$, and neglecting the transients at the end points of the τ-interval, we obtain

$$c_k(\omega, \tau) = \frac{g_k(\omega, \tau)}{i\omega + Dk^2} \tag{3.11}$$

where $c_k(\omega, \tau)$ is given by Eq. (3.7) and $g_k(\omega, \tau)$ is given by an analogous equation. Forming the spectral density matrices we get for the diagonal elements

$$C_{kk'}(\omega) = \frac{G_{kk}}{\omega^2 + D^2 k^4} \tag{3.12}$$

The matrix $G_{kk'}$ can now be evaluated by the thermodynamic theory of fluctuations (See Appendix II). This theory gives

$$c_k(t) c_{k'}^*(t) = \frac{\chi \delta_{kk'}}{A_v s''} \tag{3.13}$$

where

$$\delta_{kk'} = \begin{cases} 1 \text{ if } k = k' \\ 0 \text{ otherwise,} \end{cases}$$

$$s'' = -\left\{\frac{\partial^2 s}{\partial c^2}\right\}_{c=\bar{c}} + \frac{1}{\bar{T}} \left\{\frac{\partial^2 e}{\partial c^2}\right\}_{c=\bar{c}} \tag{3.14}$$

s and e being the entropy and energy, respectively, per unit area or volume, $\bar{T}$ the average temperature, and χ the Boltzmann constant. In the case where c is the concentration of particles whose configurational energy is constant, $s'' = \chi/\bar{c}$. If c be the temperature T then $s'' = C/\bar{T}^2$ where C

is the heat capacity per unit area or volume. Now by a general theorem concerning spectral density matrices (see Appendix I) we have

$$\overline{c_k(t)c_{k'}^*(t)} = \int_0^\infty C_{kk'}(\omega)\, d\omega,$$

giving finally by combination with (3.12) and (3.13),

$$G_{kk'} = \frac{2}{\pi}\frac{\chi D k^2}{A_\nu s''}\delta_{kk'}, \tag{3.15}$$

and

$$C_{kk'}(\omega) = \frac{2}{\pi}\frac{\chi D}{A_\nu s''}\frac{k^2\delta_{kk'}}{\omega^2 + D^2k^4}. \tag{3.16}$$

The spectral density $S(\omega)$ of $R_1(t)$ then becomes

$$S(\omega) = \frac{2}{\pi}\frac{\chi A_\nu D}{s''}\sum_k \frac{k^2|f_k|^2}{\omega^2 + D^2k^4}. \tag{3.17}$$

If we are concerned with frequencies greater than a characteristic frequency

$$\omega_0 = 4\pi^2 D/L^2 \tag{3.18}$$

where L is the smallest of L_i, $i = 1, \cdots, \nu$, then the summation in (3.17) may be replaced by an integration giving

$$S(\omega) = 2^{\nu+1}\pi^{\nu-1}\frac{\chi D}{s''}\int \frac{|f(k)|^2 k^2\, dk}{\omega^2 + D^2k^4} \tag{3.19}$$

where

$$f(k) = \frac{1}{(2\pi)^\nu}\int_{A_\nu} f(r)e^{-ik\cdot r}\, dr. \tag{3.20}$$

The integration in Eq. (3.19) is carried out over the entire ν-dimensional k-space. If the range of the function $f(r)$ is sufficiently small compared with the region A_ν, or if we let A_ν become indefinitely large, then the integration in Eq. (3.20) may be extended to all of ν-dimensional r-space.

It is perhaps revealing to rephrase Eqs. (3.17) and (3.19) in terms of distributions of relaxation times. In the theory of dielectrics we speak of the real part of the dielectric constant being equal to a series of terms summed over a distribution of relaxation times: $\Sigma_i a_i\tau_i/(1 + \tau_i^2\omega^2)$, if the distribution is discrete, or $\int_0^\infty a(\tau)\tau d\tau/(1 + \tau^2\omega^2)$, if the distribution is continuous. In the above, a_i is the weight for the relaxation time τ_i, and, in

the case of a continuous distribution, $a(\tau)d\tau$ is the weight for the relaxation times in the range $d\tau$ containing τ. In these terms Eq. (3.17) becomes

$$S(\omega) = \sum_k \frac{a_k \tau_k}{1 + \tau_k^2 \omega^2}, \tag{3.17a}$$

where

$$a_k = \frac{2}{\pi} \frac{\chi}{s''} |f_k|^2. \tag{3.17b}$$

Eq. (3.19) becomes

$$S(\omega) = \int_0^\infty \frac{a(\tau)\tau \, d\tau}{1 + \tau^2 \omega^2} \tag{3.19a}$$

where

$$a(\tau) = \frac{2^\nu \pi^{\nu-1} \chi}{s'' D^{\nu/2} \tau^{\nu/2+1}} \int |f(l/\sqrt{D\tau})|^2 \, d\Omega_\nu \tag{3.19b}$$

in which l is the unit vector in the direction of k, $d\Omega_\nu$ is the differential "solid" angle in the ν-dimensional k-space, and the integration is over the total solid angle (2π in 2 dimensions, or 4π, in 3).

It is of interest to calculate the self-covariance $\overline{R_1(t)R_1(t+u)}$. In Appendix I, it is shown that the self-covariance above is related to the spectral density $S(\omega)$ as follows:

$$\overline{R_1(t)R_1(t+u)} = \int_0^\infty S(\omega) \cos u\omega \, d\omega. \tag{3.21}$$

Using $S(\omega)$ in the form (3.17), Eq. (3.21) gives

$$\overline{R_1(t)R_1(t+u)} = \chi A_\nu / s'' \cdot \sum_k |f_k|^2 e^{-Duk^2}, \tag{3.22}$$

$$u > 0;$$

whereas with $S(\omega)$ in the form (3.19) we get

$$\overline{R_1(t)R_1(t+u)} = (2\pi)^\nu \chi / s'' \int |f(k)|^2 e^{-Duk^2} \, dk. \tag{3.23}$$

The method of the next section yields the self-covariance directly.

4. Smoluchowski Method of Solution

We call the procedure employed in this section the "Smoluchowski method" because it is based on an equation very closely analogous to the well-known Smoluchowski equation forming the basis of the theory of

Markoff processes.[19] We set out directly to calculate the self-covariance for $R_1(t)$ which, by Eq. (2.4), is given by

$$\overline{R_1(t)R_1(t+u)} = \iint f(r')f(r)\overline{c_1(r'\,t)c_1(r',\,t+u)}\,dr'\,dr. \tag{4.1}$$

Thus the problem is now reduced to the calculation of $\overline{c_1(r',\,t)c_1(r,\,t+u)}$.

The quantity $\overline{c_1(r',\,t)c_1(r,\,t+u)}$ is calculated in two steps. First we find $\overline{c_1(r,\,t+u)}^{(t+u)}$, the average value of c_1 at the point r at the time $t+u$ with the restriction that c_1 is known at every point r' with certainty to be $c_1(r',\,t)$ at the time t (assuming, of course, that $u > 0$). Then we find that the required self-covariance for c_1 is given by multiplying the above $\overline{c_1(r,\,t+u)}^{(t+u)}$ by $c_1(r',\,t)$ and averaging over-all values of $c_1(r,\,t)$ at time t; thus:

$$\overline{c_1(r',\,t)\overline{c_1(r,\,t+u)}^{(t+u)}}^{(t)} = \overline{c_1(r',\,t)c_1(r,\,t+u)}. \tag{4.2}$$

Now we assume that $\overline{c_1(r,\,t+u)}^{(t+u)}$ is related to $c(r',\,t)$ by an integral equation, analogous to the Smoluchowski equation, as follows:

$$\overline{c_1(r,\,t+u)}^{(t+u)} = \int \rho(|\,r-r'\,|,\,u)c_1(r',\,t)\,dr'. \tag{4.3}$$

In the case that c represents a concentration as in the diffusion of particles, $\rho(|\,r-r'\,|,\,u)\,dr$ is the probability that a particle be in the ν-dimensional volume element dr at time $t+u$ when it is known with certainty to be at r' a time t. Now the number of particles in dr' at r' at time t is evidently $[\bar{c}+c_1(r',\,t)]\,dr'$; consequently, the probable number of particles in dr at time $t+u$ which were in dr' at time t is $\rho(|\,r-r'\,|,\,u)[c+c_1(r',\,t)]\,dr\,dr'$. Integration over dr' gives the total probable number $(\bar{c}+\overline{c_1(r,\,t+u)}^{(t+u)})\,dr$ of particles in dr equal to $\left(\int \rho(|\,r-r'\,|,\,u)[\bar{c}+c_1(r',\,t)]\,dr'\right)dr$ which reduces to $\left(\bar{c}+\int \rho(|\,r-r'\,|,\,u)c_1(r',\,t)\,dr'\right)dr$. Division by dr and subtraction of $\bar{c}$ from both sides of the equality leads directly to Eq. (4.3). For the case of heat flow in crystal lattices the above picture can be used approximately if one uses the concept of phonons.[20] For a diffusional process $\rho(|\,r-r'\,|,\,u)$ is the normalized singular solution of the diffusion equation[21]; thus

$$\rho(|\,r-r'\,|,\,u) = \frac{1}{(4\pi Du)^{\nu/2}}\exp\left[-|\,r-r'\,|^2/4Du\right] \tag{4.4}$$

[19] Loc cit.
[20] J. Weigle, *Experientia*, 1, 99–103 (1945).
[21] Chandrasekhar, *Rev. Mod. Phys.* 15, 1 (1943).

where ν, as previously defined, is the number of dimensions of the region in which the process occurs.

Combining Eqs. (4.2) and (4.3) we get

$$\overline{c_1(r',\ t)c_1(r,\ t+u)} = \int \overline{c_1(r',\ t)c_1(r'',\ t)}^{(t)}\, \rho(|\, r - r''\,|, u)\, dr''. \quad (4.5)$$

Now using the fact that

$$\overline{c_1(r',\ t)c_1(r'',\ t)}^{(t)} = \overline{c_1(r',\ t)c_1(r'',\ t)} \quad (4.6)$$

and using the relation

$$\overline{c_1(r',\ t)c_1(r'',\ t)} = \frac{\chi}{s''}\,\delta(r' - r'') \quad (4.7)$$

proved in Appendix II, Eq. (4.5) reduces to

$$\overline{c_1(r',\ t)c_1(r,\ t+u)} = \frac{\chi}{s''}\,\rho(|\, r - r'\,|, u). \quad (4.8)$$

Introducing the expression (4.8) into Eq. (4.1) we obtain at once the desired result

$$\begin{aligned}\overline{R_1(t)R_1(t+u)} &= \frac{\chi}{s''}\iint f(r)f(r')\rho(|\, r - r'\,|, u)\, dr\, dr' \\ &= \frac{\chi}{s''(4\pi Du)^{\nu/2}}\iint f(r)f(r')\,\exp\left[-|\, r - r'\,|/4Du\right] dr\, dr'.\end{aligned} \quad (4.9)$$

For the sake of comparison with Eq. (3.23) it is necessary to write (4.9) in terms of the Fourier space-transforms of the pertinent quantities. We write

$$f(r) = \int f(k)\, e^{ik\cdot r}\, dk$$

where

$$f(k) = \frac{1}{(2\pi)^\nu}\int f(r)e^{ik\cdot r}\, dr.$$

Also, we write

$$\begin{aligned}\rho(|\, r - r'\,|, u) &= \frac{1}{(4\pi Du)^{\nu/2}}\exp\left[-|\, r - r'\,|^2/4Du\right] \\ &= \frac{1}{(2\pi)^\nu}\int \exp\left[-Duk^2 + ik\cdot(r - r')\right] dk.\end{aligned}$$

After introduction of these expressions into (4.9) a short calculation yields the result

$$\overline{R_1(t)R_1(t+u)} = (2\pi)^\nu\,\frac{\chi}{s''}\int |f(k)|^2 e^{-Duk^2}\, dk \quad (4.10)$$

which is identical with Eq. (3.23) (provided that we let $A_\nu \to \infty$ in the latter). Thus the methods of approach used in Section 3 and in this Section are completely equivalent.

5. Special Physical Models

In the previous two Sections we have developed by two different methods the consequences of the general mathematical model discussed in Section 2. Here we apply the general results to some special physical cases. In this task we will be principally concerned with finding the form of the function $f(r)$ and establishing the number of dimensions ν of the diffusion field. The main objective here is to provide some orientation on what mechanisms are or are not reasonable and to find at least one mechanism leading to the observed spectral density (inversely proportional to the frequency).

a. *A General Class of Models.* Here we consider all at once mechanisms which can be adequately represented by having $f(r)$ a ν-dimensional Gaussian function of the form

$$f(r) = \prod_{i=1}^{\nu} \frac{b_i}{(2\pi\Delta_i)^{1/2}} e^{-x_i^2/2\Delta_i}, \tag{5.1}$$

where $\Delta_i^{1/2}$ is the "width" of the function measured along the i-th coordinate x_i. This form of $f(r)$ can represent approximately several types of localization of the coupling between R_1 and c_1, as will be seen in the special examples later. Now if we work with $A_\nu = \infty$, we will then have to consider the Fourier space-transform of $f(r)$, which is readily shown to be

$$\left.\begin{aligned} f(k) &= \frac{1}{(2\pi)^\nu} \int f(r) e^{-ik\cdot r}\, dr \\ &= \prod_{i=1}^{\nu} b_i/2\pi \cdot e^{-\Delta_i k_i^2/2} \end{aligned}\right\} \tag{5.2}$$

Inserting this result into Eq. (3.19) we obtain immediately

$$S(\omega) = \frac{2\chi D}{\pi s''} \left(\prod_{i=1}^{\nu} \frac{b_i^2}{2\pi} \right) \int \frac{\exp\left(-\sum_{i=1}^{\nu} \Delta_i k_i^2 \right) k^2\, dk}{\omega^2 + D^2 k^4} \tag{5.3}$$

$$k = \sum_{i=1}^{\nu} k_i^2 .$$

Inserting this expression (5.2) into Eq. (3.23) gives

$$\overline{R_1(t)R_1(t+u)} = \frac{\chi}{s''} \prod_{i=1}^{\nu} \frac{b_i^2}{[4\pi(\Delta_i + Du)]^{1/2}}; \qquad u > 0 \tag{5.4}$$

In order that (5.3) give the observed $S(\omega) \propto 1/\omega$ as a result, the integral must reduce to something proportional to $\int k\,dk/(\omega^2 + D^2k^4)$. It is clearly impossible that any choice of ν and any set of Δ_i can achieve this result. Furthermore the self-covariance $\overline{R_1(t)R_1(t+u)}$ corresponding to the observed $S(\omega)$ should depend explicitly on the way $S(\omega)$ deviates from $1/\omega$ as ω goes to zero. The expression (5.4) is finite for all $u > 0$ and does not depend upon any cut-off phenomena in $S(\omega)$ at low frequencies. Therefore we can exclude any physical mechanisms belonging to the class considered here. However, since several mechanisms that have been proposed do fall into this class, we consider them below:

(*i*) *Schiff's Mechanism.* Schiff[22] considered tentatively that the fluctuations in contact resistance may be due to the variation in concentration of diffusing ions (atoms, or molecules) in a high resistance region bounded by parallel planes of very small separation. Schiff arrived at a noise spectrum proportional to $1/\omega$ but at the expense of disagreeing in a fundamental way with thermodynamic fluctuation theory. Here we will show what the correct consequences of this mechanism are.

Consider that the high resistance region is bounded on either side by planes parallel to the (x_1, x_2)-plane and that the thickness in the x_3-direction is very small. Now this is obviously a case of the general model just considered in which we take $\nu = 3$ and

$$\left.\begin{aligned} \Delta_{1,2} &\gg Du, \\ \Delta_3 &\ll Du, \end{aligned}\right\} \tag{5.5}$$

where $1/u$ is of the order of magnitude of the frequencies of interest. It is then a matter of algebraic manipulation to show that

$$S(\omega) \simeq \frac{\chi D}{s''} \cdot \frac{b_1^2 b_2^2 b_3^2}{2\pi^3 \Delta_1^{1/2} \Delta_2^{1/2}} \cdot \int_0^\infty \frac{k_1^2\,dk_1}{\omega^2 + D^2 k_1^4} = \frac{\chi}{D^{1/2} s''} \cdot \frac{b_1^2 b_2^2 b_3^2}{2^{5/2} \pi^2 \Delta_1^{1/2} \Delta_2^{1/2}} \frac{1}{\omega^{1/2}} \tag{5.6}$$

and

$$\overline{R_1(t)R_1(t+u)} = \frac{\chi}{D^{1/2} s''} \cdot \frac{b_1^2 b_2^2 b_3^2}{(4\pi)^{3/2} \Delta_1^{1/2} \Delta_2^{1/2}} \cdot \frac{1}{u^{1/2}} \quad u > 0. \tag{5.7}$$

Thus we see that Shiff's mechanism leads to a noise spectrum proportional to $1/\omega^{1/2}$, not $1/\omega$. The explanation of the singularity of the self-covariance (5.7) at $u = 0$ lies in the inequalities (5.5).

[22] L. I. Schiff, *BuShips Contract NObs-34144*, "Tech. Rpt. #3", (1946). Before the publishing of this paper, Schiff informed the writer that he has discarded this mechanism.

The above treatment could just as well be applied to the case in which the diffusing quantity is heat instead of ions.

(*ii*) *Resistance of a Localized Contact Disturbed by a Diffusing Surface Layer.* Here we consider the case of two conductors covered with diffusing surface layers. It is supposed that the conduction from one conductor to the other is distributed Gaussianly with a width $\Delta^{1/2}$. Finally, it is supposed that the conductivity through the above area varies with the surface concentration of the surface layer in that region. This situation is well represented by the above general model by taking $\nu = 2$, $\Delta_1 = \Delta_2 = \Delta$, and $b_1 = b_2 = b$.

The self-covariance is readily calculated with the result

$$\overline{R_1(t)R_1(t+u)} = \frac{\chi}{s''} \cdot \frac{b^4}{4\pi(\Delta + Du)} \tag{5.8}$$

The corresponding spectral density is

$$S(\omega) = \frac{1}{2\pi^2}\frac{\chi b^4}{s''}\int_0^\infty \frac{\cos u\omega\, du}{\Delta + Du} = \frac{1}{2\pi^2}\frac{\chi b^4}{s''D}\left[-\cos(\omega\Delta/D)Ci(\omega\Delta/D) + \sin(\omega\Delta/D)\left(\frac{\pi}{2} - Si(\omega\Delta/D)\right)\right] \tag{5.8a}$$

where $Ci(x)$ and $Si(x)$ are the cosine and sine integrals[23] respectively. When $\omega \ll D/\Delta$

$$S(\omega) \simeq -\frac{1}{2\pi^2}\frac{\chi b^4}{s''D}\log(\delta\omega\Delta/D), \tag{5.8b}$$

$$\delta = 0.5772,$$

and when $\omega \gg D/\Delta$

$$S(\omega) \simeq \frac{1}{2\pi^2}\frac{\chi b^4 D}{s''\Delta^2}\frac{1}{\omega^2}. \tag{5.8c}$$

Thus we see that this case does not lead to the experimental form of the spectral density. It must be remarked that here $S(\omega)$ is very sensitive to the form of the self-covariance for small u.

b. Contact between Relatively Large Areas of Rough Surfaces Covered with Diffusing Surface Layers. We consider this case in detail since it leads to results in agreement with experiment. Furthermore, the more detailed consideration of this case will illustrate more fully the use of the general mathematical model, which may be of use in studying other diffusional mechanisms should they be postulated at some future time. This mechanism does not fall into the class just considered.

[23] See Jahnke and Emde, "Tables of Functions," p. 3, Dover (1943).

Suppose that the contact in an idealized form consists of two rough surfaces close together. Let positions on the surfaces be measured with respect to a plane between the surfaces, which we will call the mid-plane. Let the coordinate system be oriented so that the x_1 and x_2 axes lie in the mid-plane. Furthermore let the region in the mid-plane corresponding to close proximity of the rough surfaces be a rectangular area $A_2 = L_1 \times L_2$. Now, for convenience, we describe positions on the mid-plane by a two dimensional vector $\mathbf{r} = (x_1, x_2)$, and henceforth it will be understood that all vector expressions refer to this two-dimensional space. Let the distance between the upper and lower surfaces at $\mathbf{r}$ be denoted by $h(\mathbf{r})$. The geometry of the above model is illustrated in Fig. 1.

Now suppose that each surface is covered by a diffusing absorbed layer, such that the sum of the concentrations on both surfaces is $c(\mathbf{r}, t)$ at the time t in the neighborhood of $\mathbf{r}$. Now consider the conduction of current between the surfaces. Let us assume that the conductance per unit area (of mid-plane) is a function of the separation h of the surfaces and the total concentration c of absorbate near the point in question, i.e., $F(h, c)$. The total conductance will be the sum of the conductances through each element of area: hence, the instantaneous resistance $R(t)$ at time t will be given by

$$1/R(t) = \int_{A_2} F(h(\mathbf{r}), c(\mathbf{r}, t))\, d\mathbf{r} \tag{5.9}$$

where $d\mathbf{r}$ is the differential area on the mid-plane and the integration extends over the rectangle $A_2 = L_1 \times L_2$. Behind the above statements lies the tacit assumption that the radii of curvature of the rough surfaces are generally considerably larger than the values of h. However, we will not explicitly concern ourselves with this implied restriction.

At this point it is expedient to imagine that we have an ensemble of contacts identical in all respects except for different variations of the separation $h(\mathbf{r})$. If we have any function of h, $\psi(h)$ say, which we wish to average with respect to the variations of h, we simply average the function over the above ensemble giving a result which we denote by $\overline{\psi(h)}^{(e)}$.

Now let us write

$$h(\mathbf{r}) = \bar{h}^{(e)} + h_1(\mathbf{r}), \tag{5.10}$$

and, as before,

$$\left.\begin{aligned} R(t) &= \bar{R} + R_1(t), \\ c(\mathbf{r}, t) &= \bar{c} + c_1(\mathbf{r}, t). \end{aligned}\right\} \tag{5.11}$$

We assume that the ensemble average $\bar{h}^{(e)}$ and the time averages $\bar{R}$ and $\bar{c}$ are constants independent of $\mathbf{r}$ and t. Let us also assume that the integrals

of $h_1(r)$ and $c_1(r, t)$ over A_2 vanish. Inserting (5.10) and (5.11) into (5 9) and expanding, we get

$$\left.\begin{aligned} &1/\bar{R} - R_1(t)/\bar{R}^2 + \cdots = A_2 F(\bar{h}^{(c)}, \bar{c}) \\ &+ \left(\frac{\partial^2 F}{\partial h \partial c}\right)^{\circ} \int_{A_2} h_1(r) c_1(r, t)\, dr + \tfrac{1}{2}\left(\frac{\partial^2 F}{\partial h^2}\right)^{\circ} \int_{A_2} h_1^2(r)\, dr + \cdots, \end{aligned}\right\} \tag{5.12}$$

where the super zero on the derivatives indicates that they are evaluated at $h = \bar{h}^{(c)}$ and $c = \bar{c}$. In accordance with previous approximations in this memorandum we neglect[24] terms of the order of c_1^2 and R_1^2. We also neglect terms of the order of h_1^2. After taking the time average of (5.12) and subtracting the result from (5.12) we get

$$\left.\begin{aligned} R_1(t) &= \int_{A_2} f(r) c_1(r, t)\, dr, \\ f(r) &= \alpha \bar{R}^2 h_1(r), \\ \alpha &= -\left(\frac{\partial^2 F}{\partial h \partial c}\right)^{\circ} \end{aligned}\right\} \tag{5.13}$$

Thus we now have a special case of our general mathematical model for the number of dimensions $\nu = 2$, provided that we assume that the total concentration c on both of the rough surfaces fluctuates in the same manner as the concentration of a single adsorbed layer confined to a plane rectangular surface. The spectral density $S(\omega)$ of $R_1(t)$ is then given by Eq. (3.17) which we repeat here

$$S(\omega) = \frac{2}{\pi} \cdot \frac{\chi A_2 D}{s''} \cdot \frac{\Sigma'}{k} \frac{k^2 |f_k|^2}{\omega^2 + D^2 k^4} \tag{5.14}$$

where k is a two-dimensional vector whose components take the values $k_i = 2\pi n_i / L_i$, $n_i = 0, \pm 1, \pm 2, \cdots$, and where f_k are the Fourier space-amplitudes of $f(r)$ given by

$$f_k = A_2^{-1} \int_{A_2} f(r) e^{-ik \cdot r}\, dr.$$

It may be appropriate at this point to consider the quantity s'' in detail for this particular case. If the energy e per unit area is independent of c, we have $s'' = -\dfrac{\partial^2 s}{\partial c^2}$ evaluated at $c = \bar{c}$ where s is here the entropy of the absorbate per unit area. For the sake of illustration let us consider a single layer of absorbate in which the molecules are non-interacting. If c, the sur-

[24] We neglect these terms not because they are small compared with c_1 or $h_1 c_1$ but, because they are non-fluctuating (in time), are hence to be compared with $1/\bar{R}$.

face concentration of the absorbate, be measured in molecules (atoms, or ions) per unit area, then, for the ideal system above, it follows that $s = -\chi c \log c$ and finally that $s'' = \chi/\bar{c}$. However, in the mechanism discussed in this part we have a compound system consisting of two separate layers on the upper and lower surfaces respectively. Nevertheless, a detailed analysis reveals that with c equal to the sum of the concentrations of both layers we still have $s'' = \chi/\bar{c}$ even though s itself is no longer given by an expression the same as that above. In conclusion let us consider the factor χ/s'' in Eq. (5.14). This factor is under the above idealization simply equal to $\bar{c}$. That is, the spectral density $S(\omega)$ is directly proportional to the average concentration of absorbed molecules, meaning simply that each molecule makes its contribution to the resistance fluctuations independently of the others. Of course, in any real system this will not be quite true; however, the existence of interactions will be manifested only by making χ/s'' not equal to $\bar{c}$ in Eq. (5.14).

The results quoted thus far apply to a system with a given $h(r)$. Now we shall average the right-hand side of Eq. (5.14) over the ensemble of variations of $h(r)$, it being supposed that $S(\omega)$ itself on the left-hand side will be negligibly affected by this operation. This amounts to replacing $|f_k|^2$ by $\overline{|f_k|^2}^{(e)}$. We then have

$$\overline{|f_k|^2}^{(e)} = \alpha^2 \bar{R}^4 \, \overline{|h_k|^2}^{(e)} \tag{5.15}$$

where h_k are the Fourier space-amplitudes of $h_1(r)$.

We now consider more closely the problem of calculating $\overline{|h_k|^2}^{(e)}$. We want to assume that $h_1(r)$ is a more or less random function of r. If $h_1(r)$ were a random function of r in the same way that the thermal noise voltage is a random function of the time t, then $\overline{|h_k|^2}^{(e)}$ would be a constant independent of k and the self-covariance $\overline{h_1(r)h_1(r')}^{(e)}$ would vanish for $r \neq r'$. This clearly cannot be so, since the function $h_1(r)$ with such statistical properties would represent a highly discontinuous type of surface incapable of physical existence. We then fall back upon the more reasonable assumption that the *gradient* of h_1 possesses statistical properties of the above type. This notion is precisely formulated by means of the following equations:

$$\vec{\nabla} h_1(r) = p(r) \tag{5.16}$$

where

$$\int_{A_2} p(r)\, dr = 0, \tag{5.17}$$

and

$$\overline{p(r)p(r')}^{(e)} = \beta \underset{\sim}{1} \delta(r - r'). \tag{5.18}$$

In Eq. (5.18) β is a parameter (with the dimensions of area) characterizing the amplitude of the surface roughness, and $\underset{\sim}{1}$ is the unit tensor in two dimensions. Expressing (5.16) in terms of the Fourier space-amplitudes h_k and p_k of h_1 and p respectively, we have

$$-ik\, h_k = p_k\,, \tag{5.19}$$

giving finally

$$\overline{|h_k|^2}^{(e)} = k \cdot \overline{p_k p_k^*}^{(e)} \cdot k/k^4 \tag{5.20}$$

Expressing (5.18) in terms of Fourier space-amplitudes we get

$$\overline{p_k b_{k'}^*}^{(e)} = \beta A_2^{-1} \underset{\sim}{1} \delta_{kk'}, \tag{5.21}$$

which, when inserted into (5.20) gives the following desired result:

$$\overline{|h_k|^2}^{(e)} = \beta A_2^{-1}\, k^{-2}. \tag{5.22}$$

Now replacing $|f_k|^2$ by $\overline{|f_k|^2}^{(e)}$ in Eq. (5.14) and substituting the expression (5.22) with the use of Eq. (5.15), we obtain

$$S(\omega) = \frac{2}{\pi} \cdot \frac{\chi D}{s''} \cdot \beta \alpha^2 \bar{R}^4 \sum_k \frac{1}{\omega^2 + D^2 k^4} \tag{5.23}$$

If the frequencies of interest are larger than a certain characteristic frequency $\omega_0 = 4\pi^2 D/L^2$ where L is the smaller of L_1 and L_2, the summation in (5.23) may be replaced by an integration giving finally

$$\left.\begin{aligned} S(\omega) &= \chi D/\pi^2 s'' \cdot \alpha^2 \beta \bar{R}^4 A_2 \cdot \int_0^\infty \frac{k\, dk}{\omega^2 + D^2 k^4} \\ &= \chi/4\pi s'' \cdot \beta \alpha^2 \bar{R}^4 A_2 \cdot 1/\omega \end{aligned}\right\} \tag{5.24}$$

This result is in agreement with experiment in most respects. The dependence on frequency is, of course, that experimentally observed by all investigators. The non-dependence on the voltage applied across the contact is implied by the basic assumptions common to all of the mechanisms considered here, and is in approximate agreement with the results of Christensen and Pearson (see Eq. (1.2)). For our result to agree with the results of CP as regards the dependence on the average resistance[25] $\bar{R}$, the factor $c^2 \bar{R}^4 A_2$ must be proportional to $\bar{R}^{2+b}$ where $b \sim 1.25$. These authors also imply that some of

[25] It must be remembered that the resistance $\bar{R}$ in the CP formula is the total contact resistance equal to sum of the gap resistance and the spreading resistance, whereas the $\bar{R}$ in our theory evidently should be considered the gap resistance. For the purposes of comparison we make the ad hoc assumption that the gap resistance is proportional to the total contact resistance.

the parameters necessary to complete the description of a contact between given substances at a given temperature show up implicitly only through $\bar{R}$. According to our theory the factor $\alpha^2 \bar{R}^4 A_2$ does not depend in any unique way upon $\bar{R}$; it matters by what means $\bar{R}$ is varied. If the resistance $\bar{R}$ is changed by altering the contact area A_2, keeping other parameters fixed, we would find that $\bar{R}A_2$ is constant so that the factor in question would be proportional to $\bar{R}^3$, that is, $b = 1$. However, if $\bar{R}$ is changed by varying the contact pressure, the effect would show up through the factor α^2, (β also, to some extent, perhaps) and, since one would expect α to increase somewhat with pressure whereas $\bar{R}$ decreases with pressure, the factor of interest would probably depend upon some power of $\bar{R}$ between 3 and 4, that is, $1 < b < 2$.

The theory formulated here suffers from the difficulty that the integral of the power spectrum with respect to frequency is logarithmically divergent at 0 and ∞, that is

$$\int_{\omega_1}^{\omega_2} S(\omega)\, d\omega \doteq \int_{\omega_1}^{\omega_2} d\omega\, \omega = \log(\omega_2/\omega_1) \to \infty \text{ as } \omega_1 \to 0 \text{ and } \omega_2 \to \infty .$$

The divergence at ∞ does not bother us as much as the divergence at 0 since, with only a divergence at ∞, the self-covariance $\overline{R_1(t)R_1(t+u)}$ exists for all non-vanishing values of u; whereas, with a singularity at 0, the self-covariance does not exist for any value of u. For this reason we cannot consider the self-covariance here. In Part *c* of this Section we consider a possible way of removing the divergence at 0, and consequently, then, we are able to calculate the self-covariance for non-vanishing values of u.

c. Refinement of the Theory of Part b. Here we propose a simple modification of the model of Part b, removing the divergence of the integral of $S(\omega)$ at $\omega = 0$. The modification considered here, although it is one of several possibilities any one of which is sufficient for removing the divergence (See Section 6.), is perhaps the only one that is sufficiently simple to treat in a memorandum of this scope. The results of this section are thus intended to be only provisional and suggestive.

Let us reconsider the statistics of the function $h(r)$ giving the separation between the surfaces near a point r on the mid-plane. The distribution of h's considered in the last section is open to several criticisms: (1) it possesses no characteristic length parallel to the mid-plane; and (2) the self-covariance $\overline{h_1(r)h_1(r')}^{(e)}$ does not exist for any value of $r - r'$.

To correct partially for these difficulties we replace Eq. (5.22) by

$$\overline{|h_k|^2}^{(e)} = \frac{\beta \ell^2}{A_2(1 + \ell^2 k^2)}, \tag{5.25}$$

where ℓ is a new characteristic length. The self-covariance $\overline{h_1(r)h_1(r')}^{(e)}$ based upon (5.25) now exists for all values of $r - r'$ except 0. Thus we still

have the objection that the variance $\overline{h_1^{2(e)}}$ is infinite; however, this will cause us no trouble.

With Eq. (5.25) instead of (5.22) the spectral of density R_1 takes the form

$$\left.\begin{aligned} S(\omega) &= \chi D/\pi^2 s'' \cdot \beta\alpha^2 \bar{R}^4 A_2 \cdot \int_0^\infty \frac{\ell^2 k^2}{1+\ell^2 k^2} \cdot \frac{k\,dk}{\omega^2 + D^2 k^4} \\ &= (\chi/4\pi s'') \cdot \beta\alpha^2 \bar{R}^4 A_2 \cdot 1/\omega \cdot Q(y), \\ Q(y) &= \frac{y\left(y - \frac{2}{\pi}\log y\right)}{1+y^2}, \qquad y = \ell^2\omega/D. \end{aligned}\right\} \tag{5.26}$$

In obtaining the above equation we have made the usual assumption that the frequencies of interest are larger than $\omega_0 = 4\pi^2 D/L^2$, and have replaced the original sum by an integral. The function $Q(y)$ has the following properties:

$$\left.\begin{aligned} Q(y) &\simeq -\frac{2}{\pi} y \log y \quad \text{for} \quad y \ll 1 \\ Q(y) &\simeq 1 \quad \text{for} \quad y \gg 1 \end{aligned}\right\} \tag{5.27}$$

Hence for $\omega \ll D/\ell^2$, $S(\omega) \propto \log \omega$, the integral of which converges as $\omega \to 0$; whereas, for $\omega \gg D/\ell^2$, $S(\omega)$ differs negligibly from that given by the unrefined theory (Eq. (5.24)).

The self-covariance $\overline{R_1(t)\,R_1(t+u)}$ now exists for all non-vanishing u and is given by

$$\left.\begin{aligned} \overline{R_1(t)R_1(t+u)} &= (\chi/2\pi s'') \cdot \beta\alpha^2 \bar{R}^4 A_2 \cdot \int_0^\infty \frac{\ell^2 e^{-Duk^2}k\,dk}{1+\ell^2 k^2} \\ &= (\chi/4\pi s'') \cdot \beta\alpha^2 \bar{R}^4 A_2 \cdot e^{Du/\ell^2}[-Ei(-Du/\ell^2)] \end{aligned}\right\} \tag{5.28}$$

where

$$\begin{aligned} -Ei(-x) &= \int_x^\infty e^{-v}\,dv/v, \\ &\simeq -\log \gamma x \quad \text{for} \quad x \ll 1, \\ &\simeq \frac{e^{-x}}{x} \quad \text{for} \quad x \gg 1, \\ \gamma &= 0.5772. \end{aligned}$$

Thus for $u \ll \ell^2/D$, $\overline{R_1(t)R_1(t+u)} \alpha - \log(\gamma Du/\ell^2)$ and for $u \gg \ell^2/D$, $\overline{R_1(t)R_1(t+u)} \alpha 1/u$.

Thus we have illustrated how one modification of the model has removed the divergence at $\omega = 0$.

It appears from the treatment here and in part b that roughness and diffusion in two dimensions are essential (at least in a linear treatment) features in obtaining $S(\omega)\alpha\ 1/\omega$. In the case of a non-linear coupling (to be considered in a later paper) a "self-induced" roughness effect may occur without introducing roughness ab initio as an intrinsic feature of the model.

6. Summary

(a) If the resistance deviation $R_1(t)$ is related to the concentration deviation $c_1(r, t)$ of a diffusing medium (particles or heat) by the *linear* functional

$$R_1(t) = \int_{A_\nu} f(r)c_1(r, t)\, dr, \tag{6.1}$$

where r is a vector and dr a volume element in a ν-dimensional space of volume A_ν, then the spectral density $S(\omega)$ of $R_1(t)$ is

$$S(\omega) = \frac{2}{\pi}\frac{\chi A_\nu D}{s''}\frac{k^2 |f_k|^2}{\omega^2 + D^2 k^4}, \tag{6.2}$$

where D is the diffusion constant, s'' is defined by Eq. (3.14), χ is the Boltzmann constant, ω is the frequency (in radians per sec.), k is the wave number vector in ν-dimensional k-space limited to a discrete lattice of points (defined by Eq. (3.2)) over which the summation is taken, and f_k is the kth Fourier component of $f(r)$ (Eq. (3.3)).

(a) If the important terms in (6.2) vary slowly between lattice points in k-space (true if $\omega > \omega_0$ given by Eq. (3.18)), then (6.1) can be replaced by the integral

$$S(\omega) = 2^{\nu+1}\pi^{\nu-1}\frac{\chi D}{s''}\int \frac{|f(k)|^2 k^2\, dk}{\omega^2 + D^2 k^4}, \tag{6.3}$$

where the integration extends over the entire k-space and where $f(k)$ is given by (Eq. 3.20)

$$f(k) = \frac{1}{(2\pi)^\nu}\int_{A_\nu} f(r)e^{-ik\cdot r}\, dr. \tag{6.4}$$

(b) Let ω' be a frequency in the middle of a wide range. Suppose $|f(k)|^2$ averaged over the total solid angle in ν-dimensional k-space is proportional to k^{2n}, where n is an integer, in a wide range of k with $k = \sqrt{\omega'/D}$ in its middle. It follows then that $S(\omega) \propto D^{-n-\nu/2}\ \omega^{-1+n+\nu/2}$ as long as $-1 < 2n + \nu + 1 < 3$. As a consequence, we see that with n an integer (as is true for the simple cases considered in Section 5) ν must be 2—the only even di-

mensionality—in order that $S(\omega)$ be inversely proportional to ω in agreement with experiment. In this case the only allowed value of n is -1.

(c) From (b) we have the interesting result that $S(\omega)$ is independent of D when it is inversely proportional to ω. This means that very slowly diffusing substances can contribute as much to contact noise as rapidly diffusing substances. This result can be derived on quite dimensional grounds and is not dependent upon the special assumptions underlying our treatment.

(d) A system comprising a high resistance layer modulated by the three-dimensional diffusion of particles or heat gives $S(\omega) \propto \omega^{-1/2}$. See Case a.(*i*) in Section 5.

(e) In a system composed of a localized contact disturbed by a diffusing surface layer (See Case a.(ii), Section 5), the self-covariance $\overline{R_1(t)R_1(t+u)}$ is inversely proportional to $\Delta + Du$ where Δ may be considered the contact area. We have $S(\omega) \propto -\log a + \text{const.}$ for $\omega \ll D/\Delta$ and $S(\omega) \propto \omega^{-2}$ for $\omega \gg D/\Delta$.

(f) In a system involving the contact between relatively large areas of rough surfaces covered with diffusing surface layers (Cases b. and c., Section 5), we have been successful in obtaining $S(\omega) \propto \omega^{-1}$, and also in obtaining a reasonable dependence upon the average resistance.

APPENDIX I

Spectral Density and the Self-Covariance

Here we consider in detail the spectral density, the self-covariance, and the relation between these two quantities, first for the case of a single random variable. The treatment is subsequently extended to the case of a *set* of random variables which necessitates the consideration of the spectral density matrix and the covariance matrix.

Let $y(t)$be a real random variable whose time average vanishes, $\overline{y(t)} = 0$. Now the m.s. value of y can be defined

$$\overline{y^2(t)} = \operatorname*{Lim}_{\tau\to\infty} \frac{1}{\tau} \int_{-\infty}^{+\infty} y^2(t, \tau)\, dt \tag{I-1}$$

where $y(t, \tau) = y(t)$ in the interval $-\frac{\tau}{2} \leq t < \frac{\tau}{2}$ and vanishes outside this interval. Evidently $y(t, \tau)$ can be expressed by the Fourier integral

$$y(t, \tau) = \int_{-\infty}^{+\infty} z(\omega, \tau) e^{i\omega t}\, d\omega \tag{I-2}$$

where

$$z(\omega, \tau) = \frac{1}{2\pi} \int_{-(\tau/2)}^{+(\tau/2)} y(t) e^{-i\omega t}\, dt.$$

By Parseval's theorem we obtain

$$\int_{-\infty}^{+\infty} y^2(t, \tau)\, dt = 2\pi \int_{-\infty}^{+\infty} |\, y(\omega, \tau)\,|^2\, d\omega,$$

which, when combined with (I-1), gives finally the desired result (using the fact that $|\, y(\omega, \tau)\,|^2$ is an even function of ω)

$$\overline{y^2(t)} = \int_0^\infty Y(\omega)\, d\omega \tag{I-3}$$

where

$$Y(\omega) = 4\pi \operatorname*{Lim}_{\tau\to\infty} \frac{1}{\tau} |\, y(\omega, \tau)\,|^2 \tag{I-4}$$

is the spectral density.

By a procedure not very different from the preceding, one can show that

$$\overline{y(t)y(t+u)} = \int_0^\infty Y(\omega) \cos \omega u\, d\omega, \tag{I-5}$$

$$Y(\omega) = \frac{2}{\pi} \int \overline{y(t)y(t+u)} \cos \omega u\, du. \tag{I-6}$$

The quantity $\overline{y(t)y(t+u)}$ is called the self-covariance.

Now let us suppose that we have a set of random variables $y_i(t)$ which are in general complex and whose time averages vanish. We are then led to consider, instead of (I-3), relations of the form

$$\overline{y_i(t)y_j^*(t)} = \int_0^\infty Y_{ij}(\omega)\, d\omega \tag{I-7}$$

where now

$$Y_{ij}(\omega) = 2\pi \operatorname*{Lim}_{\tau\to\infty} \frac{1}{\tau} [y_i(\omega, \tau)y_j^*(\omega, \tau) + y_i(-\omega, \tau)y_j^*(-\omega, \tau)] \tag{I-8}$$

in which

$$y_i(\omega, \tau) = \frac{1}{2\pi} \int_{-(\tau/2)}^{+(\tau/2)} y_i(t)e^{i\omega t}\, dt.$$

Instead of self-covariances like $\overline{y(t)y(t+u)}$ we have to consider a covariance matrix of the form $\overline{y_i(t)y_j^*(t+u)}$. Since we shall not have occasion in this paper to consider the relation between the spectral density matrix and the covariance matrix we will not consider the derivation of the analogue of Eq. (I-5).

APPENDIX II

Thermodynamic Theory of Fluctuations

The value of the quantity $\overline{c_1(r, t)c_1(r^1, t)}$ or $\overline{(c_k(t)c^*_{k^1}(t))}$ is determined from equilibrium considerations. Before going into the above continuum problem let us first consider the problem for the case of a system described by a finite set of variables. More specifically let us suppose that the state of the system subject to certain restraints (i.e. fixed total mass and energy) is described by the set of variables $x_1, \cdots, x_n$. Let the equilibrium state be given by the values $x_1^0, \cdots, x_n^0$, and let

$$x_i = x_i^0 + \alpha_i . \tag{II-1}$$

If the system is constrained to constant average energy E, the entropy of the non-equilibrium state $S = S^0 + \Delta S$ will be less than S^0, the entropy of the equilibrium state, by an amount

$$\Delta S = -\frac{1}{2}\sum_{ij} S_{ij}\alpha_i\alpha_j , \tag{II-2}$$

where

$$S_{ij} = -\left(\frac{\partial^2 S}{\partial x_i\,\partial x_j}\right)_{x_k=x_k^0} + \frac{1}{T^0}\left(\frac{\partial^2 E}{\partial x_i\,\partial x_j}\right)_{x_k=x_k^0}$$

Obviously, ΔS must be the negative of a positive definite quadratic form, otherwise the equilibrium state would not be a state of maximum entropy. The probability distribution[26] for the α's is given by

$$P(\alpha_1, \cdots, \alpha_n) = Ne^{\Delta S/\chi} \tag{II-3}$$

where N is a normalization factor and χ is the Boltzmann constant. Averaging the products $\alpha_i\,\alpha_j$ we find that

$$\sum_j S_{ij}\overline{\alpha_j\alpha_k} = \chi\delta_{ik} . \tag{II-4}$$

Multiplying (II-4) by the arbitrary set γ_i and summing over i we get

$$\sum_{ij} \gamma_i S_{ij}\overline{\alpha_j\alpha_k} = \chi\gamma_k . \tag{II-5}$$

The generalization to a system described by a continuous set of variables is not difficult on the basis of (II-5). Now suppose that, in a ν-dimensional space A_ν, we have a system whose state at time t is defined by the continuous set of values of the variable $c(r, t) = \bar{c} + c_1(r, t)$; we have

$$\Delta S = -\frac{1}{2}\int_{A_\nu} s''\, c_1^2(r, t)\, d\tau \tag{II-6}$$

[26] H. B. G. Casimir, *Rev. Mod. Phys.* **17**, Nos. 1 and 3, 343–4 (1945).

where

$$s'' = -\left(\frac{\partial^2 s}{\partial c^2}\right)_{c=\bar{c}} + \frac{1}{T^0}\left(\frac{\partial^2 e}{\partial c^2}\right)_{c=\bar{c}}$$

when s and e are the entropy and energy, respectively, per unit volume (of ν-dimensional space). In calculating (II-6) it was assumed that

$$\int_{A_\nu} c_1(r, t)\, dr = 0,$$

expressing the fact that the system is closed. In order to put (II-6) into a form strictly analogous to (II-2) we write it

$$\Delta S = -\frac{1}{2}\int_{A_\nu}\int_{A_\nu} s''\delta(r - r')c_1(r, t)c_1(r', t)\, dr\, dr'. \qquad \text{(II-7)}$$

We see that the equation analogous to Eq. (II-5) must be

$$\int_{A_\nu}\int_{A_\nu} \gamma(r')s''\delta(r - r'')\overline{c_1(r'', t)c_1(r, t)}\, dr\, dr' = \chi\gamma(r) \qquad \text{(II-8)}$$

where $\gamma(r)$ is an arbitrary function. Integrating (II-8) with respect to r'' and using the fact that the delta function is defined by

$$\int \gamma(r')\delta(r' - r)\, dr' = \gamma(r)$$

we readily arrive at the result

$$\overline{c_1(r, t)c_1(r', t)} = \frac{\chi}{s''}\delta(r - r'). \qquad \text{(II-9)}$$

Using the Fourier space-expansions of C_1 and $\delta(r)$

$$c_1(r, t) = \sum_k{}' c_k(t)e^{ik\cdot r},$$

$$\delta(r) = \frac{1}{A_\nu}\sum_k e^{ik\cdot r},$$

in the region $A_\nu = L_1 \times \cdots \times L_\nu$ with $k_i = 2\pi n_i/L_i$, we can write (II-9) over into the equivalent expression:

$$\overline{c_k(t)c_k^*(t)} = \frac{\chi}{A_\nu s''}\delta_{kk'}, \qquad \text{(II-10)}$$

where

$$\delta_{kk'} = \begin{cases} 1 & \text{if } k = k', \\ 0 & \text{otherwise.} \end{cases}$$

Abstracts of Technical Articles by Bell System Authors

Audio-Frequency Measurements.[1] † W. L. BLACK* and H. H. SCOTT. This paper indicates the theory involved in making measurements of gain, frequency response, distortion, and noise at audio frequencies, with particular emphasis on such measurements made on high-gain systems. There are also discussed techniques of measurement and factors affecting the accuracy of results. This subject is not new art but has not previously been published in correlated form, to the knowledge of the authors.

Growing Quartz Crystals.[2] † E. BUEHLER and A. C. WALKER. The Bell Telephone Laboratories started an investigation of this subject in March 1946, based on information gleaned from several investigators who visited Germany after the war, particularly Mr. J. R. Townsend of these Laboratories, and Professor A. C. Swinnerton of Antioch College. After a relatively few experiments made with equipment similar to that used by Professor Richard Nacken in Germany, and with the process he described, it became apparent that Nacken had made substantial progress in the art of growing quartz at temperatures and pressures near the critical state of water, i.e., about 374°C, and 3,200 pounds per square inch. This report summarizes further progress that has been made in the Laboratories since March 1946.

Corrosion of Telephone Outside Plant Material.[3] † K. C. COMPTON and A. MENDIZZA. Problems resulting from corrosion in the telephone outside plant are many and varied. In this article an attempt is made to give a broad overall picture of these problems and the manner in which they are met and solved by the telephone plant engineer.

Magnetic Recording in Motion Picture Techniques.[4] JOHN G. FRAYNE and HALLEY WOLFE. Development of magnetic recording at the Bell Telephone Laboratories is described with the application of such facilities to Western Electric recording and reproducing systems. A method of driving 35-mm. magnetic film with a flutter content not greater than 0.1 per cent is described, as is a multigap erasing head.

Semi-Conducting Properties in Oxide Cathodes.[5] † N. B. HANNAY, D. MACNAIR, and A. H. WHITE. It has been widely assumed, without ade-

[1] *Proc. I. R. E.*, v. 37, pp. 1108–1115, October 1949.
* Of Bell Tel. Labs.
[2] *Sci. Monthly*, v. 69, pp. 148–155, September 1949.
[3] *Corrosion*, v. 5, pp. 194–197, June 1949.
[4] *S. M. P. E. Jour.*, v. 53, pp. 217–234, September 1949.
[5] *Jour. Applied Physics*, v. 20, pp. 669–681, July 1949.
† A reprint of this article may be obtained by writing to the Editor of the Bell System Technical Journal.

quate experimental verification, that barium-strontium oxide, as used in the oxide cathode, is an excess electronic semi-conductor. Accordingly, the electrical conductivity of (Ba,Sr)O has been studied as a function of temperature before and after activation with methane, extensive precautions being taken to exclude spurious effects. The increase in conductivity obtained characterizes (Ba,Sr)O as a "reduction" semi-conductor, and hence very probably as an electronic semi-conductor whose conduction electrons arise from a stoichiometric excess of (Ba,Sr) atoms in solid solution.

A basic prediction of the semi-conductor theory has been tested quantitatively with the finding that the electrical conductivity and the thermionic emission of a (Ba,Sr)O cathode are directly proportional through three orders of magnitude of activation; well-defined chemical and electrical activation and deactivation procedures were used in obtaining this result. It may be concluded that activation represents an increase in the chemical potential of the electrons in the oxide, little or no change in the state of the surface occurring. It has also been found that deviations from the proportionality of conductivity and emission may be expected under conditions leading to inhomogeneity in the oxide, in agreement with the semi-conductor theory also.

Electron Microscope and Diffraction Study of Metal Crystal Textures by Means of Thin Sections.[6] † R. D. HEIDENREICH. Bethe's dynamical theory of electron diffraction in crystals is developed using the approximation of nearly free electrons and Brillouin zones.

The use of Brillouin zones in describing electron diffraction phenomena proves to be illuminating since the energy discontinuity at a zone boundary is a fundamental quantity determining the existence of a Bragg reflection. The perturbation of the energy levels at a corner of a Brillouin zone is briefly discussed and the manner in which forbidden reflections may arise at a corner pointed out. It is concluded that the kinematic theory is inadequate for interpreting electron images of crystalline films.

An electrolytic method for preparing thin metal sections for electron microscopy and diffraction is introduced and its application to the structure of cold-worked aluminum and an aluminum-copper alloy demonstrated. It is concluded that cold-worked aluminum initially consists of small, inhomogeneously strained and disoriented blocks about 200A in size. These blocks are not revealed by etching but would contribute to line broadening in conventional diffraction experiments. By means of a reorientation of the blocks through a nucleation and growth process, larger disoriented domains about 1–3μ in size found experimentally could be accounted for. It is sug-

[6] *Jour. Applied Physics*, v. 20, pp. 993–1010, October 1949.

† A reprint of this article may be obtained by writing to the Editor of the Bell System Technical Journal.

gested that such a nucleation and growth reorientation phenomenon is responsible for self-recovering in cold-worked metals.

The formation of $CuAl_2$ precipitate particles is demonstrated with both electron micrographs and diffraction patterns. A fine lamellar structure found in the quenched Al-4 per cent Cu alloy is at present unexplained.

Path-Length Microwave Lenses.[7]† WINSTON E. KOCK. Lens antennas for microwave applications are described which produce a focusing effect by physically increasing the path lengths, compared to free space, of radio waves passing through the lens. This is accomplished by means of baffle plates which extend parallel to the magnetic vector, and which are either tilted or bent into serpentine shape so as to force the waves to travel the longer-inclined or serpentine path. The three-dimensional contour of the plate array is shaped to correspond to a convex lens. The advantages over previous metallic lenses are: broader band performance, greater simplicity, and less severe tolerances.

Refracting Sound Waves.[8]† WINSTON E. KOCK and F. K. HARVEY. Structures are described which refract and focus sound waves. They are similar in principle to certain recently developed electromagnetic wave lenses in that they consist of arrays of obstacles which are small compared to the wave-length. These obstacles increase the effective density of the medium and thus effect a reduced propagation velocity of sound waves passing through the array. This reduced velocity is synonymous with refractive power so that lenses and prisms can be designed. When the obstacles approach a half wave-length in size, the refractive index varies with wave-length and prisms then cause a dispersion of the waves (sound spectrum analyzer). Path length delay type lenses for focusing sound waves are also described. A diverging lens is discussed which produces a more uniform angular distribution of high frequencies from a loud speaker.

Double-Stream Amplifiers.[9]† J. R. PIERCE. This paper presents expressions useful in evaluating the gain of a double-stream amplifier having thin concentric electron streams of different velocity and input and output gaps across which both streams pass.

Direct Voltage Performance Test for Capacitor Paper.[10]† H. A. SAUER and D. A. MCLEAN. Performance of capacitors on accelerated life test may vary over a wide range depending upon the capacitor paper used. Indeed, at present a life test appears to be the only practical means for evaluating

[7] *Proc. I. R. E.*, v. 37, pp. 852–855, August 1949.
[8] *Acous. Soc. Amer. Jour.*, v. 21, pp. 471–481, September 1949.
[9] *Proc. I. R. E.*, v. 37, pp. 980–985, September 1949.
[10] *Proc. I. R. E.*, v. 37, pp. 927–931, August 1949.
† A reprint of this article may be obtained by writing to the Editor of the Bell System Technical Journal.

capacitor paper, since, within the limits observed in commercial material, the chemical and physical tests usually made do not correlate with life. Lack of correlation is ascribed to obscure physical factors which have not yet been identified.

Generally, several weeks are required to evaluate a paper by life tests of the usual severity. Unfortunately, the duration of these tests is too long for quality control of paper.

The desire for a life test which requires no more than a day or two for evaluation led to the development of a rapid d-c. test. The philosophy of rapid life testing is based upon the experimental evidence that the process of deterioration under selected temperature and voltage conditions is principally of a chemical nature, and also upon the well-known fact that rates of chemical reaction increase exponentially with temperature.

Life tests on two-layer capacitors conducted at 130°C. provide an acceleration in deterioration many fold more than that obtained in the lower-temperature life tests, and correlate well with these tests.

Contributors to this Issue

SIDNEY DARLINGTON, Harvard University, B.S. in Physics, 1928; Massachusetts Institute of Technology, B.S. in E.E., 1929; Columbia University, Ph.D. in Physics, 1940. Bell Telephone Laboratories, 1929–. Dr. Darlington has been engaged in research in applied mathematics, with emphasis on network theory.

RICHARD C. EGGLESTON, Ph.B., 1909 and M.F., 1910, Yale University; U. S. Forest Service, 1910–1917; Pennsylvania Railroad, 1917–1920; First Lieutenant, Engineering Div., Ordnance Dept., World War I, 1918–1919. American Telephone and Telegraph Company, 1920–1927; Bell Telephone Laboratories, 1927–. Mr. Eggleston has been engaged chiefly with problems relating to the strength of timber and with statistical investigations in the timber products field.

J. R. PIERCE, B.S. in Electrical Engineering, California Institute of Technology, 1933; Ph.D., 1936. Bell Telephone Laboratories, 1936–. Engaged in study of vacuum tubes.

S. O. RICE, B.S. in Electrical Engineering, Oregon State College, 1929; California Institute of Technology, 1929–30, 1934–35. Bell Telephone Laboratories, 1930–. Mr. Rice has been concerned with various theoretical investigations relating to telephone transmission theory.

J. M. RICHARDSON, B.S., California Institute of Technology, 1941; Ph.D., Cornell, 1944. Bell Telephone Laboratories, 1945–49. Dr. Richardson at these Laboratories had been mainly associated with studies of ferroelectric materials, noise contacts, and contact erosion. At present he is with the Bureau of Mines at Pittsburgh.